University of Dundee

DOCTOR OF PHILOSOPHY

Genetic and molecular analysis of drop out, the single homolog of the vertebrate MAST kinases in Drosophila melanogaster

Hain, Daniel

Award date:
2011

Link to publication

Genetic and molecular analysis of drop out, the single homolog of the vertebrate MAST kinases in Drosophila melanogaster

Daniel Hain

2011

University of Dundee

University of Dundee

College of Life Sciences

Genetic and molecular analysis of *drop out*, the single homolog of the vertebrate MAST kinases in *Drosophila melanogaster*

Daniel Hain

A thesis submitted for the degree of

Doctor of Philosophy

University of Dundee

March 2011

Parts of this thesis have been submitted with the following title:

Acknowledgements

Declaration

I declare that the following thesis is based on the results of investigations conducted by myself, and that this thesis is of my own composition. Work other than my own is clearly indicated in the text by reference to the relevant researchers or to their publications. This dissertation has not in whole, or in part, been previously submitted for a higher degree.

Daniel Hain

I certify that Daniel Hain has spent the equivalent of at least nine terms in research work at the College of Life Sciences, University of Dundee, and that he has fulfilled the conditions of the Ordinance General No. 14 of the University of Dundee and is qualified to submit the accompanying thesis in application for the degree of Doctor of Philosophy.

Dr. Arno Müller

The life cycle of *Drosophila melanogaster*
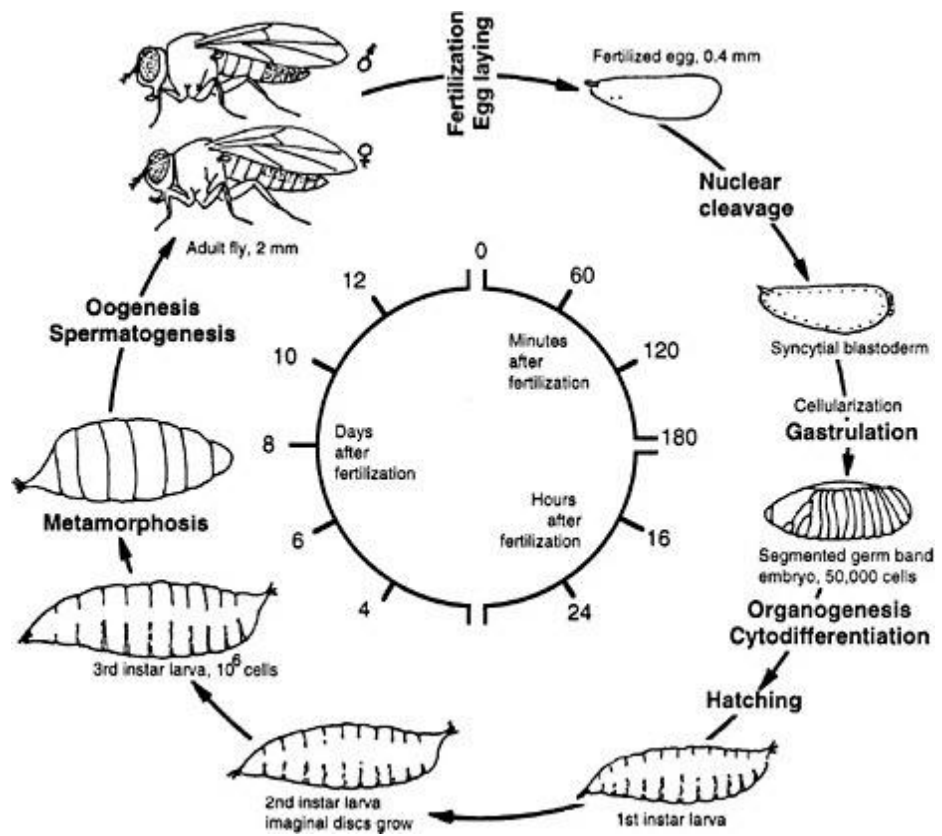
Lewis Wolpert, 1998

Abbreviations

Amp	Ampicillin
ATP	Adenosine triphosphate
BSA	Bovine Serum Albumin
°C	Degree Celsius
Da	Dalton
dH2O	Distilled water
DNA	Desoxyribonucleic acid
E.coli	*Escherichia coli*
EDTA	Ethylenediamine tetraacetic acid
ER	Endoplasmatic Reticulum
g	gram (or gravity)
GDP	Guanosine Di-Phosphate
GFP	Green Fluorescent Protein
GTP	Guanosine Tri-Phosphate
h	hour(s)
HA	Hemagglutinin
HRP	Horseradish peroxidise
Kan	Kanamycin
kDa	Kilodalton
l	litre
m	Milli
M	Molar
MT	Micro Tubule
µ	Micro
min	Minute
mol	Mole
MTOC	Microtubule Organizing Centre
n	Nano
pH	Potential of Hydrogen
PM	Plasma membrane
PVDF	Polyvinylidene fluoride
RE	Recycling Endosome
rpm	Revolutions per minute
SAJ	Spot Adherens Junction
SAR	Sub-Apical Region
SDS	Sodium dodecyl sulfate
SDS-PAGE	Sodium dodecyl sulphate polyacrylamide gel electrophoresis
sec	second
SJ	Septate Junction
Tris	Tris (hydroxymethyl) aminomethane
TJ	Tight Junction
U	Units
UV	ultraviolet
V	Volts
ZA	Zonula Adherens

Summary

Cellularisation is a specialised form of cytokinesis in *Drosophila melanogaster*. Cellularisation occurs after the first 13 syncytial cell cycles of the embryo and involves targeted insertion of membrane to form the blastoderm, which represents a polarised epithelium made out of about 6000 cells. The molecular machinery driving cellularisation is complex and not well understood. In this work a novel gene regulating this process is identified and characterised. The mutation *drop out* causes defects in intracellular transport, cell polarity and nuclear positioning. Previous work provided evidence that dop^1 is an allele of the RNA silencing gene *argonaute*2 (*ago2*). However, results presented in this thesis showed that *ago*2 functions are unimpaired in *dop* mutant embryos using genetic and biochemical tools. Moreover genetic and molecular mapping revealed that *dop* mutants carry a mutation in a gene within close proximity to *ago*2. This work demonstrates that *dop* encodes the sole *Drosophila* homolog of the mammalian MAST (microtubule associated serine/threonine) kinase family. The molecular lesion in the dop^1 allele of *dop* leads to an amino acid exchange in the kinase domain and results in a significant reduction of Dop protein levels. A detailed investigation of the mutant phenotype indicated that dop^1 affects microtubule rigidity and Dynein-dependent microtubule associated transport. Search for possible Dop targets revealed reduced phosphorylation of the Dynein intermediate chain (DIC). DIC is a subunit of Dynein and has been shown to be involved in the binding of cargo to the Dynein complex. Therefore, a possible function for Dop might be the phosphorylation of DIC to regulate microtubule dependent transport by controlling Dynein-cargo interaction.

Contents

Chapter III: Results Part I:

The *dop* mutation as an allele of *argonaute2*

Chapter IV: Results Part II: Developmental functions of the Dop kinase

Chapter V: Discussion

Figures and Tables

Chapter I: Introduction

1. <u>**Introduction**</u>

1.1. Overview

This thesis was created over the course of three years with the aim to gain deeper understanding of how epithelial cells are polarised. As an experimental system, the early embryonic development of the fruit fly *Drosophila melanogaster* was investigated. The model organism *D. melanogaster* is widely used and provides excellent genetic tools to study developmental and cell biological questions. The straightforward handling of fruit flies allows large genomic screens using mutagenesis to create mutant phenotypes and identify the associated genes. Such forward genetics were used to create a class of non-complementing mutations called *drop out* (*dop*) mutations. *dop* mutations disrupt the formation of the polarised blastoderm epithelium in *Drosophila* embryos. In this thesis *dop* mutations have been investigated and the results are grouped into two parts. Part I is based on the previous finding that the *dop*[1] allele might be an allele of the *argonaute2* gene, which provides RNA silencing functions. In part II the molecular nature of *dop* mutations are identified and the functions of the associated gene in the regulation of cell polarity are investigated.

1.2. Acquisition of apico/basal polarity

A defined apico/basal polarity is important for the functions of cells and tissues. Cell polarity has been shown to be necessary for diverse functions from directed migration of solitary cells to the secretory functions of epithelial tissues. Mutations in polarity complex proteins have been shown to result in delamination of cells from epithelial

layers, which subsequently might induce the formation of invasive tumors ({Mani, 2008 4 /id}Abbott et al., 1992; Bilder et al., 2000; Pastor-Pareja et al., 2004; Mani et al., 2008). Polarity complexes are also needed to create diffusion barriers between epithelial cells. In the gut apical cellular junctions prevent liquid from the lumen of the gut from diffusing between the epithelial cells and causing inflammations (Hermiston and Gordon, 1995; Whitney et al., 2010). These cellular junctions define apico/basal polarity and are characterised by transmembrane receptors and membrane associated protein complexes. Nevertheless, the interaction and regulation of polarity complexes is not well understood. *Drosophila* cellularisation is used as a model to understand the regulation of polarity complexes (Schejter, 1993; Tepass and Hartenstein, 1994; Sullivan and Theurkauf, 1995).

The formation of polarity complexes occurs gradually throughout embryogenesis (Müller, 2001). Rudimentary cues for polarity are given prior to cellularisation. The early cell cycles of the embryonic development in *Drosophila* occur without cytokinesis. The early embryo proceeds rapidly through 13 syncytial division cycles (Fig. 1.1A, B). During cycles 1-9 the nuclei divide in the centre of the egg. At the end of the 10th cycle most nuclei migrate to the cortex of the plasma membrane of the embryo. As soon as the nuclei are arranged at the periphery of the embryo the membrane is specified into a pseudo-epithelial structure (Karr and Alberts, 1986). The establishment of an actin matrix at the membrane between the nuclei induces structural changes that lead to invagination of the membrane into pseudo cleavage furrows (Mavrakis et al., 2009). The membrane region on top of the nuclei develops apical characteristics such as microvili-like membrane protrusions, while the pseudo-cleavage furrow between nuclei aggregates proteins that later separate into the basal and lateral membrane compartments (Mavrakis et al., 2008; Lecuit, 2004). The pseudo-cleavage

furrows surround the nuclei during the rapid cell cycles 10-13 and after each division additional furrows form to surround every nucleus in a honeycomb shaped pattern.

In cell cycle 14 the rapid division cycles stop and cellularisation begins (Fig. 1.1C). During cellularisation the furrow membrane grows towards the centre of the embryo. Membrane growth can be divided into a slow phase and a fast phase. In the slow phase the membrane grows 0.3 microns per minute for 40 minutes. At the end of slow phase the membrane furrows have passed the nuclei. During the following fast phase the membrane grows almost three times as fast as during slow phase until the furrows reach a depth of 30 microns. Marker proteins that localised uniformly to the pseudo cleavage furrow are separated and indicate different membrane compartments such as the apical region, the baso lateral region and the furrow canal. The furrow canal is a tear shaped structure at the leading edge of the growing membrane. The furrow canal maintains basal marker proteins like Slam, DPatJ and RhoA, while the lateral membrane aggregates proteins like Neurotactin, Dlg and Scribbles. Between the furrow canal and the lateral membrane transient basal junctions are established at onset of cellularisation. The basal junctions contain DE-Cadherin and β-Catenin (Müller and Wieschaus, 1996; Peifer and Wieschaus, 1990). Cadherin molecules are transmembrane proteins that mediate Ca^{2+}-dependent cell-cell contacts. Through their cytoplasmic domains they bind to Catenin proteins that establish the connection to the actin-cytoskeleton. Progenitors of apical junctions are observed during the fast phase of cellularisation. During the fast phase of cellularisation spot adherens junctions (SAJ) form in the apico-lateral region of the growing membrane. Diffusely localised clusters of DE-Cadherin/beta-Catenin and Bazooka (the *Drosophila* homologue of Par-3) interact in the membrane to form the SAJ (Tepass, 1994; Harris and Peifer, 2005; McGill et al., 2009). The SAJ are a precursor to the adherens junction also called Zonula

Adherens (ZA). As the lateral membrane extends further basally, lateral marker proteins are highly concentrated above the basal junctions and less concentrated in apical regions. At the end of cellularisation the polarity complexes rearrange. The baso/lateral proteins shift upwards along the lateral membrane. The basal junction is resolved and the cadherin/catenin complex is primarily found at the SAJ. At this time the ZA is formed from the SAJ and adopts a belt like structure surrounding the apico/lateral membrane. In addition the apical polarity proteins Crumbs and Stardust gradually accumulate apical of the ZA and define the sub-apical region (SAR). Proteins of the SAR and the ZA interact vividly to establish distinct polarity regions (for overview see Harris and Peifer, 2005). The maturation of epithelial polarity is only completed in late embryogenesis with the formation of the apico/lateral septate junction (SJ) during hypodermis differentiation (Tepass and Hartenstein, 1994). SJs are tight membrane boundaries that restrict diffusion across the intracellular space and within the membrane constituting an analogue to the mammalian tight junction.

In summary essential polarity regulators arrange at the membrane during cellularisation while mature apico/basal junctions are established during later development. How the polarity regulators are recruited to the membrane is not well understood. A likely model suggests that these proteins are transported to the membrane via microtubule-associated transport of membrane material (Lecuit and Wieschaus, 2000).
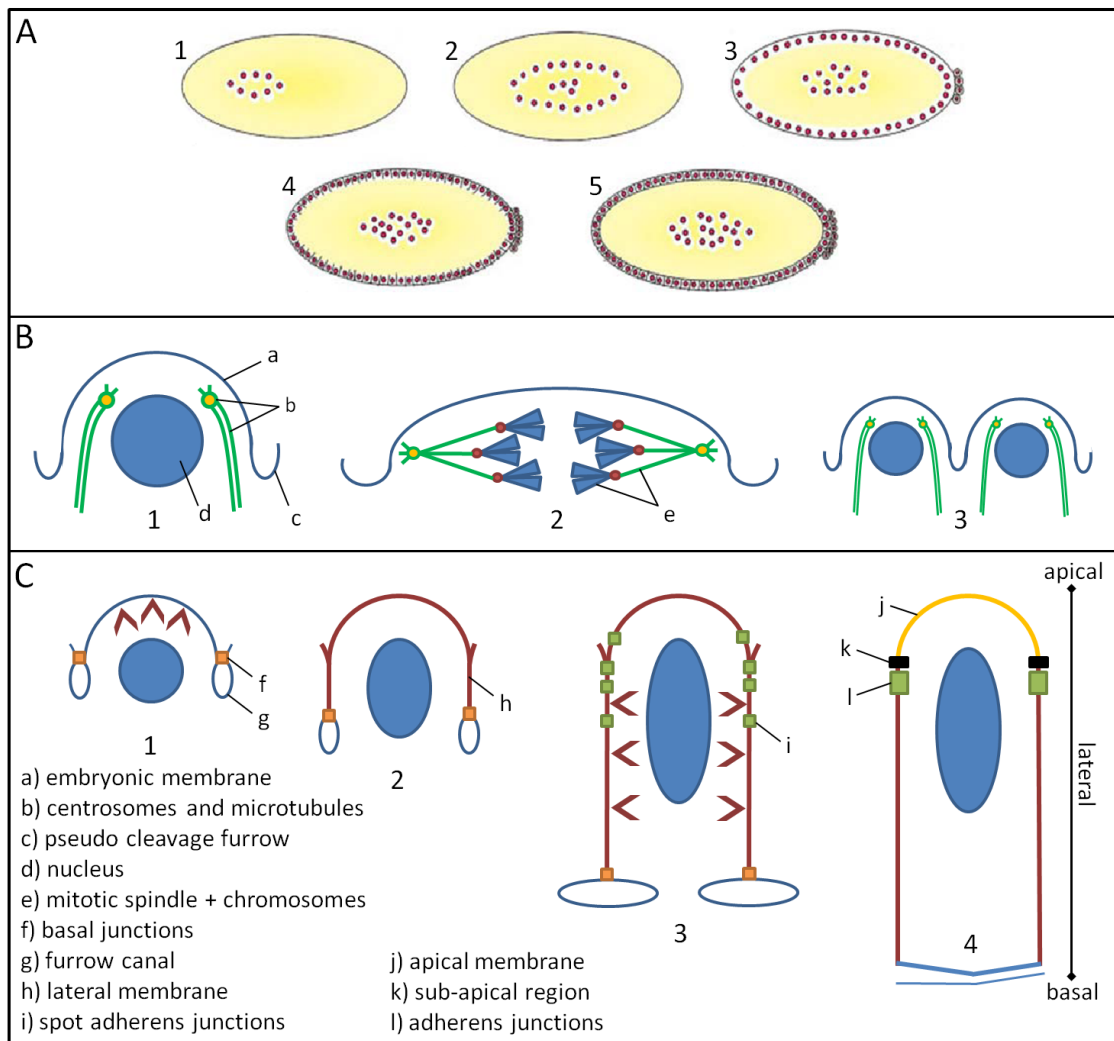
Fig. 1.1: Cellular structure of embryos during syncytial divisions and cellularisation. The first syncytial divisions occur in the yolk of the egg (A1, A2). During cell cycle 10 the nuclei (red) arrange at the outer membrane (A3). Syncytial divisions occur at the membrane (A4, B1-3) until the rapid divisions halt in interphase of cell cycle 14. Then cellularisation occurs (A5, C1-4). To drive membrane growth membrane material is inserted into the apical membrane during slow phase (arrows in C1) and into the lateral membrane during fast phase (arrows in C3). The basal junctions form first; apical junctions are assembled during fast phase as spot adherens junctions that are transformed into adherens junctions during later development (Mazumdar and Mazumdar, 2002; Müller, 2001).

1.3. Membrane transport during cellularisation

1.3.1. Membrane transport routes

During cellularisation the membrane surface of the embryo increases ≈25-fold in 60 min (Beronja and Tepass, 2002). Membrane transport is an inevitable process to provide raw material for the membrane growth during cellularisation. Initially apical extensions of the plasma membrane called villous projections were favoured as source

of membrane material for cellularisation (Turner and Mahowald, 1976). However, membrane labelling experiments showed that the villous projections only provide material for the formation of the furrow canals (Lecuit and Wieschaus, 2000). In fact, the majority of the material needed for membrane growth derives from insertion of vesicles originating from internal organelles (Fig. 1.2). The membrane material deployed during cellularisation derives in part from the endoplasmatic reticulum (ER) and the Golgi. During cellularisation ER and Golgi are aligned in a dispersed pattern at the basal side of the nuclei. The transport of membrane material from ER and Golgi to the growing membrane is microtubule dependent as microtubule depolymerisation leads to inhibition of membrane growth and disrupts Golgi structures (Lecuit and Wieschaus, 2000). Furthermore, inhibition of ER-to-Golgi transport by injection of brefeldin A reduces the speed of membrane growth (Sisson et al., 2000).

The recycling endosome (RE) is another internal membrane organelle involved in cellularisation. The RE is a tubulo-vesicular structure that localises to the apical cytoplasm surrounding the centrosomes. The RE connects the endocytic and exocytic pathways (Ang et al., 2004; Lock and Stow, 2005; Murray et al., 2005). The GTPases Dynamin and Rab11 are necessary for vesicle trafficking through the RE (van der Bliek and Meyerowitz, 1991; Ullrich et al., 1996; Dollar et al., 2002). In addition Dynamin regulates vesicle budding from membranes during endocytosis (Chen et al., 1991; van der Bliek and Meyerowitz, 1991) while Rab11 is involved in the exocytic pathway (Riggs et al., 2007; Royou et al., 2003). Mutations in Dynamin as well as overexpression of dominant negative Rab11 result in inhibition of membrane growth (Grant et al., 1998; Pelissier et al., 2003). As the RE connects endocytic and exocytic vesicle transport it might have two roles during cellularisation (reviewed in Lecuit, 2004): First,

Endocytosis of membrane material from the apical membrane (dependent on the small GTPase Rab5) might pass through the RE for re-direction to the growing membrane. Second, vesicles derived from the ER/Golgi network are transported through RE pathways before being exocytosed. In conclusion membrane material is transported from internal membrane pools to fuse with the growing membrane by exocytosis.

Intracellular vesicle transport might also be necessary to recruit polarity proteins to the membrane. Tracking of the transport of the transmembrane protein Neurotactin (Nrt) has revealed an intracellular transport route for membrane proteins during cellularisation (Lecuit and Wieschaus, 2000). Nrt is synthesised during early cellularisation in the ER and accumulates in the lateral membrane in later stages. Disruption of microtubules leads to accumulation of Nrt near the Golgi, while disruption of RE function by a Dynamin mutation leads to accumulation in the RE (Pelissier et al., 2003). These experiments show that intracellular vesicle transport is a possible mechanism to recruit trans-membrane proteins and polarity regulators during cellularisation.
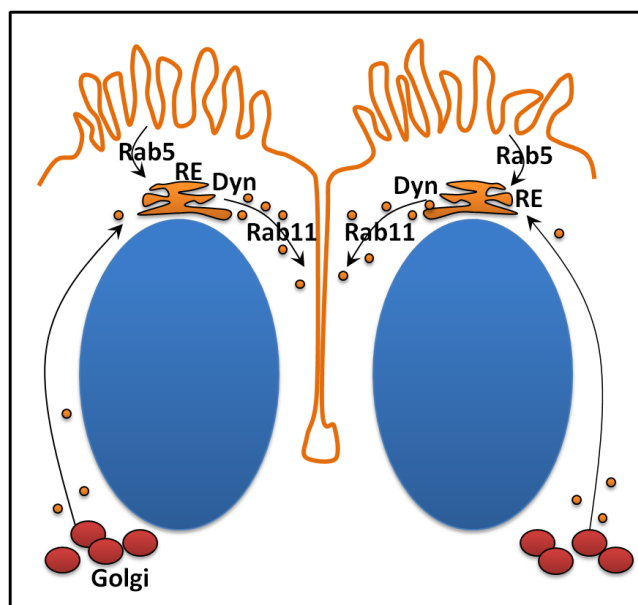
Fig. 1.2: Routes of membrane transport during cellularisation. The material needed for the membrane growth during cellularisation derives mainly from the Golgi. The apical transport of Golgi vesicles is dependent on microtubules and Dynein. The RE is participating in the exocytosis of internal membrane material. RE function is dependent on the GTPases Dynamin (Dyn) and Rab11. Membrane is also provided by endocytosis from the villous projections in the external membrane. Rab5 positive early endosomes are routed to the RE to provide membrane material (Lecuit, 2004).

1.3.2. Microtubule associated transport

The regulation of membrane transport during cellularisation is complex and not well understood. Membrane reservoirs like the Golgi and the RE have been identified as sources of membrane vesicles that can be used for membrane growth. However, it is not known how the transport of Golgi or RE vesicles towards distinct target sites is regulated. A likely mechanism for site directed exocytosis is the microtubule associated vesicle transport. Microtubules have a polarised structure with defined minus and plus ends. Transport along the microtubules is accomplished by Dynein and Kinesin motor complexes. Dynein motors catalyse cargo transport towards the minus ends of microtubules, while most Kinesin motors move in direction of the plus ends.

Several studies have indicated an important role of Dynein in cellularisation (Robinson et al., 1999; Papoulas et al., 2005; Riggs et al., 2007). Dynein is a multi-protein complex consisting of two heavy chains of $\sim$ 500 kDa as well as multiple intermediate chains, light intermediate chains and light chains. The heavy chains fold to form globular domains that provide the motor function. These "head" structures are connected by a stem structure to the light, light intermediate and intermediate chains. These smaller subunits have been found to regulate motor activity and the binding of cargo; however their precise functions are not well understood. In metazoan organisms Dynein is essential for survival. Mutations that lead to loss of the Dynein heavy chain are recessive lethal. Therefore, hypomorphic alleles have been used to study Dynein functions in the early embryo. These studies showed that Dynein is needed for nuclear attachment to the membrane and proper structure of the cytokinetic spindle (Robinson et al., 1999). 94% of these Dynein mutants die during embryonic development. Most of these embryos show defects during the syncytial divisions or fail

to cellularise. The mutant embryos entering cellularisation display defects in recruitment of Baz and DE-Cadherin (Harris and Peifer, 2005). Furthermore, inhibition of Dynein functions by injection of a Dynein antibody during cellularisation results in slowed membrane growth and blocks the apical transport of Golgi vesicles (Papoulas et al., 2005). Therefore, Dynein dependent transport is necessary for the directed transport of membrane vesicles and polarity regulators during cellularisation. The various functions of Dynein motors during mitosis, cytokinesis and cellularisation indicate complex regulation of Dynein activity and cargo selectivity but how Dynein dependent transport is regulated is not understood.

The functions of Kinesins are not well investigated during cellularisation. A very recent report showed that the Kinesin Pavarotti (Pav) is needed for membrane growth (Sommi et al., 2010). Pav is the *Drosophila* homolog of Kinesin-6 (also named MKLP1), which is known to regulate cell division and formation of the cytokinetic furrow. Inhibition of Pav affects membrane growth during syncytial divisions as well as cellularisation and leads to changes in the localisation of actin and vesicles. During cellularisation Pav functions in two possible ways: First, Pav might transport membrane vesicles towards microtubule plus ends to supply membrane material needed during cellularisation. Second, the motor activity of Pav might provide a force to pull the growing membrane towards the centre of the embryo. Both models strengthen the idea that the control of microtubule associated transport is of high importance during cellularisation.

A process that allows investigation of the control of microtubule-associated transport during early embryogenesis is the transport of lipid droplets (Fig. 1.3). Lipid droplets are storage sites for energy, sterols and precursors of membrane phospholipids
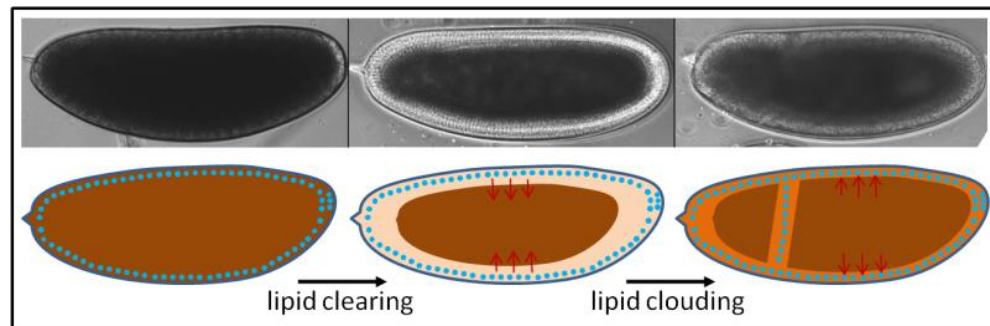
Fig. 1.3: Lipid droplet transport. Microscopic and schematic pictures of embryos during early development. Before lipid clearing the embryo is filled with light scattering lipid droplets. By lipid clearing the outer region is cleared of droplets and becomes translucent. The apical transport during lipid clouding restores the lipid droplets in the blastodermal cells. Red arrows show direction of transport.

(Welte, 2009). Because the lipid droplets scatter light this process can easily be monitored using bright field microscopy. Before cellularisation the droplets are localised throughout the embryo. At onset of cellularisation they are transported basally from the cortex into the centre of the embryo. This movement leads to the clearing of the outer embryonic region and is called lipid clearing. The reverse process, the so-called lipid clouding, occurs at the end of cellularisation. During lipid clouding the droplets are transported into the blastoderm cells, which thereby become dark again. This later phase of transport has been shown to be dependent on Dynein (Gross et al., 2000; Welte et al., 1998) while lipid clearing is solely Kinesin-dependent (Shubeita et al., 2008). The investigation of lipid droplet transport revealed molecular switches controlling the activity of Dynein and Kinesin motors that are simultaneously bound to lipid droplets. One gene being suggested to act as a switch for the direction of microtubule based transport is the nesprin 4 homolog *klarsicht* (*klar*) (Welte et al., 1998; Guo et al., 2005). *klar* mutants do show lipid clearing but no lipid clouding and the protein encoded by *klar* was found to interact with Kinesin-1 and cytoplasmic dynein (Yu and Welte 2010; unpublished). Therefore, Klar is suggested to affect the direction of the bidirectional transport of lipid droplets by physical interaction with the motor proteins. The movement of these droplets can be studied to identify novel

regulators of microtubule-associated transport. The mutant allele this thesis is based upon does show a lipid-clouding defect and therefore might offer new insights into the regulation of lipid droplet transport and Dynein function.

1.4. The cytoskeleton during early development

Directed transport of membrane material and proteins towards the outer membrane demands specific arrangements of the cytoskeleton. The correct regulation of microtubules and actin filaments has been shown to be essential for syncytial divisions and cellularisation. The organisation of the actin and microtubule networks during syncytial divisions and cellularisation is explained in the following sections.

1.4.1. Regulation of the cytoskeleton during syncytial divisions

During the syncytial cleavage cycles 10-14 the nuclei divide at the membrane. During the nuclear division the microtubules arrange as mitotic spindles surrounded by the pseudo-cleavage furrows (Fig. 1.4). The pseudo cleavage furrows are associated with actin filaments. These filaments are needed to shape the furrow and thereby create boundaries around the mitotic spindle. The mitotic spindle consists of microtubules originating from centrosomes which function as microtubule-organising centres (MTOCs). Microtubules are arranged in a bipolar manner. The microtubule ends at the MTOC are described as the minus ends while the plus ends of the microtubules are reaching into different intracellular regions. This organisation enables a classification into distinct microtubule subfamilies. The kinetochore microtubules associate with the chromosomes. Their function is needed to correctly align the chromosomes during

metaphase and to provide a scaffold for chromatid segregation in ana- and telophase. Interpolar microtubules build antiparallel bundles of microtubules that
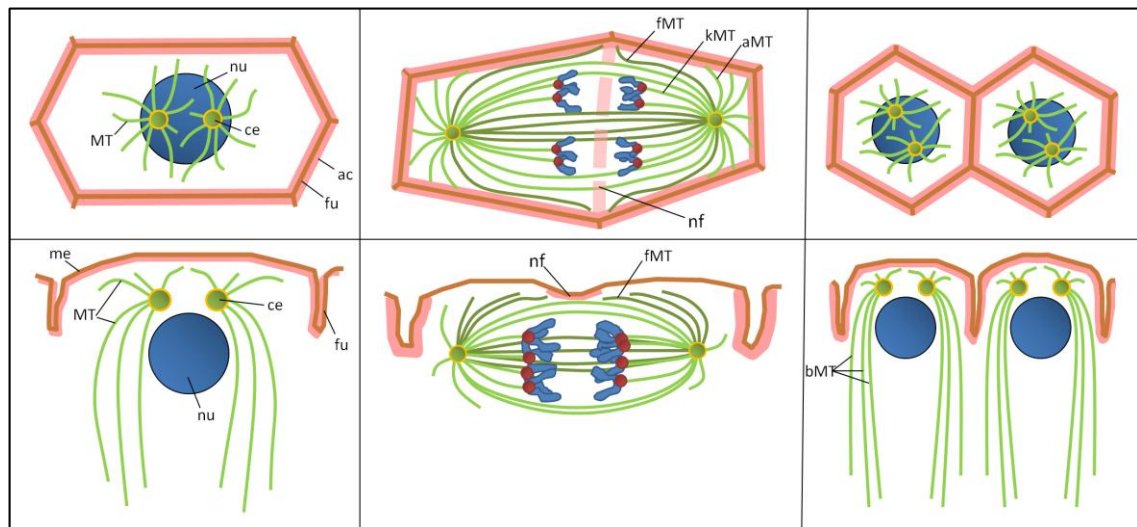
Fig. 1.4: Organisation of the cytoskeleton during syncytial divisions. The top panel shows an *en face* view on the surface of the embryo while the bottom panel represents a longitudinal section. Schematics are representing the cellular compartments before (left), during (middle) and after (right) a syncytial division. The microtubules are shown in green, the actin matrix is shown in pink. Membrane is shown in brown. Nuclei and compacted chromosomes are shown in blue. MT=microtubule, nu=nucleus, ce=centrosome, fu=membrane furrow, me=membrane,nf=new furrow, fMT=furrow MT, kMT=kinetochor MT, aMT=astral MT, bMT=basket MT.

reach from one centrosome to the other. Together with the kinetochore microtubules the interpolar microtubules define the elliptic shape of the mitotic spindle. Astral microtubules radiate from the spindle-opposing sides of the centrosomes. The plus ends of astral microtubules are thought to interact with the actin network at the cell cortex to aid in spindle orientation. The fourth subfamily of microtubules is first appearing in anaphase. The midzone microtubules are antiparallel microtubules in the centre of the spindle. These microtubules are bundled into a dense structure by plus-end directed kinesin motors and microtubule bundling proteins. An interesting class of microtubules are furrow microtubules (Albertson et al., 2008). The plus ends of the furrow microtubules are localised in close distance of the membrane that is going to form the membrane furrow. Furrow microtubules function in the recruitment of membrane vesicles and proteins to induce and shape the membrane furrow (Danilchik et al., 2003; Albertson et al., 2008).

Formation of novel pseudo cleavage furrows after the segregation of the chromosomes is necessary to separate the syncytial nuclei and prevent the formation of multinuclear cells. Depolymerisation of microtubules or actin leads to dissociation of the nuclei from the membrane and degradation of the pseudo-cleavage furrows (Foe et al., 1993; Schejter and Wieschaus, 1993). A likely model suggests that the microtubules are needed to deposit actin at the site of furrow formation. Correct deposition of actin and regulators of actin structure is needed for the formation of the furrows. In addition actin is needed to allow anchoring of basal and lateral polarity proteins (Foe et al., 2000). A major regulator of actin assembly and actin structure is the GTPase Rho1. Effectors of Rho1 are the ROCK (Rho-associated kinase – also see 5.1) and the formin Diaphanous (Dia). Interaction of Rho1 and ROCK leads to activation of myosin II, which regulates the contraction of actin fibres (Amano et al., 1996) while Dia has been implicated in stimulating actin fibre growth (Wallar and Alberts, 2003; Watanabe et al., 1999) and regulation of microtubule stability (Ishizaki et al., 2001; Palazzo et al., 2001; Wen et al., 2004). Inhibition of Rho1 activity prevents the arrangement of nuclei at the outer membrane and disrupts the localisation of myosin II at the furrow (Royou et al., 2004). In the early embryo Rho1 is activated by the GEF (GDP-GTP exchange factor) RhoGEF2. Mutations in RhoGEF2 lead to the loss of actin rich furrows during syncytial cleavage cycles (Grosshans et al., 2005; Padash Barmchi et al., 2005). In *Drosophila* S2 cells RhoGEF2 is associated with microtubule plus ends. This finding shows that the activation of Rho1 at the cortex might be regulated by the orientation of the microtubules and suggests a possible way to define the area where the furrow is initiated.

Also the Dystrophin-like protein Dah (discontinuous actin hexagon) is needed for assembly of the pseudo-cleavage furrow (Zhang et al., 1996; Cao et al., 2008). Dah has

been shown to bind to the membrane to anchor actin matrices. Recruitment of Dah to the furrow is dependent on the small GTPase Rab11 and its interactor Nuf (nuclear fallout). Rab11 and Nuf are needed for vesicle trafficking through the recycling endosome (Rothwell et al., 1999; Riggs et al., 2003; Riggs et al. 2007). In conclusion the position of the pseudo-cleavage furrow is defined by microtubule-associated transport of membrane material, actin and regulators of actin dynamics. After initiation of the furrow the actin network allows aggregation of polarity proteins.

1.4.2. Regulation of the cytoskeleton during cellularisation

While the syncytial divisions end in incomplete cytokinesis, cellularisation is often described as modified cytokinesis (Tepass and Tanentzapf, 2001; Mazumdar and Mazumdar, 2002). Although both processes show strong resemblance to cytokinesis syncytial divisions and cellularisation are regulated in very different ways. While the syncytial divisions are entirely controlled by maternally provided genes, cellularisation is dependent on zygotic gene transcription. A systematic screen for zygotic genes that regulate cellularisation revealed three genes called *nullo*, *serendipity-alpha* and *bottleneck* (Merrill et al., 1988; Wieschaus and Sweeton, 1988;). All of these genes were found to control the integrity of the actin cytoskeleton at the furrow canal (Rose and Wieschaus, 1992; Scheijter et al., 1992; Schweisguth et al., 1990; Scheijter and Wieschaus, 1993(2)). During cellularisation actin and myosin II aggregate at the furrow canal (Fig. 1.5). Therefore establishment of a contractile actin cytoskeleton was thought to drive cellularisation (for a review see Glotzer, 1997). Depolymerisation of actin fibres by injection of cytochalasin A inhibits cellularisation if the drug is injected before onset of cellularisation. Surprisingly, cytochalasin A injection during

cellularisation did not affect membrane growth and had only an effect on the contraction of the furrow canals at the end of cellularisation (Royou et al., 2004).
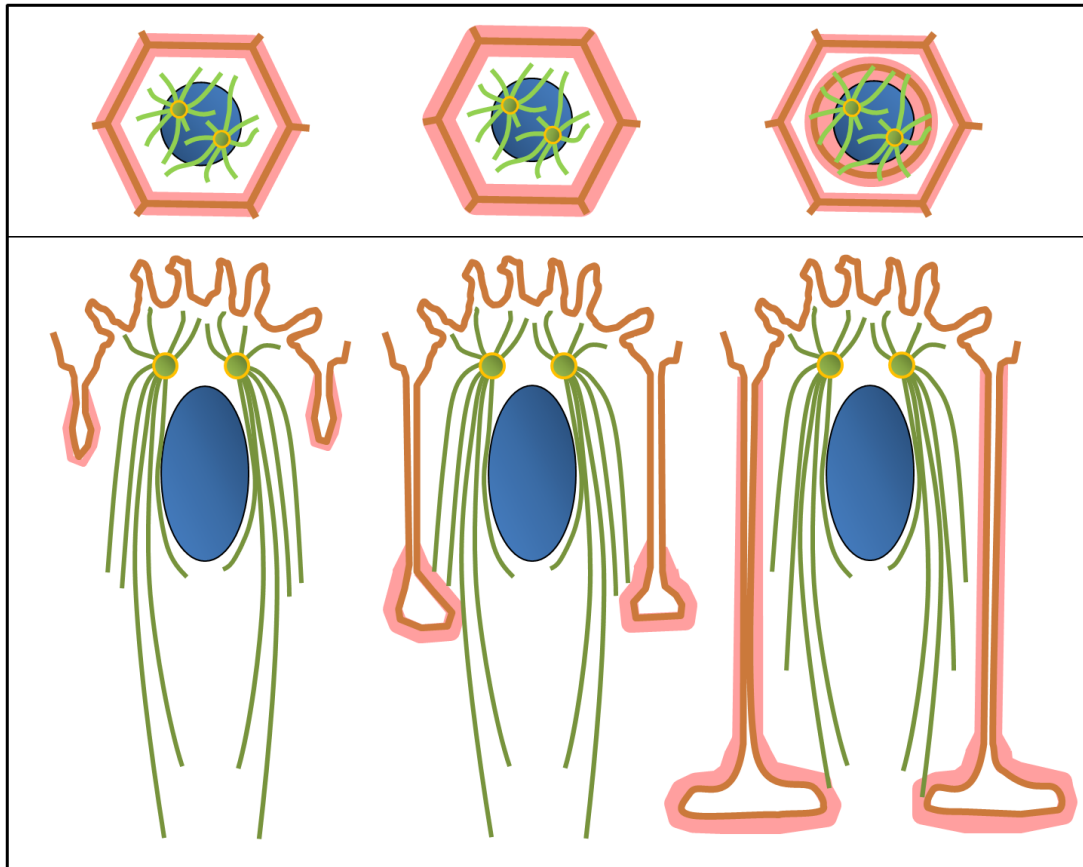
Fig. 1.5: Organisation of the cytoskeleton during cellularisation. The organisation of actin (red) and microtubules (green) is shown at onset (left), during the fast phase (middle) and at the end of cellularisation (right). Membrane with the apical villous projections is shown in brown. Top panel represents an *en face* view on the surface of the embryo while the bottom panel represents a longitudinal section.

These experiments showed that the actin cytoskeleton is needed for furrow initiation but not for the membrane growth during cellularisation. A more important role is understood for microtubules. During cellularisation two centrosomes are located between each nucleus and the membrane. Microtubules extend from the centrosomes towards the centre of the embryo and towards the outer membrane (Karr and Alberts, 1986; Webb et al., 2009). Thereby the microtubules build a scaffold that is polarised along the apico/basal axis of the cells and allows directed transport of internal membrane reservoirs and proteins. The microtubules might also provide directional cues for the membrane growth actively by exerting a force pushing the membrane and

forcing it inward (Foe et al., 1993; Sommi et al.; 2010) and passively by directing membrane insertion to specific sites. However, the way microtubules interact with the growing membrane is not understood.

1.5. Developmental defects caused by the *drop out* mutation

The *dop^1* mutation was created in an EMS (Ethylmethane Sulfonate) induced mutagenesis for maternal effect genes in the 71 C-F region on the left arm of chromosome 3 by Samuel Galewsky (Galewsky and Schulz, 1992). The maternal effect characteristics of the *dop^1* mutation indicate that the products of the associated gene are passed on from the mother to the embryo by deposition of maternal mRNA or protein into the egg. Embryos from *dop^1* homozygous mutant mothers (called *dop^1* embryos from here on) lack maternal contribution of this gene, which leads to defects in cellularisation. The developmental defects described for *dop^1* embryos are first
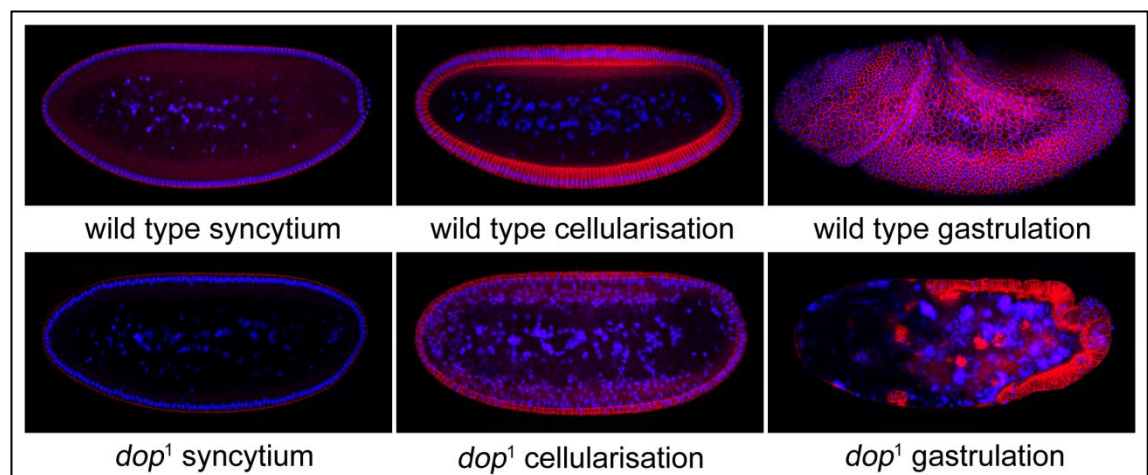
Fig. 1.6: Defects in *drop out* mat/zyg mutant embryos. Fixed embryos stained for nuclei (blue) and membrane (red). Mutants show normal syncytial division cycles but nuclei drop from the membrane at onset of cellularisation. Mutant embryos display varying percentages of nuclear drop out, leading to loss of blastoderm structures during gastrulation.

appearing during onset of cellularisation. Wild type embryos have a highly regular organisation during cellularisation. Their nuclei are aligned in a single row along the

outer membrane as they are enveloped with membrane. In dop^1 embryos nuclei detach from the membrane after onset of cellularisation. Furthermore, during slow phase of cellularisation the speed of membrane growth is strongly reduced while the fast phase of cellularisation is not affected. These defects lead to formation of a blastoderm with decreased depth, containing cells without nuclei or holes in the blastoderm (Fig. 1.6) (Meyer et al., 2006, Galewski and Schulz, 1992). Another dop^1 defect occurring during cellularisation is affecting the microtubule-associated transport of lipid droplets. Lipid droplets are transported in a bidirectional manner. Basal transport is dependent on Kinesin, while apical transport is dependent on cytoplasminc Dynein motor proteins. dop^1 embryos show basal transport of lipid droplets but no apical transport. These findings indicate that the defects in dop^1 embryos might derive from failure of Dynein dependent transport. The investigation of the molecular mechanism behind the defects of dop^1 mutants will reveal details of how membrane transport is regulated and how apico/basal polarity is established.

1.6. Aim of the study

The aim of this study is to gain novel insight into cellularisation and the formation of epithelial polarity. Due to the findings made during the ongoing project this thesis is split into two parts. The first part (chapter 3) investigates the relationship between *dop*[1] and the RNA silencing mediator Argonaute2 which has previously been suggested to be the gene associated with the *dop*[1] allele. The second part (chapter 4) describes the findings about the reasons for the developmental defects in *dop*[1] mutants. Genetic and biochemical methods as well as a detailed microscopic analysis are applied to examine the developmental mechanisms involved in the control of cellularisation.

Chapter 2: Material and Methods

2. Material and Methods

2.1. Material

2.1.1. Chemicals

The chemicals used in this work were acquired from the companies *Invitrogen* (Carlsbad, USA), *Sigma-Aldrich* (St. Louis, USA), New England Biolabs (Ipswich, USA), *Bio-Rad* (München, Germany), *Fluka* (Buchs, Switzerland), *GE Healthcare/Amersham* (Chalfont St. Giles, UK), *Fermentas* (St. Leon-Rot, Germany), and *Roche* (Mannheim, Germany) unless stated otherwise.

2.1.2. Oligonucleotides

Oligonucleotides were produced by the *Oligonucleotide Synthesis Service* (CLS Dundee, UK). A list of used olinucleotides is found in the supplemental material.

2.1.3. Cloning vectors

- pCR 2.1 TOPO TA (*Invitrogen*), 3.9 kb, Amp^R, Can^R

- pJet 1.2 (*Fermentas*), 2.9 kb, Amp^R

- pBluescript II KS+ (*Agilent Technologies*; Santa Clara, USA), 3 kb, Amp^R

- pUAST - expression vector for transgenesis (Brand and Perimon, 1993), 8.9 kb, Amp^R

- K10 UASP - expression vector for transgenesis (Koch et al., 2009), 9 kb, Amp^R

2.1.4. Antibodies

The antibodies used for Immunofluorescence (IF) and Western blot (WB) experiments

in this work are listed in Tab. 2.1.

Antibody	Dilution	Purpose	Reference
m-α-Neurotactin	1/10	IF	DSHB BP106
m-α-KlarM	1/50	IF	(Guo et al., 2005)
rb-α-βGal	1/500	IF	Promega
m-α-HA	1/1000	IF, WB	Roche 12CA5
rb-α-Slam	1/5000	IF	(Stein et al. 2002)
m-α-Dlg	1/500	IF	DSHB 4F3
rb-α-Baz (n-term)	1/5000, 1/10000	IF, WB	(Wodarz et al., 1999)
m-α-RhoA	1/50	IF	DSHB PID9
rb-α-DpatJ	1/1000	IF	(Richard et al., 2005)
-α-alphaTubulin	1/1000	IF, WB	DSHB 12G10
-α-betaTubulin	1/100	IF	DSHB E7
-α-Baz-pS151	1/200	WB	(Krahn et al., 2009)
-α-Baz-980	1/200	WB	(Krahn et al., 2009)
-α-Baz- S1085	1/200	WB	(Krahn et al., 2009)
m-α-DIC	1/2000	WB	Millipore MAB1618
rb-α-PTEN	1/1000	WB	(Wodarz et al., 1999)
m-α-Smaug	1/1000	WB	(Tadros et al., 2007)
rb-α-Dop1302	1/2000	WB	this work
rb-α-Dop1303	1/2000	WB	this work
rb-α-Dop1303 (purif.)	1/2000	WB	this work
rb-α-Dop2073	no affinity to antigen		this work
rb-α-Dop2074	1/8000 (?)	WB	this work
rb-α-Dop2074 (purif.)	1/20	WB	this work

Tab. 2.1: Antibodies

2.1.1. Fly lines

The fly lines used in this thesis are listed in Tab. 2.2. The fly lines were either derived

from one of the *Drosophila* stock collections in Bloomington (Indiana, USA), Szeged

(Hungary), Kyoto (Japan), from other *Drosophila* labs or created in the work shown

here.

Name	Genotype	Reference
Or R	standard laboratory wild-type strain	(Lindsley and Zimm, 1992)
w^{1118}	standard laboratory wild-type strain, w^-	(Lindsley and Zimm, 1992)
st e	$st^1\ e^1$	(Nüsslein-Vollhardt, 1986)
red e	$red^1\ e^1$	B #1662
Tai255.1	wild type strain	(Joly, 1987)
dop^1	w-, $dop^1\ st/\ TM3\ [ftz::lacZ]$	(Schreiber, 2003)
Df(3L)XG9	w^-; $Df(3L)XG9/\ TM3$	(Grosshans et al., 2003)
Df MR15	$Df(3L)EP3417^{MR15}/TM6$	Müller 1998
Df MR20	$Df(3L)EP1754^{MR20}$	Müller 1998
dop^{LH} alleles	div.	(Müller and Hauer, 2003)
Pl(3)s1754	$P\{lacW\}l(3)s1754^{s1754}$	(Spradling et al., 1999)
$ago2^{51B}$	$ago2^{51B}/\ ago2^{51B}$	(Xu et al., 2004)
$ago2^{321}$	$ago2^{321}/TM3$	this work
$ago2^{454}$	$ago2^{454}/TM3$	this work
Klc^{8ex94}	Klc^{8ex94},FRT/TM3	Gindhart et al., 1998
UAS::ago2	w^-; UAST::ago2/ UAST::ago2	(Schreiber, 2003)
mat15::GAL4	w^-; mat-tub::Gal4-VP16/ TM3	(Dawes-Hoang et al., 2005)
mat67::GAL4	w-; mat-tub::Gal4-VP16/ CyO	(Dawes-Hoang et al., 2005)
NGT::Gal4	Scer\GAL4$^{nos.PG}$	(Barrett et al., 1997)
GMR::Gal4, DIAP1^{RNAi}	*GMR::Gal4, symDIAP1^{RNAi}/ CyO*	(Huh et al., 2004)
ZH-attP-58A	$M\{vas\text{-}int.Dm\}ZH\text{-}2A$, $M\{3xP3\text{-}RFP.attP'\}ZH\text{-}58A$	(Bischof et al., 2007)
UAS::dop	w^-; UASP::dop$^{ZH\text{-}attP\text{-}58A}$	this work
UAS::dop-GFP	w^-; UASP::dop-GFP$^{ZH\text{-}attP\text{-}58A}$	this work
UAS::dop-HA	w^-; UASP::dop-HA$^{ZH\text{-}attP\text{-}58A}$	this work
UAS::dop$^{\Delta DUF}$-HA	w^-; UASP::dop-HA$^{ZH\text{-}attP\text{-}58A}$	this work
UAS::dop$^{\Delta Kinase}$-HA	w^-; UASP::dop-HA$^{ZH\text{-}attP\text{-}58A}$	this work
UAS::dop$^{\Delta PDZ}$-HA	w^-; UASP::dop-HA$^{ZH\text{-}attP\text{-}58A}$	this work
UAS::PDZ^{dop}-HA	w^-; UAST::PDZ^{dop}-HA	this work
UAS::DUF^{dop}-HA	w^-; UAST::DUF^{dop}-HA	this work
jupiter-GFP	$P\{PTT\text{-}un1\}Jupiter^{GFP}$	(Karpova et al., 2006)
UAS::baz-GFP	baz$^{Scer\backslash UAS.cSa.T:Avic\backslash GFP}$	(Sanchez-Soriano et al., 2005)
GFP-tubulin	*ubi:GFP-Tubulin-GFP/CyO*	J. Raff
DE-Cad-GFP	*ubi::DE-Cad-GFP;MKRS/TM6*	(Oda and Tsukita, 2001)

Tab. 2.2: used fly stocks

2.1.2. Commonly used buffers

- PBS: 137 mM NaCl, 2.7 mM KCl, 10 mM Na_2HPO_4, 1.76 mM KH_2PO_4, pH 7.4

- PBT: PBS, 0.05 % Tween 20

- TBE: 89 mM Tris, 8.9 mM Boric acid, 2 mM EDTA, pH 8.0

2.1.3. Instruments

- UV Spectrophotometer: Gene Quant II, *Pharmacia Biotech* (Cambridge, UK)

- Centrifuge *Heraeus* Instruments Biofuge fresco

- Centrifuge 5424 (*Eppendorf*)

- Master Cycler Gradient (*Eppendorf*)

- Consort EV202 Electrophoresis Power Supply (*Consort*)

- IPGphor Isoelectric Focusing System (*Amersham*)

- *Olympus* BX61 Microscope / Aquisition and Shutter Hubs *Improvision* / Orca ER Digital Camera *Hamamatsu*

- *Leica* Confocal SP2 / NeHe (Helium/Neon) laser

- IX81 Spinning disc confocal (*Olympus*), Yokogawa CSU-X1, CascadeII camera

2.1.4. Software

- Volocity Acquisition and Volocity Visualisation, *PerkinElmer* (Massachusetts, USA)

- ImageJ (Abramoff et al., 2004) and ImageJ Plugins: Multi measure (*Optinav*), Multi tracker by J. Kuhn (University of Texas at Austin), ImageJ Kymograph written by J. Rietdorf (FMI Basel) and A. Seitz (EMBL Heidelberg)

- Photoshop CS4, *Adobe* (San Jose, California)

- DNA STAR, *Lasergene* (Wisconsin, USA)

2.2. Methods

2.2.1. Methods for *Drosophila melanogaster*

2.2.1.1. Cultivation of *Drosophila*

Flies were kept on standard medium (356 g corn grist, 47.5 g soy flour, 84 g dry yeast, 225 g malt extract, 75 ml 10 % Nipagin, 22.5 ml propionic acid, 28 g agar, 200 g sugar beet molasses, 4.9 l dH2O) at 18°C, RT and 25°C. For egg collection, flies were kept on apple juice agar plates (40 g agar, 340 ml apple juice (100 %), 17 g sucrose, 30 ml Nipagin (10 %; 100 g Nipagin were dissolved in 1 l 70 % Ethanol) ad 1 l H2O), which were supplied with yeast for stimulation.

2.2.1.2. Hatching rate determination

Flies were placed on yeasted apple juice plates for 4 hours or overnight. The laid eggs were counted immediately. After 48 h the remaining embryos that did not hatch were counted and the hatching rate was determined by calculation of the percentage of hatched vs. unhatched embryos.

2.2.1.3. Creation of transgenic flies

Transgenic fly lines were produced by injection of transformation vectors into the germline of *Drosophila* embryos. This method is based on the integration of a transformation vector into the genomic DNA of the injected germ cells and subsequent crosses to raise individual flies carrying stable transgenes. The injection was performed by the company *Rainbow transgenic flies* (Camarillo, USA). Two distinct transgenesis

systems were used for the integration of vector DNA into the genome. A P-Element based approach was used to insert transgenes at random positions into the genome. Transformation vectors containing inverted repeats derived from transposable elements were injected together with a plasmid encoding a transposase gene. Transposase expression in the germline induces recombination of the inverted repeats with semi-random sites of the genome.

The insertion of the vector at random sites can affect the expression level of the transgene and make a comparison of the effects of different transgenes complicated. To create transgenic lines that are directly comparable to each other the attB/attP recombination system was used. This system relies on the PhiC31 integrase which is a serine-type recombinase that mediates the sequence-specific recombination between two largely different attachment sites, called *attB* and *attP*. The PhiC31 recombinase catalyses the recombination between the *attB* and *attP* sequences which leads to a change in the attachment site sequence. Recombined attachment sites are called *attR* and *attL* and are distinct from *attB* and *attP* sites; therefore the recombination reaction is unidirectional. This property of the *attB*/*attP* recombination system makes it significantly more effective than the conventional P-element based method. Transgenic flies carrying *attP* sites at known genomic positions were produced by Johannes Bischof (University of Zurich, Switzerland)(Bischof et al., 2007). In this work an *attP* line with an insertion at chromosomal localisation 58A on the second chromosome was used for the insertion of transgenes in an expression vector carrying *attB* sites.

2.2.1.4. Balancing of transgenic flies

Flies developing from embryos, which were injected during the transgenesis process, were crossed with balancer flies (*w⁻; If/CyO; MKRS/TM6*) to prevent chromosomal recombinations and gene loss. Transgene bearing flies were recognised by red eye colour and were crossed again with the balancer flies in single fly crosses in order establish the line and to identify on which chromosome the insertion occurred.

2.2.1.5. Creation of germ line clones

Embryos that lack the maternal contribution of a homozygous lethal gene can be produced by the induction of germ line clones. The FRT-FLP system was used to induce recombination in the germ line of heterozygous mutant females to create germ line mosaic clones that carry the Klc^{8ex94} mutation homozygously. To achieve this, the mutation of interest was combined with a Flipase recombination target (FRT) site in the proximal region of the chromosome. With the expression of a Flipase (FLP) enzyme the FRTs of metaphase chromosomes can be cleaved to create a mitotic cross over. If such a cross over occurs in a germ cell during development a possible result is the formation of homozygous mutant ovaries. The crosses shown in Fig. 3.1 were used to bring FLP and FRT sites together. After combining FLP and FRT the recombination was induced by two successive heat shock treatments of L3-larvae (1 h incubation at 37°C, 1 h at 25°C and again 1 h at 37°C). Exclusive collection of eggs derived from mutant clones was enabled by using an additional mutant allele. The ovo^{D} allele leads to dominant female sterility and the flies fail to produce eggs. Successful recombination can remove the ovo^{D} allele from the recombinant germ cell and allows the production of eggs for further analysis.
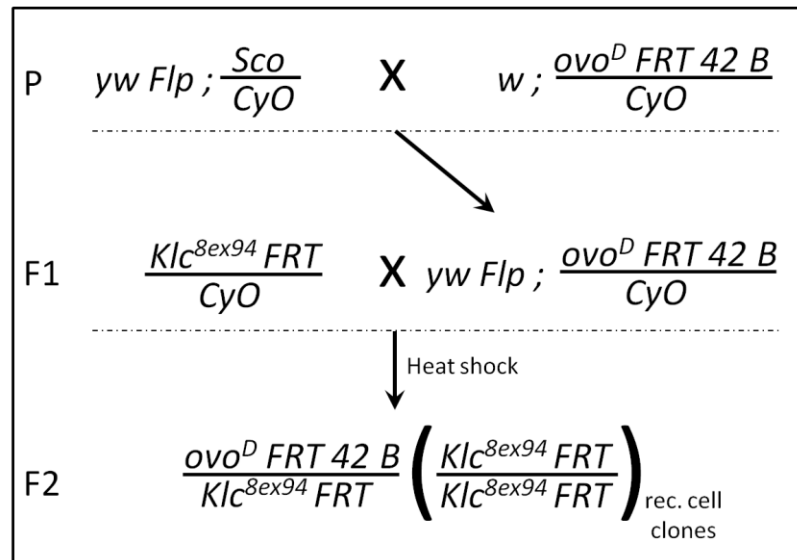
Fig. 2.3: Crosses performed for the creation of Klc mutant germ line clones. The in the first cross (P), female flies carrying the Flipase gene on the first chromosome were crossed with male flies harbouring the *ovo*^D mutation and the FRT site. Some flies originating from this cross carry FLP and FRT and the male flies with this genotype could be crossed against female flies carrying the Klc mutation (F1). The larvae hatching from this cross were subjected to 37 °C for two hours which elevates the Flipase activity. The hatching flies were collected and subjected to egg collection.

2.2.2. Methods for nucleic acid analysis

2.2.2.1. Preparation of genomic DNA from flies

A modified protocol of E. J. Rehm from the Berkeley Drosophila Genome Project (BDGP) was used to obtain genomic DNA: 30 flies were collected in a reaction tube and frozen in liquid nitrogen. 200 µl Buffer A (100 mM Tris-HCl, pH 7.5, 100 mM EDTA, 100 mM NaCl, 0.5 % SDS) were added. The flies were homogenised using the Bio-Vortexer (*Biospec Products*, Bartlesville, USA), additional 200 µl Buffer A were added and the homogenisation procedure was continued until only cuticle remained. The solution was incubated at 65°C for 30 min. 800 µl of a LiCl/KAcetate-solution (1 part of 5 M KAcetate and 2.5 parts of 6 M LiCl) were added and incubated on ice for at least 10 min. Afterwards the sample was centrifuged at 13000 rpm for 15 min at RT and the supernatant was transferred into a fresh reaction tube. The DNA was precipitated

adding 600 µl Isopropanol and spinning for 15 min at 13000 rpm at RT. The pellet was washed with 70 % Ethanol and then air dried. The DNA was resuspended in 150 µl H_2O.

2.2.2.2. Extraction of DNA for deficiency mapping

Embryos with a homozygous deficient genome were identified by X-Gal staining (*The little blue book*, Wilson et al., 1989) and collected. 5 embryos per genotype were collected, snap frozen in N_2 and crushed using a plastic pestle. Instantly, 50 µl of slurry containing Chelex beads (Biorad, part 143-3832, 100-200 mesh Chelex, sodium form) were added and the embryos were homogenised using the pestle. Afterwards the solution containing the DNA bound beads was boiled for 10 min and centrifuged to separate the supernatant from the beads. 1-5 µl of the supernatant were used per PCR reaction.

2.2.2.3. Isolation of RNA from embryos

RNA was extracted using Trizol reagent (Invitrogen). 50 µl of embryos at the desired age were collected and lysed in 600 µl Trizol. The lysate was centrifuged for 10 min, 12000 rpm at 4 °C. The supernatant was collected, incubated 5 min at room temperature and mixed with 100 µl Chloroform. The mixture was incubated for 2 min and subsequently centrifuged for 15 min. After centrifugation the RNA was precipitated from the aqueous phase by addition of 250 µl Isopropanol. The pellet was washed with 75 % EtOH and resuspended in RNAse free water.

2.2.2.4. **Polymerase chain reaction (PCR)**

For molecular cloning, DNA fragments were amplified from plasmid DNA or genomic DNA by PCR (Saiki et al., 1985). A standard reaction contained 10 pmol oligonucleotides and 10 – 100 ng template DNA and was performed according to the protocol of the manufacturer. The reaction volume was set to 50 µl in all reactions. Annealing temperature and amplification time of a standard PCR protocol are indicated in Table 2.4 and were adjusted according to the needs of the particular experiment.

	Duration	Temperature
Initial denaturation	3 min	95 °C
Denature	**50 sec**	**95 °C**
Anneal	**50 sec**	**55-60 °C**
Extend	**1 min per kb (*Taq*)**	**72 °C**
Cycle	36 times	
Final extension	10 min	72 °C

Table 2.4: Standard PCR program

2.2.2.5. **RT-PCR**

RT-PCR was carried out using the OneStep RT-PCR kit from *QIAGEN* (Hilden, Germany) according to the manufacturer's instructions. A standard RT-PCR reaction contained 1 µg RNA and 0.60 µM oligonucleotides specific for the gene of interest. Annealing temperature and amplification time of a standard RT-PCR protocol are indicated in Table 2.5 and were adjusted according to the needs of the particular experiment.

	Duration	Temperature
Reverse Transcription	30 min	45 °C
Initial activation	15 min	95 °C
Denature	**10 sec**	**95 °C**
Anneal	**1 min**	**55-60 °C**
Extend	**1 min per kb (*Taq*)**	**72 °C**
Cycle	20-40 times	
Final extension	10 min	72 °C

Tab. 2.5: standard RT-PCR program

2.2.2.6. Quantitative real time PCR

The template DNA for the PCR reaction was synthesised from 5 µg purified total RNA (DNAse treated) using Superscript II Reverse Transcriptase and random primers (*Invitrogen*). Qrt-PCR was conducted using 3 µl cDNA and primers specific for either *ago2*^{long} or *ago2*^{short}. The ribosomal protein gene *RpL32* was used as a control. To control pipetting errors three replicate PCR reactions per strain/gene were performed. The SYBR Green JumpStart Taq ReadyMix for QPCR (Sigma-Aldrich, Product #S4438) was used to set up the PCR reactions. Reactions were conducted and analysed on a BIO-RAD myIQ thermocycler using a standard 40-cycle protocol, and amplification products were verified via gel electrophoresis and melting curves.

2.2.2.7. Cultivation of *E. coli*

E. coli-strains were grown in Luria-Bertani medium (LB medium; 1 % Trypton, 0.5 % yeast extract, 1 % NaCl) at 37°C. For selective growth Ampicillin was added at a final concentration of 100 µg/ml. Kanamycin was used at a concentration of 50 µg/ml. Solid medium for LB plates contained 2 % agar.

2.2.2.8. Isolation of plasmid DNA from *E. coli*

For the purpose of cloning, sequencing and transformation of flies plasmid DNA was obtained using the Plasmid Plus Midi Kit (*Qiagen*, Hilden, Germany). The preparation was performed according to the manufacturer's protocol.

E. coli cultures were grown over night in 5 ml selective LB medium at 37°C. 1.5 ml of the overnight culture were sedimented by centrifugation at 13000 rpm for 1 min. The pellet was resuspended in 150 µl P1 buffer (50 mM Tris-HCl pH 8.0; 10 mM EDTA; 100 µg/ml RNaseA, stored at 4 °C). To lyse the cells, 150 µl of the buffer P2 (200 mM NaOH; 1 % SDS) were added, inverted and incubated for 5 min at RT. The reaction was stopped adding 150 µl of buffer P3 (3.0 M KAcetate pH 5.5). The samples were centrifuged for 10 min at 13000 rpm. The supernatant was transferred into a fresh reaction tube. The DNA was precipitated with 300 µl isopropanol and spun at 13000 rpm for 30 min. The pellet was then washed with 70 % Ethanol at 13000 rpm for 5 min. The pellet was air dried, resuspended in 30 µl H_2O and stored at -20°C until further use.

2.2.2.9. DNA restriction

For analytical restriction reactions, 0.5 µg DNA were digested with 1 – 2 units restriction enzyme (acquired from *Roche* and *NEB*) in a total volume of 30 µl at 37°C for 2 h. For cloning purposes this protocol was scaled up to 5 µg of DNA.

2.2.2.10. **Agarose gel electrophoresis**

For the analysis of DNA fragments 0.2 volumes of DNA sample buffer (30 % Glycerol, 0.25 % Bromphenol blue, 0.25 % Xylene cyanol) were added to the DNA solution. The DNA fragments were electrophoretically separated in a horizontal agarose gel (1 %) in TAE buffer (40 mM Tris-Acetate, 20 mM NaAcetate, 2 mM EDTA, pH 8.3) in the presence of Ethidiumbromide (0.5 µg/ml). DNA bands were detected with UV light (λ = 254 nm). The size of the DNA bands was estimated by comparing them with the standard Gene Ruler 1 kb ladder (*Fermentas*).

2.2.2.11. **Isolation of DNA fragments from agarose gels**

PCR products or DNA restriction samples were electrophoretically separated on an agarose gel. The corresponding band was excised using a scalpel and transferred into a reaction tube. To isolate the DNA fragments from the gel the Wizard SV Gel and PCR Clean-Up System from *Promega* (Madison, USA) was used according to the manufacturer's protocol.

2.2.2.12. **Ligation of DNA fragments**

Linearised DNA fragments were ligated in a reaction mixture (total volume 20 µl) containing 5 units T4-DNA-Ligase (*Fermentas*) and 1 to 10 µg/ml DNA at 16°C over night. The molar Vector/Insert DNA ratio was between 1:5 and 1:10. The correct DNA amounts were calculated via the formula shown in Tab. 2.6. The ligation reaction was incubated for 18 h and used immediately for transformation into *E. coli*.

$$\frac{100 \text{ ng }_{(vector)} \quad \times \quad X \text{ kB }_{(insert)}}{X \text{ kB }_{(vector)}} \times 5\text{-}10_{(exess)} = X \text{ ng }_{(insert)}$$

Tab. 2.6: Calculation of DNA insert amount for ligation reactions

2.2.2.13. Transformation of *E. coli*

E. coli aliquots stored at -80 °C were defrosted on ice. 1 - 5 µl DNA from ligation reactions or 10 ng of plasmid were added to 25 µl of *E. coli* suspension and incubated for 30 min on ice. After this heat shock was induced by transferring the vials in a water bath (45 sec at 42 °C). To cool the solution 800 µl LB medium were added with successive incubation at 37 °C for 1 hour. Finally, 200 µl of the transformation reaction were plated on selective medium (LB Amp) and incubated at 37 °C over night. If colonies grew over night they were isolated and used to inoculate 2 ml pre-cultures, which were later transferred into 50 ml LB cultures for large scale purification of the vector.

2.2.2.14. Colony PCR

To screen efficiently high numbers of transformed *E. coli* colonies after ligation and transfection of new constructs, colonies were touched with a pipette tip and partially transferred into a prepared PCR reaction by stirring the PCR mix with the tip. The remaining bacteria on the pipette tip were used to inoculate 2 ml liquid cultures. As a negative control one PCR reaction was stirred with a pipette tip that touched a region of the agar plate, which did not contains colonies.

2.2.2.15. **Plasmid rescue**

The genomic insertion site of *EP(3)3417* was determined using a cycle sequencing method developed by A. M. Huang and colleagues (Huang et al., 2000). DNA was extracted from flies carrying the P-element. 10 µl of the genomic DNA were digested with the restriction enzyme Sau3A for 2.5 hrs. The digested DNA was then incubated with T4 ligase over night (10 µl DNA, 40 µl 10x ligation buffer, 350 µl dH2O, 2 units ligase). After ligation the DNA was precipitated and resuspended in 150 µl TE buffer. 10 µl of the DNA were used for a PCR reaction with primers specific to the P-element (see supplementary material). The amplified DNA was separated by gel electrophoresis, purified and sequenced.

2.2.3. **Protein biochemical methods**

2.2.3.1. **Extraction of protein from embryos and adult flies**

Embryos collected from apple juice agar plates or 3 day old adult flies were filled in a reaction tube and snap frozen in liquid nitrogen. The embryos were dechorionised in 50 % commercial bleach prior to freezing. Using a plastic pestle the frozen tissues were fractured before they were covered with an amount of lysis buffer corresponding 5 -10 times of their volume. The thawing tissue was again briefly grinded with the pestle and then incubated for 30 min on ice. Thereafter, the lysate was centrifuged twice (10 min, 18000 rpm) to remove the insoluble fraction. The protein extract was immediately used for subsequent experiments or stored at -80 °C. Used lysis buffers are listed in Table 2.7. For extraction of phospho-proteins phosphatase inhibitors (*Roche*) were added. Purification of some proteins required adaption of the lysis protocol.

Triton-X buffer	NP-40 buffer	RIPA buffer
50 mM Tris-HCL pH 8.0 150 mM NaCl 1 % Triton-X (0.1 % β-Mercaptoethanol)	20 mM Tris-HCL pH 8.0 137 mM NaCl 10 % Glycerol 1 % NP-40 2 mM EDTA	50 mM Tris-HCL pH 8.0 150 mM NaCl 1 % NP-40 0.5 % Sodiumdeoxycholate 0.1 % SDS
Complete protease inhibitor cocktail (*Roche*) one tablet/10 ml freshly added before use		

Tab. 2.7: Lysis buffers

2.2.3.2. Protein estimation using Bradford reagent

0.5 – 2 µl protein extract were diluted with H_2O to a volume of 20 µl. 700 µl of room temperate Bradford reagent (*Sigma-Aldrich*) were added and mixed with the protein. The solution was transferred into plastic UV cuvettes and after 1-2 min the absorbance at 600 nm wavelength was measured in a photometer. The measured values were compared to a standardisation curve created from bovine serum albumin (BSA) dilutions with known concentration (40 µg, 20 µg, 10 µg, 5 µg, 2.5 µg in 20 µl).

2.2.3.3. Protein precipitation with TCA

To clean and concentrate protein extracts 1 volume of Trichloroacetic acid (TCA) stock solution (50 %) was added to 5 volumes of protein sample and incubated for 10 min on ice. The mixture was centrifuged at 14000 rpm for 5 min to collect the precipitate in a pellet. After removing the supernatant the pellet was washed three times with cold (stored at -20 °C) acetone with centrifugation in between the washing steps. After the last wash the acetone was driven off by placing the tube on the lab bench for 2-5 min.

Precipitated protein was either resolved in sample buffer (NuPage SB, *Invitrogen*) for gel loading or in rehydration solution for 2DGE (see below).

2.2.3.4. Protein estimation for 2D-PAGE

Extracted protein was precipitated using TCA and resolved in rehydration buffer. As the Rehydration buffer prevents readability of protein concentration using the Bradford protocol the 2-D Quant assay (GE Healthcare) was used. 5-10 µl of protein solution were precipitated and resolved in staining solution by following the manual of the assay. To control pipetting error and changes in precipitation efficiency the samples were measured in duplicates. The absorbance of each sample was measured in a photometer at 480 nm and compared to a BSA standard curve.

2.2.3.5. PAGE and Western blotting

Proteins were denatured in sample buffer with added 50 mM dithiothreitol (DTT) and loaded onto protein gels. Depending on the size of the investigated protein either 4-12 % Bis-Tris or 3-8 % Tris-Acetate precast acrylamide gels (*Invitrogen*) with the corresponding buffers (MOPS SDS running buffer or TA buffer respectively) were used. As a molecular weight marker protein ladders (PageRuler prestained protein ladder or Spectra high range multicolour ladder (*Fermentas*)) were used. The gels were run at 200 V for 45 min – 1 h. After the gel electrophoresis the acrylamide gels were transferred to a Whatman filter paper soaked in transfer buffer (10x stock: 288 g Glycine, 60.4 g Tris-Base in 2 l H_2O; 1x buffer: 1 volume 10x stock solution, 2 volumes

Methanol, 7 volumes H_2O). Gel sized sheets of polyvinylidene fluoride (PVDF) membrane were prepared in methanol and arranged on top of the acrylamide gel. Gel and membrane were sandwiched between Whatman filters and sponges soaked in transfer buffer. This assembly was placed in the blotting chamber filled with transfer buffer and the transfer was performed at 100 V for 60 – 120 min. The success of the protein transfer was checked by shaking the membrane in a solution containing Ponceau S (0.1 % Ponceau S in 5 % acetic acid). Antigen detection on the membrane was performed like shown in Tab 2.8. Afterwards the horseradish peroxidase (HRP) tag on secondary antibodies was detected by using ECL as a chemiluminescent substrate. The luminescence was detected using photographic film.

Step	Duration	Solution
Wash	1x 10 min	TBS
Block	2 h - over night	5 % milk powder in TBS
Primary antibody incubation	2 h	5 % milk powder in TBS+AB
Wash	3x 10 min	TBS
Secondary antibody incubation	2 h	5 % milk powder in TBS+AB
Wash	4x 15 min	TBS

Tab. 2.8: Antibody labelling

2.2.3.6.   2D-PAGE

25 µg of protein were solubilised in 125 µl Rehydration buffer (Tab. 2.9) by shaking the solution for 2 h at room temperature. After the solubilisation step the solution was transferred into the strip holders of the IPGphor apparatus. 7 cm long dried polyacrylamide gel strips (Immobiline DryStrip pH4-7, *GE Healthcare*) were cut to size and laid on top of the solution in the strip holder without covering bubbles that block the solution from touching the strip. The strip in the protein solution was covered with mineral oil and incubated for 18 h at 25 °C in the IPGphor apparatus. After the

rehydration the focussing program was set up to start the isoelectric focussing using 50 µA per strip and gradually increasing voltage (Tab. 2.10).

IPG Rehydration solution	
Ingredients	Amount (for 100 ml)
7 M Urea	42.04 g
2 M Thiourea	15.2 g
1.2 % CHAPS	1.2 g
0.25 % Ampholytes	0.25 ml
0.4 % ASB-14	0.4 g
43 mM DTT	0.66 g

Tab. 2.9: IEF Rehydration solution

Focussing program		
Step	Duration	Voltage
1 rehydration	18 h	0 V
2 run	1 h	100 V
3 run	1 h	500 V
4 run	1 h	1000 V
5 run	1 h	2000 V
6 run	1 h	4000 V
7 run	4 h	8000 V

Tab. 2.10: IEF focussing program

After the focussing the strips were removed from the strip holders, cleaned from the oil with a water stream and incubated in 2 ml SDS Equilibration buffer with moderate agitation (Tab. 2.11). Equilibration was performed in two steps each lasting for 10 min: first step Equilibration buffer + DTT (10 mg/ml); second step Equilibration buffer + iodoacetamide (25 mg/ml). Thereafter the strips were loaded onto an acrylamide gel (ZOOM gel, *Invitrogen*). To keep the gel strip fixed it was embedded in a agarose sealing solution (MOPS SDS running buffer, 0.5 % agarose, bromphenol blue). The following steps were conducted according to 2.2.3.5.

SDS Equilibration buffer	
Ingredients	Amount (for 200 ml)
50 mM Tris pH8.8	10 ml (of 1 M stock)
6M Urea	72.07
30 % Glycerol	60 ml
2 % SDS	4 g
Bromphenol blue	trace

Tab. 2.11: SDS Equilibration buffer

2.2.3.7. Phosphatase treatment of protein extract

Dephosphorylation of purified proteins was achieved by the use of Lambda protein phosphatase (*NEB*). In absence of phosphatase inhibitor 100 µg of protein were extracted using Triton-X lysis buffer. The dephosphorylation was prepared like stated in Tab. 2.12 and incubated at 30 °C for 30 min. In the following the protein was directly precipitated and continued to be processed following the 2DGE protocol. For the negative control the phosphatase was heat inactivated for one hour at 65 °C in the presence of 50 mM Na_2EDTA and then combined with 100 µg of protein prepared with phosphatase inhibitor cocktail.

Protein dephosphorylation	
Ingredient	Amount
Protein	25 µl
NEBuffer for Protein Metallophosphatases (10x)	5 µl
MnCl2 (10 mM)	5 µl
Phosphatase	5 µl
Protease Inhibitor (20x)	2.5 µl
H_2O	7.5 µl

Tab. 2.12: Protease treatment

2.2.3.8. Immunoaffinity purification

For pull-downs with GFP-Trap beads (Muyldermans et al., 2009; Rothbauer et al., 2008), embryos were lysed on ice with ice-cold Triton-X lysis buffer. The extract was incubated with 50 µl Sepharose beads coupled to protein G for preclearing for 30 min. A tabletop centrifuge was used to spin the beads down and the lysate was separated from the beads for incubation with 5 µl GFP-Trap beads (2 h at 4 °C). Afterwards the beads were washed with IP wash buffer (3x buffer 1, 3x buffer 2) and boiled in 1x loading dye.

IP wash buffer 1	IP wash buffer 2
50 mM Tris pH 7.4	50 mM Tris pH 7.4
270 mM Sucrose	270 mM Sucrose
1 % Triton-X	1 % Triton-X
150 NaCl	0.1 % Mercaptoethanol
0.1 % Mercaptoethanol	Protease Inhibitor
Protease Inhibitor	

Tab. 2.13: IP wash buffers

2.2.3.9. Production of peptide antibodies

Peptide antigens were synthesised and injected by Eurogentec (Southhampton, UK). The immunisation of Rabbits followed a three month program with four successive injections of antigen and four collections of serum (pre-immune, 1st bleed, 2nd bleed and final bleed). Antibodies were raised against antigens of Dop indicated in Tab. 2.14. Keyhole limpet haemocyanin (KLH) was conjugated to the injected peptides as a carrier.

Peptides	Rabbit No.
(1) MSRQEGAASRPADGAC and (2) ISTSTPQKNDEHQEQC	1303
	1304
(3) CPQPPKPTQLQPQKSM and (4) GRMSPYFRPRSRSLSS	2073
	2074

Tab. 2.14: Produced antibodies

2.2.3.10.   Sucrose gradient centrifugation

Embryos were homogenised in TKM buffer (50mM Tris pH7.4, 25 mM KCl, 5mM $MgCl_2$, protease inhibitor) containing 1M sucrose. The lysate was centrifuged through a sucrose gradient, and the lipid droplets at the surface were separated. The lipid droplet fraction was second subjected to an additional sucrose gradient centrifugation and the protein amount of the final fraction was determined. 0,5mg of each lysate were subjected to Western blotting procedures. Duplicate samples were processed for each type of embryo.

2.2.3.11.   RISC assembly assay

Protein was extracted from 0-4 h embryo collections using non-denaturising conditions. Wild type and mutant protein extracts were diluted to an equal protein concentration, frozen in liquid nitrogen and stored at -80 °C.

A master mix was prepared for the RISC assembly reaction (Tab. 2.15), which was mixed in a 1/1 ratio with a row of dilutions of embryonic extract (for example: 5 µl extract + 5 µl M.mix; 2.5 µl extract + 2.5 µl H2O + M.mix; 1.25 µl extract + 3.75 µl H2O + 5 µl M.mix...). The reactions were incubated for 1 h at 25 °C. Afterwards, the *in vitro* reaction mixtures were diluted with 10 µl of loading buffer (1x lysis buffer, 6% Ficoll 400), and part of the sample was analysed on a 3.9% (39:1 acrylamide-bisacrylamide) native acrylamide gel in 1xTBE buffer. The gels were dried and exposed to a autoradiography film over night at -80 °C.

RISC assembly Master Mix (2x)	
Ingredience (concentration)	Amount
Creatine Kinase (2 µg/ µl)	1.5 µl
Creatine Phosphate	5 µl
ATP (200 mM)	1 µl
DTT (1 M)	0.5 µl
RNAsine (20 U/µl)	0.5 µl
Glycerol	10 µl
Lysis buffer (5x)	10 µl
H_2O	11.5 µl
siRNA*	10 µl

Tab. 2.15: RISC assembly master mix

2.2.4. Fixation of embryos

2.2.4.1. Heat fixation

Embryos were dechorionated using 6.5 % NaOCl and transferred to a scintillation vial containing boiling 2 ml Triton-X Salt solution (3 ml Triton X-100, 40 g NaCl, ad 1 l with H_2O). The embryos were shortly incubated and then immediately cooled by adding 10 - 15 ml cold salt solution. The scintillation vial was kept on ice for some minutes. The salt solution was discarded and replaced by heptane and methanol. By vigorous shaking the vitelline membrane of the embryos was removed. Embryos were transferred to a reaction tube and washed twice with methanol. The embryos were stored at -20 °C in methanol.

2.2.4.2. Formaldehyde fixation

Embryos of the desired age were collected from yeasted apple juice plates and dechorionated using 50 % commercial bleach. The embryos were rinsed and transferred to a scintillation vial containing 4 ml fixative (4 % formaldehyde in PBS) and 4 ml heptane. The embryos were incubated for 25 min under agitation. The lower

phase was discarded and 4 ml methanol was added. By vigorous shaking the vitelline membrane of the embryos was removed. Embryos were transferred to a reaction tube and washed twice with methanol. The embryos were stored at -20 °C in methanol for at least one day before continuing of the staining protocol.

2.2.4.3. In vivo organelle fractionation

Separation of embryo organelles by centrifugation in vivo was performed after a protocol of Michael Welte (Tran and Welte, 2010). Flies aged between 3-5 days were transferred into an egg collection chamber and eggs were collected for one hour at 25 °C. The embryos were dechorionated in 50 % commercial bleach and transferred into a 1.5 ml reaction tube containing 1 ml buffer (0.4 % NaCl, 0.03 % TritonX-100). The embryos were centrifuged for 10 min at 1250 rpm. Centrifuged embryos were immediately subjected to heat fixation.

2.2.4.4. Immunofluorescence

Indirect immunofluorescence was used exclusively for detection of proteins in fixed embryos. All steps were performed under agitation. The fixed embryos were washed three times with PBT for 20 min each. Unspecific binding sites were saturated by blocking with blocking solution (10 % normal horse serum in PBT) for 45 min at RT. The incubation with the primary antibody followed in blocking solution at 4 °C over night. The following day, the embryos were washed three times with PBT for 20 min and incubated with a fluorescently labelled secondary antibody in blocking solution for 2 h

at RT. DAPI (1/1000 from a 1 mg/ml stock solution) was added at this step. After three washing steps with PBT for 20 min each, embryos were embedded in Mowiol containing DABCO to prevent bleaching of fluorescence during confocal microscopy.

2.2.4.5. Life imaging

Embryos were collected on apple juice plates and dechorionated chemically using 50 % bleach or manually using forceps. Embryos of the desired developmental stage were selected and placed on a glass cover slip covered with glue (scotch tape dissolved in Heptane). The embryos were covered with halocarbon oil (*Sigma*) and the cover slip was mounted on a glass slide using two cover slips as spacer to prevent squeezing the embryo. Embryos mounted this way develop normally and were imaged using bright field microscopy as well as confocal scanning microscopy.

Chapter III - Results Part I:

The *dop* mutation as an allele of *argonaute2*

3.1. Introduction of Part I

Previous complementation and genomic sequencing experiments showed that dop^1 is an allele of the *argonaute2* (*ago2*) gene (Meyer et al. 2006). The Ago2 protein provides important functions to the RNA silencing pathway. RNA silencing is the targeted destruction of RNA to suppress gene expression. To date the role of Ago2 for early embryonic development is not well understood. A process involving RNA silencing that is essential for early development and might be affected in dop^1 mutants is the maternal-to-zygotic transition.

3.1.1. Argonaute dependent RNA silencing in *Drosophila*

RNA silencing is a mechanism to negatively regulate gene expression by destruction or translational repression of messenger RNA (mRNA) and other RNA species (Baulcombe, 1999; Fire et al., 1998). The RNA silencing machinery is directed by short double stranded RNA (dsRNA) molecules complementary to the target RNA. Argonaute proteins are the key protein component of this machinery.

The molecular pathway of RNA silencing is activated by dsRNA molecules and their processing into molecules with the length of 21-23 nucleotides. This trimming process is catalysed by multi-domain RNAse III-like Dicer proteins which bind to the RNA by interaction with RNA binding proteins (Bernstein et al., 2001). After processing of the RNA the Dicer protein interacts with the Argonaute containing RISC (RNA induced silencing complex) to form the RISC-loading complex. Argonaute proteins have been shown to be capable of catalysing all of the following steps of the silencing process (Rivas et al., 2005). First Argonaute binds to the dsRNA, which leads to separation of

the passenger strand and the guide strand. The guide strand contains the complementary sequence of the target RNA and stays within the RISC while the passenger strand is degraded. Argonaute protein "armed" with the guide strand is then able to dissociate from the protein complex and eventually bind to the target mRNA. The target mRNA is degraded by Argonaute via a single endo-nucleolytic cleavage event known as slicing (Liu et al., 2004; Meister et al., 2004; Rand et al., 2004; Rivas et al., 2005; Song et al., 2004; Okamura et al., 2004). In addition Argonaute proteins can interfere with translation by shortening the poly(A) tail of mRNA targets or inhibition of ribosomes (Iwasaki et al., 2009;Iwasaki and Tomari, 2009; Miyoshi et al., 2005).

The *Drosophila* genome encodes five characterised Argonaute proteins: Ago1, Ago2, Ago3, Piwi and Aubergine (Carmell et al., 2002; Li et al., 2009; Kataoka et al., 2001; Williams and Rubin, 2002). The functional domains of Argonaute family proteins are conserved PAZ and PIWI domains. The PAZ (PIWI/Argonaute/Zwille) domain contains a nucleic acid binding pocket with high affinity to 3' ends of single and double stranded RNA (Lingel et al., 2003; Ma et al., 2004; Song et al., 2003; Yan et al., 2003). The PIWI domain has RNAse-H homology and catalyses the slicing activity (Liu et al., 2004; Meister et al., 2004; Song et al., 2004). In addition to the broadly conserved PAZ and PIWI domains *Drosophila* Ago2 carries an extended amino-terminal region of 397 amino acids containing two sets of imperfect glutamine rich repeats (GRR1 and GRR2). The GRRs are only found in insects and their function is unknown (Meyer et al., 2006; Hain et al., submitted). Functional studies using mutants of Ago1 and Ago2 showed that these proteins act in two separate silencing pathways (Fig. 3.1).
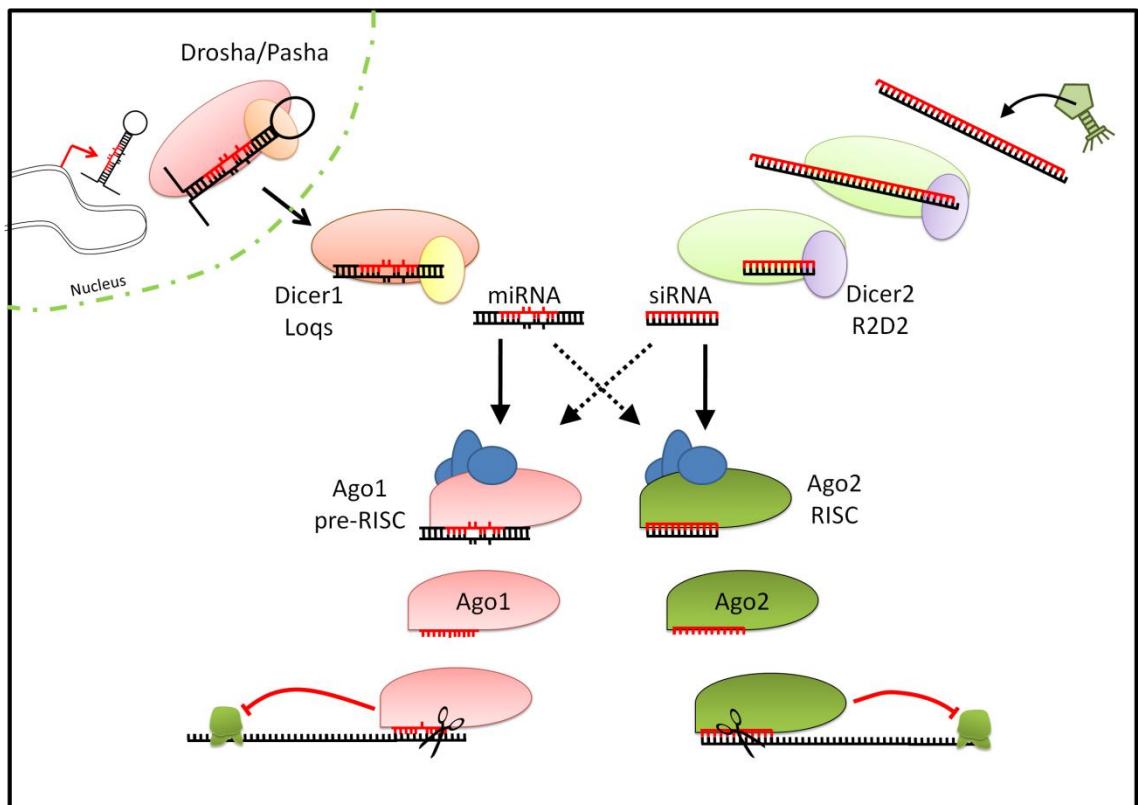
Fig. 3.1: RNA silencing pathways in *Drosophila*. Two distinct pathways mediate miRNA and siRNA dependent silencing. miRNAs are expressed from genomic sequences. They are pre-processed in the nucleus by the Drosha/Pasha proteins and exported by Exportin-5. The loop structure is cleaved by Dicer1/Loqs. The processed miRNA is then handed over to the Ago1 RISC. After passenger strand elimination Ago1 can bind to target mRNA and trigger degradation or translational repression. The siRNA pathway is triggered by viral or external RNA fragments that are processed by Dicer2/R2D2. Processed siRNAs are loaded into the Ago2/RISC which can cleave target RNAs. Depending on the structure of the RNA duplex structure miRNAs and siRNAs can be sorted into the neighbouring pathway.

The micro RNA (miRNA) mediated silencing pathway is directed by Ago1. Ago1 mediated silencing regulates developmental processes. miRNA precursor molecules are transcribed from miRNA genes in the genome by the RNA polymerase II to regulate gene expression by degradation of mRNAs. Mutations affecting components of the miRNA mediated silencing pathway such as *dicer1* and *ago1* are homozygous lethal (Kataoka et al., 2001; Lee et al., 2004) and miRNA genes have been identified that have specific targets to control early embryonic development (Leaman et al., 2005).

In contrast, a role for the small interfering RNA (siRNA) directed pathway in development has not been sufficiently established. The siRNA pathway is conducted by Ago2. siRNAs are double stranded RNAs that are not directly expressed by the

genome. siRNAs either derive from viruses or selfish DNA elements like retro-transposons. Disruption of siRNA directed silencing in flies by mutations in *dicer2* or *ago2* results in poor viral defence and only weakly affects overall viability and fertility (Lee et al., 2004; Okamura et al., 2004; Xu et al., 2004). Embryos with various defects during the syncytial division cycles are reported for *ago2* mutants but these defects show a very low penetrance (Deshpande et al. 2005). Because of the low penetrance of these developmental phenotypes it is widely believed that *ago2* does not regulate major developmental steps in *Drosophila*.

Despite of the lack of a lethal phenotype indications for a developmental function of *ago2* are given. The first indication is the interaction of Ago1- and Ago2-dependent signalling pathways. Experiments using labelled miRNA showed that miRNAs can be loaded onto Ago2 depending on their structure. miRNAs usually contain several base mismatches between guide and passenger strand as well as between guide strand and the target RNA. miRNA structures with mismatches are preferentially bound by Ago1 while miRNAs with no mismatches are bound by Ago2. Because of this sorting mechanism a small number of miRNAs is found associated to Ago2 (Förstermann et al., 2007; Tomari et al., 2007; Ghildiyal et al., 2010). A direct interaction between Ago1 and Ago2 was suggested by co-immunoprecipitation experiments. Precipitation of Ago2 from embryonic extracts using an Ago2 antibody co-purified Ago1 indicating that Ago1 and Ago2 might be present in a single protein complex (Meyer et al., 2006). In conclusion Ago2 might at least have a minor or very specific role in the miRNA silencing pathway that is regulating developmental processes.

The second and most interesting evidence that Ago2 has functions in development that have not been revealed so far is the fact that *ago2* alleles, published as null

alleles, retain expression of an *ago2* isoform (preliminary data from W. Meyer). The *ago2* gene expresses two annotated isoforms *ago2*-RB and *ago2*-RC (Fig. 3.2). The expressed proteins Ago2-PB and Ago2-PC only differ in the amino-terminal 6-9 amino acids. Because of the high similarity of Ago2-PB and Ago2-PC they are termed Ago2^{long} in this work. Two apparent null alleles of *ago2* were published, called *ago2*^{51B} and *ago2*^{414} (Okamura et al., 2004; Xu et al., 2004). These alleles were independently created by imprecise excision of the transposon *EP(3L)3417* and both contain genomic deficiencies that delete the first two exons of *ago2*-RB and the first exon of *ago2*-RC (Fig. 3.2). Reverse transcriptase PCR using primers located in the first two exons showed no expression of the *ago2*^{long} isoforms in
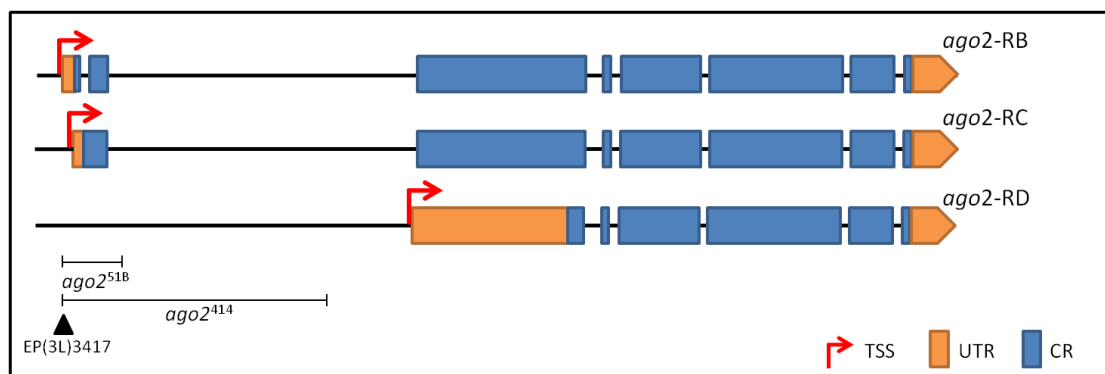
Fig. 3.2: Different transcripts of *ago2* in *Drosophila*. Intron-exon structure of the two *ago2*^{long} and the *ago2*^{short} transcripts. Transcriptional start sites (TSS) are marked by red arrows, exons in blue, untranslated regions (UTR) in orange. The published null alleles delete the first exons and intronic sequence (marked by bars). The mutants were created by imprecise excision of the *EP(3L)3417* element inserted in the 5`UTR of *ago2* (black triangle).

these mutants. However, RT-PCR with primers binding in exons 3 and 7 and northern blotting experiments with a probe binding exons 3-7 showed that a short fragment is still transcribed in these mutants. Analysis of the genomic sequence of the *ago2* locus showed an additional TSS located upstream of the third exon. This TSS might control expression of a so far uncharacterised isoform of *ago2* termed *ago2*-RD or *ago2*^{short} (Meyer, 2007). The short isoform of *ago2* includes the functional PAZ and PIWI

domains and has high similarity to mammalian Ago2. Therefore Ago2[short] might represent a fully functional member of the Argonaute family. The expression of the *ago2*[short] isoform in the published null alleles renders these mutations hypomorphic. In conclusion it seems plausible that *ago2*[51B] and *ago2*[414] do not display penetrant developmental defects as the developmental function of *ago2* is sustained by *ago2*[short].

3.1.2. Evidence for *dop*[1] affecting *ago2* function

dop[1] maternal zygotic mutant embryos display severe developmental defects that lead to failure of blastoderm formation. More recently, the *dop*[1] allele was identified as an allele of the *ago2* gene (Meyer et al., 2006). The methods used to map the *dop*[1] allele to *ago2* included deficiency mapping and transgene complementation experiments. Genomic sequencing of *ago2* in *dop*[1] mutants revealed a molecular aberration affecting the number of amino-terminal glutamine rich repeats (GRRs) of Ago2. Whether this variation on GRR pattern affects the biological function of Ago2 has remained elusive.

The annotated wild type sequence of Ago2 contains 4 repeats of GRR1 and 11 repeats of GRR2 (Fig. 3.3). *dop*[1] mutants carry 4 GRR1 repeats and 10 GRR2 repeats suggesting that the molecular lesion in *dop*[1] results in the loss of one GRR2 repeat (Meyer et al., 2006). Analysis of the *dop*[1] non-complementing allele *dop*[46] supported the GRR hypothesis. *dop*[46] was independently created by transposase-induced imprecise excision of the *EP(3L)3417* P-element which is located in the 5`UTR of *ago2.* Genomic sequencing showed that *dop*[46] mutants have lost one repeat of the GRR1 region; resulting in a 3 GRR1/ 11 GRR2 pattern. Expression of an *ago2* transgene containing

the wild type GRR combination in dop^1 or dop^{46} embryos results in a partial complementation of the severe developmental defects. Therefore, it was suggested that a change in GRR numbers is responsible for the developmental defects.
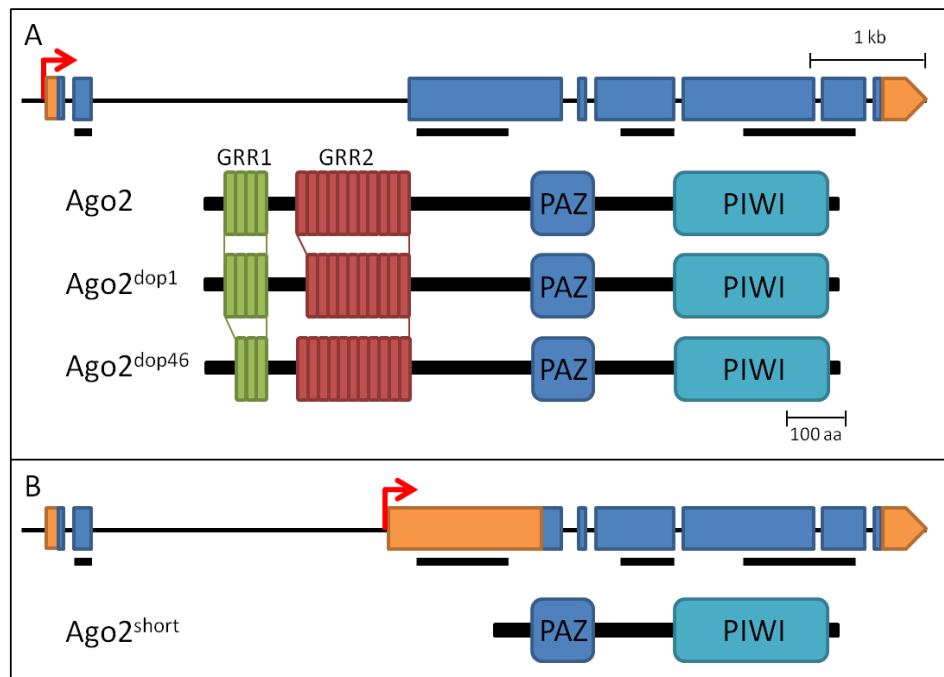
Fig. 3.3: Domain organisation of wild type and mutant Ago2 isoforms. The genomic coding regions for the $ago2^{full\ length}$ (A) and $ago2^{short}$ (B) isoforms are displayed. Regions coding for the GRRs, the PAZ and the PIWI domain are marked by black bars, untranslated region is marked orange and transcriptional start sites are indicated by red arrows. The schematics of the $Ago2^{long}$ isoforms encoded by wild type and *dop* mutant *ago2* are shown below the coding regions. Wild type Ago2 contains an amino-terminal half with the GRRs and a carboxy-terminal half with the functional PAZ and PIWI domains. The wild type gene encodes 4 copies of GRR1 and 11 copies of GRR2. The proteins encoded by dop^1 and dop^{46} fly lines contain 4xGRR1/10xGRR2 and 3xGRR1/11xGRR2 respectively.

The phenotype induced by the dop^1 allele is significantly stronger than the phenotype induced by the deficiencies in $ago2^{51B}$ and $ago2^{414}$ mutants. This finding indicates that variations in GRR number might disrupt *ago2* function more severely than the deficiency alleles. In order to understand the genetic relationship between dop^1 and the deficiency alleles one has to take into account the isoforms expressed in the different alleles. $ago2^{51B}$ and $ago2^{414}$ mutant embryos express only the short isoform of *ago2* while the dop^1 allele expresses the short isoform and the long isoform including the GRR variation. Complementation experiments showed that dop^1 is complemented by the *ago2* deficiencies and it was suggested that the expression of

the short isoforms can rescue *dop*[1] mutant embryos. Furthermore the experiments were interpreted to show that the GRR variation of the long isoform in *dop*[1] embryos affects the function of the short isoform (Meyer, 2007). To prove this model genetically, alleles are needed that are deficient for both isoforms of *ago2*. Such *ago2* null mutant alleles would also allow the investigation of the full function of *ago2* during development. A possible role for *ago2* during early embryonic development is the execution of RNA destabilisation during the maternal-to-zygotic transition.

3.1.3. The maternal-to-zygotic transition

During the first hours of development embryonic cells often go through rapid cell cycles without extended interphases. During these cell cycles the embryonic genome remains transcriptionally inactive and most mRNAs and proteins are provided by the mother. Gene expression profiling showed that approximately 65% of all *Drosophila* genes are maternally provided to the oocyte (Lecuyer et al., 2007; Tadros et al., 2007). The dependency on maternal transcripts lasts only until the zygotic gene expression of the embryo genome is activated and maternal transcripts are actively degraded. This maternal-to-zygotic transition (MZT) has been studied in model organisms including echinoderms, nematodes, insects, fish, amphibians and mammals (reviewed in Tadros and Lipshitz, 2005). Most changes in the ratio of maternal/zygotic mRNA occur during the 14th cell cycle in *Drosophila*. MZT occurs in two inseparable processes: transcriptional activation and destruction of maternal mRNAs (Newport and Kirschner 1982(1) and (2); Wieschaus 1996; Bashirullah et al., 2001; De Renzis et al., 2007). Genome activation appears to rely in part on the sequestration of transcriptional repressors by the exponentially increasing amount of DNA during cleavage divisions

and on changes in the nucleocytoplasmic ratio (Grosshans et al., 2003; McCleland et al. 2009; Lu et al., 2009). The first process dependent on zygotic gene expression is cellularisation (Edgar et al., 1986; Merrill et al., 1988; Sibon et al., 1997). One of the first zygotic genes expressed is the zinc-finger protein Zelda, which is necessary for transcriptional activation of many early transcribed genes. Loss of Zelda function causes defects in cell division and cellularisation (Liang et al., 2008; Harrison et al., 2010).

At least two separate pathways have been identified that act in concert to conduct transcript destruction during MZT. The first pathway is maternally encoded and driven by the RNA binding protein Smaug (Tadros et al. 2007(2)). Smaug is a major regulator of maternal mRNA destabilization in *Drosophila* as it is essential for the destruction of maternal transcripts (Tadros and Lipshitz, 2005). Over 20% of the maternal mRNAs regulated during MZT are destroyed in a Smaug dependent fashion. Smaug binds to maternal transcripts that contain a cis-element called SMG recognition element (Smibert et al., 1996). This leads to the recruitment of the CCR4/POP2/NOT-deadenylase complex, prompting the cleavage of the poly(A) tail (Semotok et al., 2005; Semotok et al., 2008). Recent studies of Smaug function during early embryonic development showed an involvement in the control of the syncytial cell divisions and membrane growth during cellularisation (Benoit et al., 2009). The second pathway is activated two hours after fertilisation and is driven by the zygotic expression of double stranded RNAs (Bashirullah et al,. 1999; Tadros et al., 2003; Bushati et al., 2008). The zygotic expression of miRNAs in early embryos can target the destruction of maternal mRNAs during MZT (Giraldez et al., 2006; Tang et al., 2007; Bushati et al., 2008). Loss of zygotic RNA silencing functions leads to stabilisation of 15% of the maternal mRNAs during MZT (De Renzis et al., 2007). However, to date there are no studies

demonstrating the involvement of Argonaute proteins in MZT in *Drosophila*. So far, Ago2 was shown to be involved in MZT in mouse and zebrafish (Lykke-Andersen et al., 2008; Giraldez et al., 2006). In mice, knockdown of Ago2 leads to a developmental arrest of the 2-cell stage embryo and a microarray analysis comparing the arrested embryos with wild type 2-cell embryos shows a set of maternal RNAs that were stabilised upon knock down of Ago2. Furthermore, the authors describe failure in the induction of zygotic gene expression in the arrested embryos suggesting a tight interaction of transcript destruction and genome activation (Lykke-Andersen et al., 2008).

Mutations in *Drosophila ago2* have been studied using the *ago2*[414] and *ago2*[51B] alleles. These deficiencies show no defects in cellularisation. However, these alleles do not remove all *ago2* isoforms and the remaining expression of the *ago2*[short] isoform might cover severe developmental defects. Investigation of true *ago2* null alleles is therefore required to reveal further functions of the miRNA directed control of MZT.

3.2 **Results of Part I**

3.2.1. Variation of Ago2 GRR numbers does not affect development or RNA silencing

Results from previous studies suggested that a variation of Ago2 GRR numbers can interfere with Argonaute2 functions. In addition to the conserved carboxy-terminal region *Drosophila* Ago2 harbours an unusual amino-terminal region, which contains high numbers of glutamine residues (ca. 30%) arranged in imperfect repeats. These repeats can be divided in two groups of glutamine-rich repeats (GRR) called GRR1 (6 amino acid imperfect repeat) and GRR2 (23 amino acid imperfect repeat). The amino-terminal region containing the GRRs is not conserved in mammalian homologues and its function is unknown. Genomic sequencing of the *ago*2 gene in *dop*[1] mutants revealed a reduction of one GRR2 repeat. Analysis of *dop*[46], a *dop*[1] non-complementing allele, showed loss of one GRR1 repeat (Meyer et al., 2006).

To search for effects of GRR number variations in relation to cellularisation defects the number of repeats in wild type and mutant fly strains was assessed. This analysis revealed a large variation in the pattern of GRRs (Table 4.1). In agreement with the previously published data a reduction of GRR2 number from 11 to 10 was found in *dop*[1] mutant flies compared to their progenitor strain *red e*. Other mutations were analysed for changes in GRR number. The *dop*[LH5] allele was produced by EMS mutagenesis of the scarlet/ebony (*st e*) wild type line and does not complement *dop*[1] (Hauer and Mueller, unpublished). *dop*[LH5] flies carry 3 GRR1 and 11 GRR2. This combination was also found in *dop*[46]. Strikingly, analysis of *st e* flies, the precursor strain of *dop*[LH5], showed the same number of repeats as found in *dop*[LH5] showing that the GRR combination in *dop*[LH5] did not result from the mutagenesis process. As *st e*

flies cellularise normally this finding indicates that the combination of 3 GRR1 and 11 GRR2 (3/11) is unlikely to cause the cellularisation phenotype. Also this finding suggests that there has to be another genomic aberration affecting dop^{LH5} and dop^{46} mutants. Complete sequencing of the *ago*2 locus in dop^{LH5} and dop^{46} flies did not show any other mutations (results not shown).

Line	GRR1 (6AA)	GRR2 (23 AA)	Maternal embryonic lethal
"wild type" project	4	11	
red e	4	11	
dop1	4	10	✓
st e	3	11	
dopLH5	3	11	✓
dop46	3	11	✓
3CPA120	2	13	
3CPA103	3	10	
3CPA54	3	11	
3CPA35	3	13	
3CPA122	4	11	
Ln(1)AB	4	11	
w-14 melbourne	4	11	
Tai255.1	3	11	
OreR*	4	13	
OreR**	3	16	
TM6B	4	12	

Tab. 4.1: Copy numbers of GRR repeats in different wild type strains and *dop* mutant fly lines. Numbers of repeats were analysed by PCR and subsequent sequencing. Reductions of repeat numbers are found in dop^{1} (progenitor strain *red e*) and dop^{46} (marked by asterisk). No variation of GRR repeats occurred in the production of the dop^{LH5} allele from the *st e* fly strain. The lines *3CPA120* to *TM6B* have been characterised by Brian Bettencourt. *3CPA* strains are derived from isolated flies caught from free living *Drosophila melanogaster* populations in North America. The other fly lines are widely used laboratory stocks. Note the repeat variation in a fly line that was kept in two different labs (*OreR** and *OreR***).

An analysis of naturally occurring changes in GRR pattern was done in collaboration with Brian Bettencourt (University of Massachusetts Lowell). In his study the number of repeats was analysed in isolated wild type and laboratory strains. The *3CPA* strains are derived from a single wild type North American population. Flies of this polulation were isolated in 2001 and the isolated strains were kept separately in the lab for nine years before being used in tis study (gift of B. P. Lazzaro). These strains show a variation of repeat number including the combinations of 3/11 and 3/10 in close resemblance to dop^{46} and dop^{1}. This analysis suggests a fast evolution of the GRR region of Ago2 naturally occurring in fly populations. Analysis of different laboartory strains showed a even wider range of GRR combinations (*Ln(1)AB* to *TM6B*). For example, two copies of the *Oregon-R* strain kept in different laboratories were found

to carry the combinations 4/13 and 3/16. The loss of GRR repeats in *dop*[1] and *dop*[46] might therefore be a spontaneous event without association to the mutagenesis process.

Variations of GRR numbers have been found in wild type fly lines. These changes of GRR composition might influence the functions of *ago*2 in a non-lethal manner. A change in repeat number might contribute to the defects seen in *dop* mutant embryos. The *Tai255.1* line carries an *ago2* gene encoding 3 GRR1 and 11 GRR2; the combination that is also found in *dop*[46] mutants. To investigate whether this repeat variation does induce developmental defects, embryos from *Tai255.1* flies were compared to wild type and *dop*[1] embryos (Fig. 4.1).

A characteristic defect in *dop* mutants is the lack of lipid droplet transport during lipid clouding. Lipid droplet transport occurs in two phases. In the lipid clearing phase lipid droplets are transported into the inner of the embryo, towards the microtubule plus ends. During the lipid clouding phase the droplets are transported towards the outer region of the embryo, by microtubule minus end directed transport. Successful lipid droplet transport leads to the darkening of the blastoderm in stage 8 embryos (Fig. 4.1A). *Dop*[1] embryos do not show lipid clouding as the blastoderm is much brighter than in wild type embryos. Analysis of *Tai255.1* embryos showed no defects in lipid clouding comparable to wild type.

Another effect in *dop* mutants is the delay of membrane growth during cellularisation (Meyer et al., 2006). The membrane of the pre-blastoderm embryo grows between the nuclei in two phases. The slow phase lasts 40 minutes with a membrane growth rate of
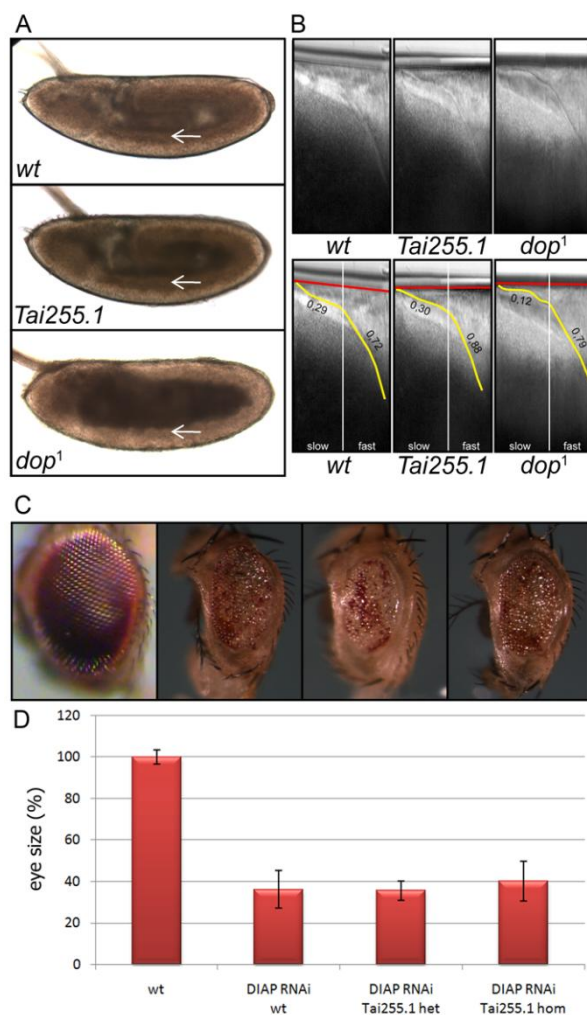
Fig. 4.1: GRR variation does not affect development or RNAi. Effects of GRR variation on early embryonic development were assessed by microscopic analysis of lipid clouding (A) and cellularisation (B). Proper lipid droplet transport leads to the darkening of the outer region of stage 8 wild type embryos observed in bright field microscopy (A). In *dop*[1] embryos lipid droplet transport fails which leads to clarity of the embryonic tissue (arrows). *Tai255.1* embryos display normal lipid clouding. Measurement of membrane growth speed during cellularisation is shown on the right (B). Movies of cellularising embryos were recorded and transformed into kymographs. Kymographs were created by selecting an area of interest of 3 by 45 pixels at the same position in every movie frame. Assembly of the selected regions creates an image showing the progression of the membrane in time (start of membrane growth left, end of cellularisation right). The speed of membrane growth was determined for slow and fast phase of cellularisation (numbers in µm/min). A Diap1[RNAi] assay shows that the effect of GRR variation on RNA silencing does not vary much between wt and *Tai255.1* flies (C, D). The size of wt eyes was determined as 100%. Induction of Diap1[RNAi] does lead to eye defects of similar strength in wild type and heterozygous or homozygous *Tai255.1*.

0.3 µm per minute. As the membrane reaches the basal end of the nuclei the fast phase of cellularisation begins with a rate of 0.8 µm per minute and lasts for 20 minutes. *dop*[1] mutant embryos show reduced membrane growth during the slow phase of cellularisation. Figure 4.1B shows kymographs created from time-lapse recordings of membrane growth in wild type, *Tai255.1* and *dop*[1] embryos. Kymographs allowed visualising the progression of the membrane furrows through time. The movement of the furrows was tracked throughout cellularisation (indicated by yellow lines) and the time point of transition between slow and fast phase of cellularisation was estimated. The distances between the membrane furrow and the outer embryonic membrane were measured in relation to time and the speed of membrane growth was calculated for slow and fast phase. Calculations showed that wild type embryos have a

membrane growth rate around 0.3 μm/min during slow phase and 0.75 μm/min during fast phase. Membrane growth in *dop*[1] mutants was slowed down to at least a third of the speed (measured speed varied between 0.06 – 0.12 μm/min) in slow phase while fast phase was not affected. Membrane growth in *Tai255.1* embryos was found to resemble wild type membrane growth rates. In conclusion the aberrant number of repeats in *Tai255.1Ago2* does not lead to developmental defects in lipid droplet transport and cellularisation as found in *dop*[1] or *dop*[46] embryos.

Unstructured amino acid repeats like the GRRs have been found in Ago1 of *Trypanosoma brucei* (TbAgo1) (Shi et al., 2009). The repeats in TbAgo1 are arginine-glycine rich motifs that have been shown to influence the strength of RNAi responses. Variations in the GRR number in Ago2 might therefore modulate Ago2`s silencing efficiency. To assay the effects of repeat variation on the siRNA pathway a double stranded RNA complementary to the cell death inhibitor Diap1 was expressed in the compound eyes (GMR::Gal4, UAS::DIAP1[RNAi]). Induction of RNAi against Diap1 in the eye leads to apoptosis of the photoreceptor cells and a reduction in eye size. Mutations that disrupt the siRNA silencing pathway lead to suppression of this eye defect. Using this assay the measurement of eye size provides a quantitative readout of RNA silencing with high sensitivity. Expression of the Diap1[RNAi] construct led to a reduction of the eye size to 36.2% of the wild type eye size (Fig. 4.1C, D). Knock down of Diap1 was then tested in flies carrying one or two gene copies of *Tai255.1 Ago2* (carrying the 3GRR1/11GRR2 variation). Flies with one copy did show eye size reduction to 35.6% and flies with two copies showed a reduction to 40.1% of the wild type eye size. Analysis of the Diap1[RNAi] effect on eye size showed no significant difference between wild type and *Tai255.1* flies (independent *t*-test between one and

two copies of *Tai255.1* Ago2: p-value is 0.36). Knock down of Diap1 in *dop*[1] homozygous mutant flies did not affect eye size significantly (data not shown).

To investigate the effects of GRR repeat variation in *dop*[1] on a biochemical basis, *in vitro* assays were performed. The RNA silencing pathway is triggered by single stranded or double stranded small RNA molecules, which are cleaved into shorter fragments by Dicer RNases. Subsequently the processed RNA is incorporated into a ribo-nucleoprotein complex called RISC. Argonaute proteins are part of the RISC complex. During RISC formation Argonaute proteins are "armed" with the guide strand of the small RNA while the passenger strand is eliminated. By incubating embryo lysate with radio-labelled siRNA RISC assembly can be visualised. Initiation of RISC assembly takes place when the siRNA is bound by Dicer2 and R2D2 (siRNA-DCR2-R2D2, complex 1). This complex binds then to an Ago2 containing multiprotein complex where the guide strand is loaded into Ago2. This complex is termed RISC loading complex (RLC, complex 2). The active RISC complex containing loaded Ago2 catalyzes then sequence-specific cleavage of the target RNA (holo-RISC, complex 3). The protein complexes that assemble around the siRNA during different steps of the silencing pathway have varying molecular weights. Therefore it is possible to observe the procession of the RNA by native protein separation.
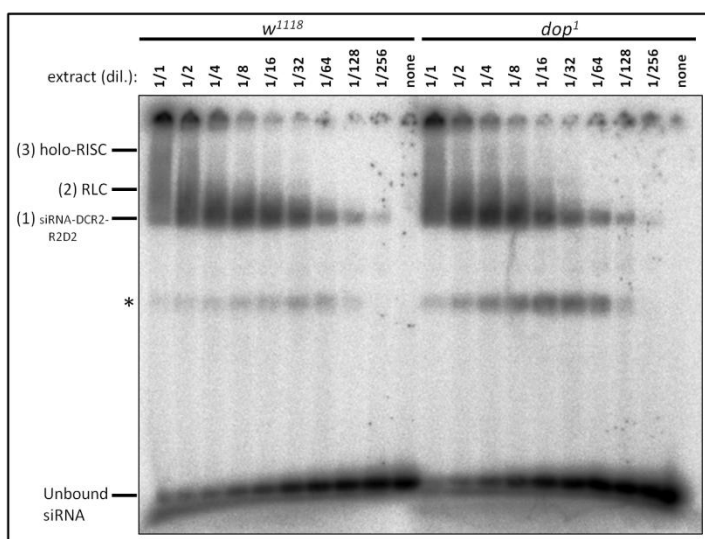
Fig. 4.2: siRNA induced RISC assembly is unaffected in *dop*[1] mutants. Radiolabelled siRNA was incubated with dilutions of extracts from wild type or *dop*[1] mutant embryos. On a native acrylamide gel the formation of the RISC complex can be monitored. Wild type and *dop*[1] mutant extracts carry both the capability to incorporate the siRNA which can be seen by the reduction of unbound RNA at the bottom of the gel as well as by the upwards band shift occurring when the RLC and holo-RISC complexes are formed. For detailed description see text and 2.2.3.11. The protein fraction labelled by an asterix is so far uncharacterised.

The integration of the radio-labelled RNA into different complexes was analysed on a native acrylamide gel (Fig. 4.2). In wild type and *dop*[1] mutant embryos radio-labelled RNA was found to be incorporated in similar extend into the Dicer/R2D2 complex, the RLC and the holo-RISC. These results show that the GRR repeat variation in *dop*[1] mutants does not interfere with the formation of the RISC. In conclusion the data obtained so far argue against an implication of GRR repeat variation in siRNA silencing pathways.

3.2.2. Genetic relationship between *ago2* and *dop*[1]

dop[1] was characterised as allele of *ago2* by several methods. The genomic region containing the *dop*[1] mutation was found by complementation tests using genomic deletions. The smallest deletion that did not complement *dop*[1] defects is the deficiency *Df(3L)XG9* which deletes the genomic regions 71D1-3 and contains 7 genes. Due to previous mapping and other genetic data only two of these genes were considered as candidate genes for *dop*[1]; *CG7739* and *ago2* (Schreiber, 2003). Both of these genes were cloned and expressed in the mutant embryos. Only expression of the *ago2* transgene was found to result in survival of embryos derived from *dop* mutant mothers (Meyer et al., 2006). Previous studies provided evidence that both *ago2* isoforms, *ago2*[long] and *ago2*[short], are expressed in *dop*[1] mutants. Since *ago2* gene products are expressed in *dop*[1] mutants and are unlikely to be affected in their function towards RNA silencing, we questioned whether the mutant defects might derive from a change in the relative expression levels of the short and long isoforms.

To test expression of the isoforms quantitatively and to test the model that the *dop*[1]

allele might affect the relative amount of the two isoforms their expression was

analysed by using quantitative real-time PCR (Qrt-PCR) (Fig. 4.3). Using primers specific

for either the long or the short isoform it could be shown that the short isoform is

expressed in wild type as well as in *dop*[1] mutants. The ratio of *ago2*^{long} and *ago2*^{short}

was 1/0.63, which means that *ago2*^{short} is roughly 30% lower expressed than *ago2*^{long}.

The observed ratio did not differ much between *wild type* and *dop*[1]. Similar expression

levels have been confirmed by collaboration with B. Bettencourt for several of the

previously described *3CPA* fly lines (Hain et al., 2010 submitted). These findings show

that although the expression of the short isoform can be confirmed there is no change

in expression levels of the *ago2* isoforms in *dop*[1] mutants. In conjunction with the

above experiments no evidence for loss or altered *ago2* function was found. These

data raise severe doubts on the hypothesis that *dop*[1] is an allele of *ago2*.

Trials to prove *ago2*^{short} expression on protein level were undertaken using a newly

produced antibody against a carboxy-terminal peptide. However, this experiment did

not reveal any data as the antibody exhibited insufficient specificity to Ago2 (see

supplemental material).
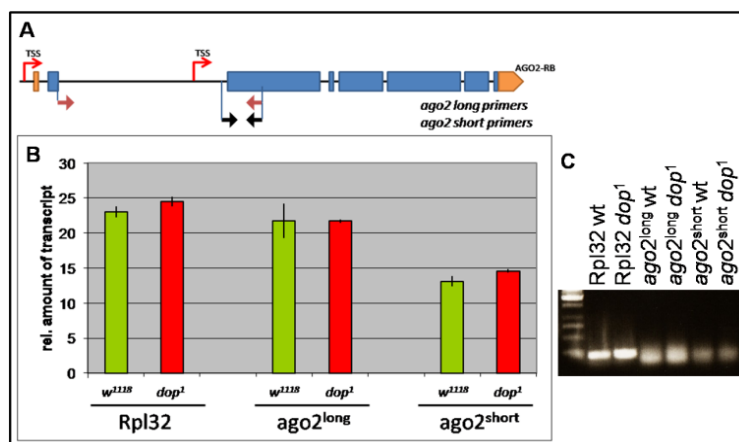
Fig. 4.3: *ago2*^{short} **is an isoform of** *ago*2 **expressed in wild type and** *dop*[1] **mutant embryos.** Qrt-PCR using specific primers (shown in A) for either the long isoforms or the putative short isoform of *ago*2 shows similar expression levels of all isoforms in *dop*[1] and wt embryos. Relative transcript amounts from the Qrt-PCR are shown in B. C shows the PCR products separated on an agarose gel.

The short isoform of *ago2* encodes the functional PAZ and PIWI domains and an alignment of the putative protein sequence encoded by *ago2*short with the human Ago2 shows a high level of conservation (Hain *et al.*, submitted). The existence of the short isoform raises the question about its potential contribution in RNA silencing pathways. To answer this question the *in vivo* RNAi assay the compound eye was performed as described above (see 4.1; Fig 4.4). Addition or reduction of different doses of the *ago*2 isoforms using combinations of different *ago*2 alleles allows modulation of RNA silencing. Induction of DIAP1RNAi in wild type eyes resulted in a decrease of the eye size (Fig. 4.4(2)). Previous experiments showed that the loss of *ago2*long did suppress the eye defect almost completely, despite the presence of two gene copies of *ago2*short (Meyer et al., 2006). A further reduction to only one expressed copy of *ago2*short showed complete suppression of the RNAi induced defects (Fig. 4.4(3)). This indicates that expression of *ago2*short alone might not provide significant function towards RNAi. These results were compared to flies expressing one copy of *ago2*short and *ago2*long each (Fig. 4.4(4)) and to flies expressing two copies of *ago2*short and one copy of *ago2*long (Fig. 4.4(5)). This comparison showed a clear difference between one or two copies of the short isoform in the presence of at least one *ago2*long isoform. A possible explanation for this result might be that the silencing function of the Ago2short is dependent on the presence of the full-length protein containing the GRRs.
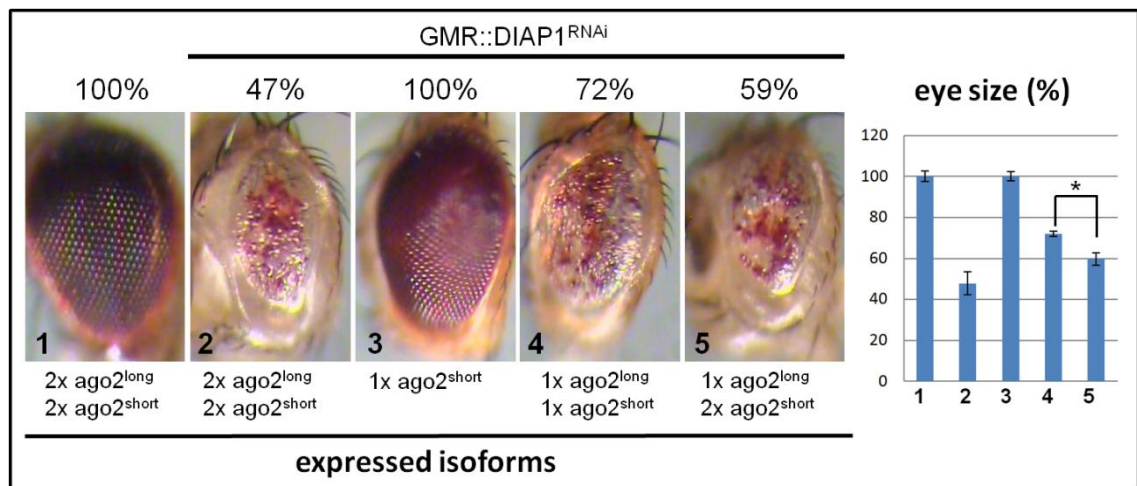
Fig. 4.4: Effects of *ago2* and *dop*[1] alleles on RNA interference. Eye tissue specific expression of a double stranded RNA against Diap1 leads to eye size reduction (**2** - 47% of wild type eye size). If flies carry deletions that only retain expression of *ago2*[short] the eye phenotype is completely suppressed (**3** - 100% of wild type eye size). Upon removal of one gene copy of *ago2* the eye size is slightly bigger (**4** - 72%) than in wild type flies expressing DIAP1[RNAi] arguing for reduced RNAi function. Adding one copy of *ago2*[short] into *ago2* hemizygous background increases the functions of the RNA silencing machinery slightly as the eye size is reduced to 59% (**5**). The graph shows measured eye size in percent (n≥12)(asterisk shows a significant difference between **4** + **5**, $p<0.005$, t-test). Genotypes are: **(1)** w^{1118}, **(2)** *GMR::Gal4,UAS::DIAP^{RNAi};+/+* **(3)** *GMR::Gal4,UAS::DIAP^{RNAi};Df(3L)XG9/ago2^{51B}* **(4)** *GMR::Gal4,UAS::DIAP^{RNAi}; Df(3L)XG9/ago2^{dop1}* **(5)** *GMR::Gal4,UAS::DIAP^{RNAi};ago2^{51B}/ago2^{dop1}*

3.2.3. Novel *ago*2 null alleles complement *dop*[1]

To functionally characterise Ago2, most studies employ the two apparent null alleles *ago2^{51B}* and *ago2^{414}* (Fig. 4.5). These alleles represent two independently derived deletions that were produced by imprecise excision of a P-element inserted into the genomic region encoding the 5 prime UTR of *ago*2 (Xu et al., 2004; Okamura et al., 2004). However, recent analysis showed that *ago2^{51B}* and *ago2^{414}* retain expression of the *ago2*[short] isoform (Meyer et al., 2006; Hain et al., submitted). Therefore these alleles do not represent true null alleles of *ago2*.

To perform a complementation analysis that clearly shows whether *dop*[1] affects *ago2* a real null mutation is needed. To identify true *ago*2 null alleles we acquired additional *ago*2 mutants, produced by mobilisation of the *EP(3L)3417* transposon, from the laboratory of Haruhiko Siomi (Keio University, Japan). In contrast to *ago2^{414}*, Northern

blot analysis of *ago2*[321] and *ago2*[454] did not show any remaining expression of *ago2*[short] (conducted by K. Okamura, Sloan Kettering Institute, U.S.A). *ago2*[454] showed expression of a 600 bp fragment. To investigate the deletions in *ago2*[321] and *ago2*[454] the molecular breakpoints were assessed using genomic PCR and sequencing. The results showed that the 5-prime breakpoint of both deficiencies is positioned at the same site 34 base pairs downstream of the transcriptional start site of the long isoforms (TSS1). Deletions of 2514 base pairs in *ago2*[321] and 3237 base pairs in *ago2*[454] could be identified (Fig. 4.5).

ago2[454] carries the largest deletion in *ago2* that has been identified so far. The deletion reaches into the core of the *ago2* gene, which is coding for the PAZ and PIWI domains. Therefore it is very unlikely that any functional Ago2 protein is expressed in these mutants. However, expression of a short c-terminal fragment corresponding to the remaining sequence has been found. Expression of this fragment might be triggered by the TSS1 which is still present in *ago2*[454].
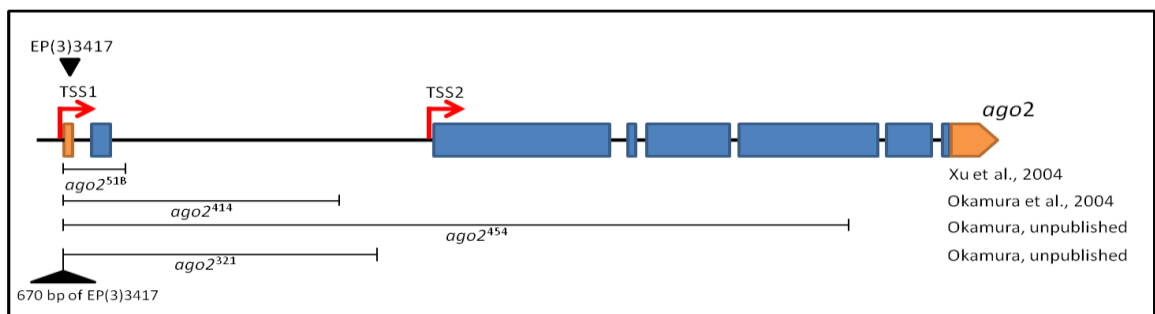
Fig. 4.5: Novel *ago2* alleles that interfere with expression of long and short *ago2* isoforms. Primer walking and genomic sequencing shows that the alleles *ago2*[454] and *ago2*[321] delete regions further downstream than other *ago2* alleles published so far. All alleles were produced by mobilisation of the *EP(3L)3417* transposon (black triangle) but only the unpublished allele *ago2*[454] deletes the second TSS (red arrows). *Ago2*[454] deletes 5751 base pairs; from 34 bp downstream of the TSS1 to the last part of the fifth exon. *Ago2*[321] deletes 2514 bases with the same upstream breakpoint. *ago2*[321] retains 670 bases of the EP element which might interfere with promoter sequences (see text).

The deletion in *ago2*[321] does differ from *ago2*[414] only by 300 bases and TSS1 and TSS2 are still present. The reason why the expression of *ago2*[short] is only absent in *ago2*[321]

and not in *ago*2^{51B} might be distinct from the size of the deletion. In *ago*2^{321} a 670 base pair fragment of *EP(3L)3417* was found at the deficiency breakpoint indicating that a fragment of the P-element was left behind in the excision process. The remnant of the P-element might interfere with the expression of *ago*2^{short} by preventing promoter read-through from the *ago2* promoter on TSS1 towards the coding region of the short isoform. In conclusion *ago*2^{321} and *ago*2^{454} are novel alleles of *ago2* that prevent expression of all *ago2* isoforms. The phenotypic features of *ago*2^{321} and *ago*2^{454} will be published elsewhere (K. Okamura et al., unpublished).

The above results provided the important conclusion that the published apparent null alleles still express *ago2* gene product and therefore complicated their use for genetic complementation analyses of *ago2* and *dop*. With the identification of *ago*2^{321} and *ago*2^{454} as true *ago2* null alleles stringent complementation studies have become possible. To test whether the new *ago*2 null alleles can complement the maternal lethality of *dop*^{1} embryos *ago*2^{321} and *ago*2^{454} mutants were crossed against *dop*^{1} mutant flies and transheterozygous flies were investigated. While *dop*^{1} homozygous flies are completely sterile transheterozygous flies carrying *dop*^{1} in combination with either *ago*2^{321} or *ago*2^{454} showed survival rates similar to wild type (Fig. 4.6E). Furthermore the *ago*2 null alleles also complement developmental defects. *dop*^{1} embryos show a defect in lipid droplet transport. In wild type embryos lipid clouding leads to the darkening of the outer embryonic region. In the *dop*^{1} mutants the outer region remains bright. In addition *dop*^{1} mutants show a defect in membrane growth and nuclear anchoring during cellularisation. *ago*2 null alleles were found to complement the lipid clouding defect and the cellularisation defect (Fig 4.6A-D and F,G) This complementation analysis showed that the novel *ago*2 null alleles fully complement the *dop*^{1} defects. Therefore it is unlikely that the severe phenotype of

dop[1] is caused by loss of function of the long and short isoforms of *ago2*. In conclusion, these experiments indicate that *dop* is not an allele of *ago2*.
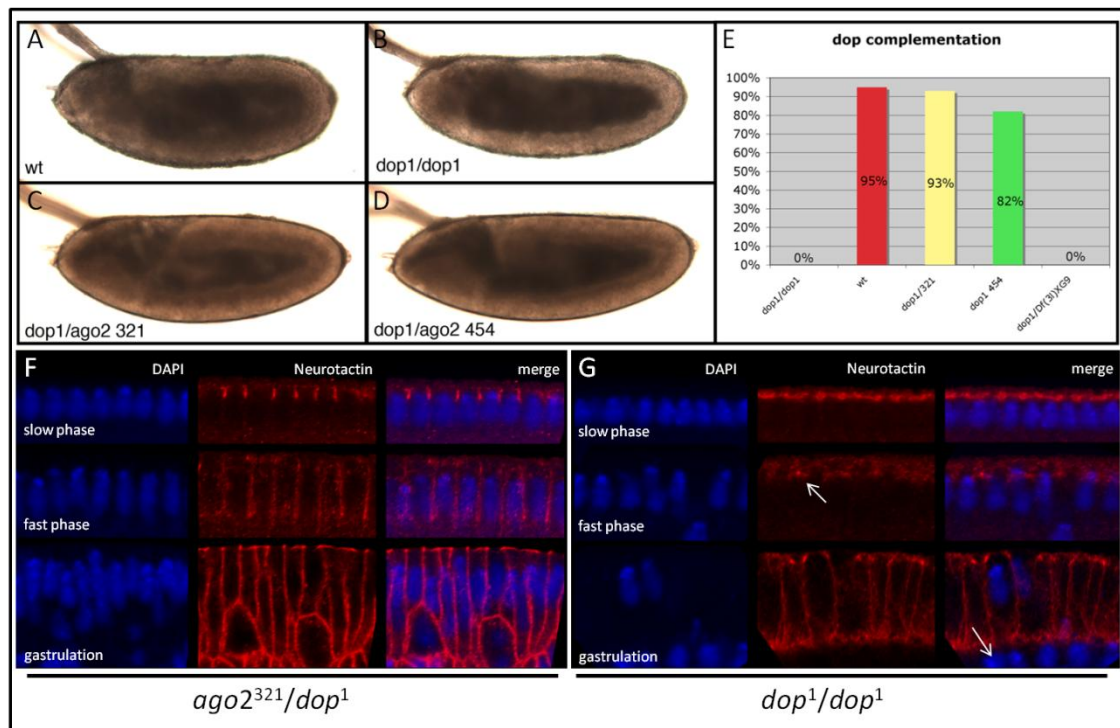
Fig. 4.6: *ago*2 null alleles fully complement *dop*[1] defects. Comparison of wild type, *dop*[1] homozygous and transheterozygous flies. Light microscopic images of embryos that show lipid clouding are shown in (A-D). Note the darkening of the ectoderm caused by the light scattering lipid droplets in A, C and D while the *dop*[1] ectoderm remains clear (B). Both *ago*2 null alleles also complement the lethality of *dop*[1] (E) and the cellularisation defects observed in *dop*[1] embryos (F and G, data for *ago2*[454] is identical to *ago2*[321]). A Neurotactin antibody was used to stain the membrane (red); nuclei were stained with DAPI (blue). Arrows indicate defects in furrow formation and nuclear anchoring in *dop*[1] mat/zyg. embryos.

3.2.4. *dop*[1] is an allele of an uncharacterised gene

Two theories of how *dop*[1] might affect *ago*2 function have been tested by using genetic methods. The hypothesis that *dop*[1] carries a mal-functional number of GRR repeats, has been disapproved genetically and biochemically. The other possibility was that *dop*[1] mutants display disproportional expression levels of the *ago*2 full-length transcript and a so far uncharacterised isoform, *ago*2[short]. Although the presence of *ago*2[short] was proven by different methods in wild type and *dop*[1], we did not obtain any evidence for a misregulation of these transcripts in *dop*[1]. Novel *ago*2 deficiencies

lacking the expression of long and short *ago*2 isoforms complement the *dop*[1] defect in

early embryos. These findings indicate that *ago*2 is not the gene affected in *dop*[1]

mutants. Based on these conclusions, the genetic mapping of *dop*[1] was revisited. The

dop[1] mutation was mapped to chromosome 3L by complementation mapping using a

set of chromosomal deficiencies (Meyer et al., 2006). The smallest deficiency found to

be unable to complement *dop*[1] defects was the deficiency *Df(3L)XG9*. *Df(3L)XG9* is a

genomic deletion that was produced by x-ray mutagenesis and the published

breakpoints are shown in Figure 4.7 (Grosshans, 2005). The distal breakpoint of

Df(3L)XG9 was mapped to the right of the *mex1* gene by PCR mapping. The proximal

breakpoint of the deficiency was based on complementation of a lethal P-element

insertion in *CG7427* (*Pl(3)s1754*)(Fig. 4.7). As flies carrying *Df(3L)XG9* over the

Pl(3)s1754 insertion were viable it was decided that the distal breakpoint is positioned

upstream of *CG7427*. Based on these data it was expected that only genes between

mex1 and *CG7427* were deleted and genes outside of this region were not considered

as candidates for *dop*[1].
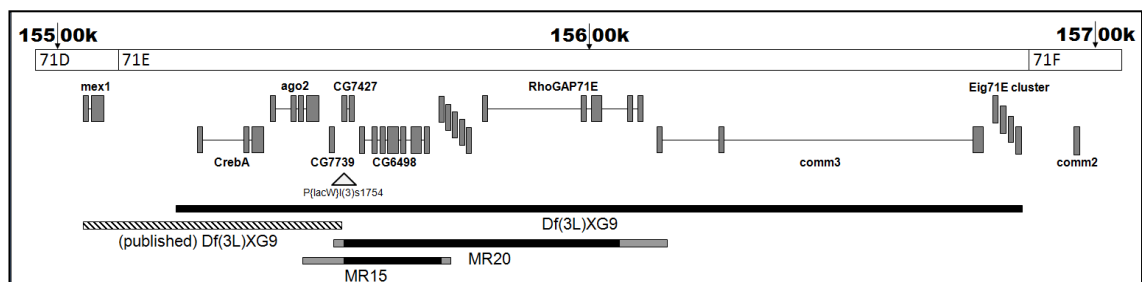
Fig. 4.7: Newly characterised deficiencies uncover the *dop*[1] locus. This figure shows the published and the corrected breakpoints of the deficiency *Df(3L)XG9* in the genomic region 71E. To break down the region with candidate genes to a smaller range, additional deficiencies were mapped by primer walking. The deficiencies *MR15* and *MR20* were identified to lie within the region deleted by *Df(3L)XG9*. *MR15* is the smallest deficiency uncovering the *dop*[1] locus. The break points of *MR15* reduce the list of candidate genes to *CG7739*, *CG7427* and *CG6498*. The position of *Pl(3)s1754* is indicated by a triangle.

To reconsider the mapping experiments of *dop*[1] the chromosomal breakpoints of

Df(3L)XG9 were defined molecularly. Using different sets of primers for PCR based

primer walking and genomic sequencing (supplemental material) breakpoints could be determined with a dramatic difference to the published breakpoints (see Fig. 4.7). This finding is surprising as the deficiency clearly deletes *CG7427* but complements the lethal recessive insertion of *Pl(3)s1754*. A possible explanation for this might be that the insertion site for the P-element is not in *CG7427*. The genomic insertion site of *Pl(3)s1754* was analysed by plasmid rescue but this analysis did confirm insertion in *CG7427*. The only remaining explanation is that the *Pl(3)s1754* insertion is not homozygous lethal and that the homozygous lethality of the chromosome carrying this insertion harbours another lethal mutation with unknown position. This mutation caused the wrong believe that the *Df(3L)XG9* deficiency is shorter than it actually is.

The newly characterised *Df(3L)XG9* breakpoints are located 134,974 bases apart from each other and delete additional genes to the ones contained by the originally published breakpoints. To investigate if any of these genes might be affected in *dop*[1] additional deficiencies were investigated. The *dop*[1] non-complementing deficiencies *MR15* and *MR20* were derived from imprecise excision of *Pl(3)s1754*. Primer walking showed that neither of these deficiencies deletes *ago*2, but further downstream regions containing the computed genes *CG7427* and *CG6498* (Fig. 4.7). To search for mutations in these genes primer pairs were designed to amplify their genomic sequence via PCR. The amplified PCR fragments were sequenced and revealed a point mutation in *CG6498*.

This first part of the thesis demonstrated that the *dop*[1] mutation does not affect *ago2*. Furthermore, the model that severe cellularisation defects result from variations in GRRs in *ago2* could be disproven by the finding that GRR variations are a common phenomenon in wild type fly populations. A major problem that prevented the proper genetic characterisation of the *dop*[1] allele was the lack of an *ago2* null allele. The identification of true *ago2* null alleles defined a breakthrough for the investigation of *dop* and will be of significant importance for the research of *argonaute* functions. The *ago2* null alleles provided final proof that *dop*[1] is not an allele of *ago2*. Subsequent mapping of the *dop*[1] gene locus revealed a mutation in *CG6498*, a gene that has not been characterised in *Drosophila*. As *dop*[1] and other *dop* mutations (see 6.1.2) carry mutations in *CG6498* from now on the name *dop* will be used for this gene. The second part of this thesis will focus on the functions of the *dop* gene.

Chapter IV - Results Part II:

Developmental functions of the Dop kinase

4.1. Introduction of PartII

4.1.1. Protein kinases

The superfamily of protein kinases is one of the largest groups of proteins encoded by eukaryotic genomes. The human genome encodes 518 kinases, roughly half of which are mapped to loci associated with genetic diseases (Manning et al., 2002). The annotation of the *Drosophila* genome predicts about 251 kinases. The difference in these numbers originates mostly from the fact that vertebrate genomes often encode many members of a protein family, which only share a single homolog in *Drosophila* (Morrison et al., 2000). The lower number of homologous proteins expressed in *Drosophila* makes an investigation of the general protein function in this organism much easier.

Protein kinases are involved in almost every signalling pathway and many other cellular processes. The function of a protein kinase is the phosphorylation of protein substrates. Kinases can influence activity, stability, localisation or the overall function of the substrate protein by addition of a phosphate group. The catalytic activity of kinases lies within the conserved kinase domain. The length of the eukaryotic protein kinase domain ranges from 250 to 300 amino acids. A phosphorylation reaction is catalysed when the active centre of the kinase domain binds to the substrate and adenosine triphosphate (ATP). The phosphate in the gamma position of the ATP molecule is removed by the kinase and added to the hydroxyl group of an amino acid on the substrate. Phosphorylated residues are serine or threonine (by serine/threonine kinases) and tyrosine (by tyrosine kinases).

Work of Steven Hanks, Anne Marie Quinn and Tony Hunter showed that most eukaryotic protein kinases can be grouped into 7 conserved subfamilies, based on the conservation of the functional amino acids (Hanks, Quinn and Hunter, 1988; Hanks and Hunter, 1995; Manning et al. 2002; Pearce et al., 2010). Their work groups kinases with specific substrate specificities into different families. By aligning the conserved amino acids in the identified protein kinases and early functional studies it was found that the catalytic kinase domain consists of two functional parts linked by a central hinge region (Hanks, Quinn and Hunter, 1988; Hanks, 2003). The amino-terminal lobe and the hinge region provide ATP-binding function. The carboxy-terminal lobe provides substrate binding and transfer of the phosphate group from ATP to a free hydroxyl group of the substrate. This region also influences the affinity to certain substrates. Kinase substrates are usually other proteins that contain a specific consensus motif, which is recognised by the kinase (Johnson et al., 1998). Modern techniques like the analysis of protein structure by x-ray crystallography revealed further functions for conserved residues for many kinases. Nevertheless, despite the conservation of distinct kinase motifs an exact prediction of substrates for an uncharacterised kinase is not possible and can only be shown by biochemical interaction studies.

Other effects on protein kinase function are created by accessory domains. Many proteins carrying kinase domains also contain conserved protein domains that regulate localisation, activity or interaction with target and non-target proteins. Pleckstrin-homology (PH) domains have been shown to be involved in protein localisation to the membrane by binding phosphatidyl-inositol phosphates. An example for the recruitment of kinases to the membrane for the induction of cytokinesis is ROCK kinase. Rock kinases harbour a PH domain and are downstream effectors of the small GTPase RhoA. Activated RhoA-GTP leads to actin assembly and activation of ROCK at

the membrane. Activated ROCK kinase is needed to suppress the function of myosin

phosphatase target subunit 1 (MYPT1) by phosphorylation of Thr696 and Thr853 of

MYPT1 (Carbajal et al., 2000; Velasco et al., 2002). MYPT1 is the targeting subunit of

the myosin light chain phosphatase (MLCP) that binds to myosin and inactivates the

myosin light chain (MLC) by dephosphorylation (through catalytic activity of the PP1c

subunit of MLCP). Therefore, ROCK activity releases the block of MLC and therefore

induces assembly of myosin II filaments, which successively leads to assembly of

contractile actomyosin bundles. An opposing role in MLC regulation is conducted by

the MLC kinase (MLCK) that phosphorylates MLC at Ser19 (Gao et al., 2001).

Formation of the contractile ring in cytokinesis involves the function of many other

protein kinases (Polo-like kinase (Plk), cyclin-dependent kinase (CDK), Checkpoint

kinase 1 (Chk1) and Aurora B that act in complex regulatory mechanisms.

4.1.2. The MAST kinase family

Mammalian microtubule-associated serine/threonine (MAST) kinases are part of the

AGC kinase subfamily. MAST kinases are modular proteins containing three conserved

domains. The kinase domain is embedded between an amino-terminal conserved

Pfam1908 domain* called DUF (domain of unknown function) and a carboxy-terminal

PDZ domain. The functions of mammalian MAST kinases are not well understood. The

first member of the MAST kinase family identified was MAST2 (MAST205). MAST2 was

found to be associated with microtubule fractions from mouse testes (Walden et al.,

1993). Biochemical fractionation experiments showed that MAST kinases are

*The Pfam database enlists protein domains represented by multiple sequence alignments and hidden Markov models (Finn et al., 2007)

associated with microtubules and this association is dependent on microtubule-associated proteins (MAPs). Until today only two phosphorylation targets of MAST are known: PTEN and NHE3. The tumor suppressor and phosphatase PTEN can be bound and phosphorylated by MAST kinases (Valiente et al., 2005). PTEN is a key regulator of cell growth and apoptosis. The kinases MAST1-3 were found to bind the PTEN carboxy-terminus via their PDZ domain. This interaction increased phosphorylation of PTEN by the kinase domain of MAST *in vitro*. Phosphorylation of the carboxy-terminal domain of PTEN by MAST2 has been shown to prevent PTEN degradation by interfering with ubiquitination (Vazquez et al., 2000). Therefore MAST kinases have been suggested to regulate PTEN functions and stability. The second MAST kinase substrate is the apical Na^+/H^+ exchanger NHE3 (Wang et al., 2005). NHE3 is bound by the PDZ domain of MAST2. Co-expression of MAST2 and HNE3 in opossum kidney (OK) cells resulted in inhibition of pH recovery indicating that MAST2 might inhibit NHE3`s ion transport function. The exact phosphorylation sites in PTEN and NHE3 have not been investigated.

Three additional proteins have been identified to bind MAST kinases. MAST1 has been found to bind β2-Syntrophin (Lumeng et al., 1999). The interaction of MAST1 and β2-Syntrophin has been shown to involve the PDZ domains of both proteins. β2-Syntrophin is a part of the Dystrophin/Utrophin network in the membrane of neuro-muscular synapses. MAST kinases are thought to link this membrane bound complex via β2-Syntrophin with microtubule filaments. This interaction might constitute a mechanism to couple the Dystrophin/Utrophin network with signal transduction pathways. Also Proto-Cadherin LKC (expressed in liver, kidney and colon tissues) (PCLKC) protein is bound by the PDZ domain of MAST2 (Okazaki et al., 2002). The

interaction of MAST2 with PCLKC is directed by the classic interaction between the PDZ domain of MAST2 and a PDZ-binding motif at the carboxy-terminus of PCLKC. Interestingly, this member of the atypical cadherin superfamily acts as a tumor suppressor by inducing contact inhibition in epithelial cells and is lost in cancer cells. Contact inhibition provides a way to arrest uncontrolled cell growth in epithelial cells. Interaction of MAST2 with PCLKC might control contact inhibition in epithelial cells. MAST2 was found to regulate immune responses by interacting with TRAF6 (Xiong et al., 2004). The site for this interaction was found to lie within an amino-terminal region, containing the DUF domain of MAST2. Xiong and colleagues proposed that association of MAST2 and TRAF6 might result in the inhibition of TRAF6 dependent NF-kappa-B activation. The NF-kappa-B signalling pathway is regulation gene transcription in response to extracellular signals, is important for many cellular functions and its incorrect regulation has been linked to may human diseases.

In conclusion there is yet no clearly defined function published for MAST kinases. MAST interactors are found in different signalling pathways regulating different cellular mechanisms. Distinct phosphorylation sites have not been found and the phosphorylation motifs are not known. The following chapters will provide new insights into the function of the MAST kinase family by investigation of the *dop* gene.

4.2. <u>Results of Part II</u>

4.2.1. Characterisation of the Dop protein

4.2.1.1.   Dop is the *Drosophila* homolog of the MAST kinase family

Genome annotation shows that *CG6498* is encoding a predicted protein of 2139 amino acids length. Amino acids 342 to 703 are annotated as a Pfam:DUF (domain of unknown function) domain, amino acids 835 to 1170 encode a serine/threonine kinase and positions 1513 to 1593 encode a conserved PDZ (PSD-95, Dlg and ZO) domain.

BLAST analysis (Basic local alignment search tool - http://www.uniprot.org) revealed that the amino acid sequence of Dop is similar to proteins of the MAST (microtubule associated serine/threonine) kinase family. The domain structures of the human MAST kinases MAST1, MAST2, MAST3 and MAST4 are very similar to that of Dop (Fig. 6.1A). Sequence alignments were performed to analyse the conservation between Dop and the human MAST kinases. The calculated overall percentage identities (PID) of the human MAST kinases and Dop in pair wise alignments are 37.74 % (MAST3), 35.66 % (MAST1), 34.66 % (MAST2) and 34.07 % (MAST4). Alignment of the annotated domains only showed higher conservation, especially the conservation of the kinase domain (Fig. 6.1B) indicating that the region surrounding domains is not conserved (for a full alignment of the proteins see supplemental material). Because of the conservation of these proteins investigation of *dop* in *Drosophila* is likely to provide an excellent model for understanding MAST kinase functions in human.

The level of conservation between MAST kinases and Dop suggests similar cellular functions. To gain more insight into this structural conservation, homologues of Dop
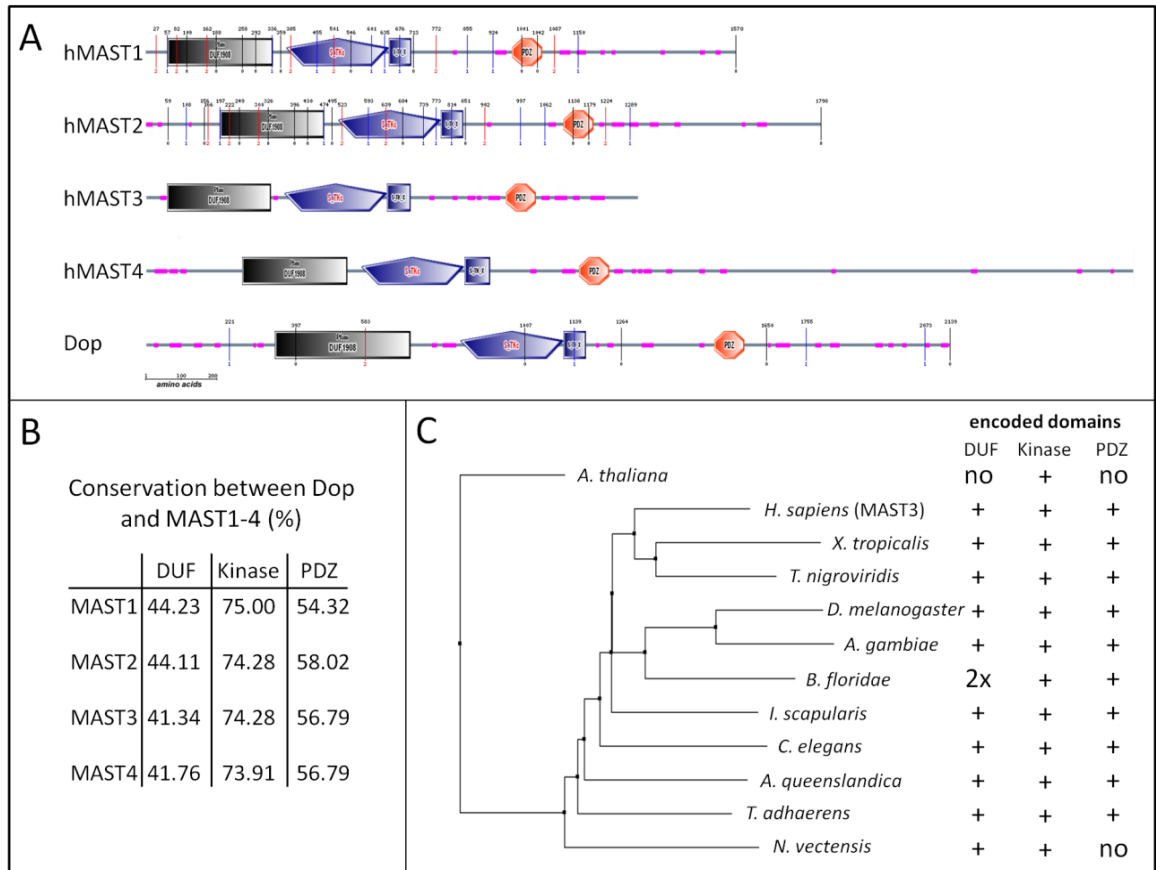
Fig. 6.1: Alignment of annotated Dop homologues and conservation of DUF, kinase and PDZ domains. The domain structure of the human MAST kinases 1-4 and *Drosophila* Dop was analysed using SMART (Simple Modular Architecture Research Tool - http://smart.embl-heidelberg.de) (A). Percentage identities of pair wise alignments of the DUF, Kinaes and PDZ domains (B). Dop homologues were also found in other organisms (B). A neighbor-joining phylogram shows the relation of the found proteins. Most homologues contain the accessory DUF and PAZ domain. *Branchiostoma floridae* encodes a Dop homolog with two DUF domains (2x). The protein in the sea anemone Nematostella *vectensis* does not contain a PDZ domain. Note: the MAST homolog in *Arabidopsis thaliana* was not found in the BLAST search but taken from Karpov *et al.* 2010 (Domains identified using SMART are marked by +, no found domain is indicated by no).

were searched in other organisms. BLAST search against annotated proteins shows a conservation of the domain structure of Dop in vertebrates, insects, nematodes and primitive metazoa (Dop homologues were found in **mammals**: *h. sapiens, M. musculus, R. norvegicus*; **fish**: *T. nigroviridis* and *B. floridae*; **insects**: *D. melanogaster, A. gambiae, I. scapularis*; **nematodes**: *C. elegans;* **cnidaria**: *N. vectensis and* **basal metazoan**: *T. adhaerens; A.queenslandica*) (Fig. 6.1C). All organisms found to encode a MAST kinase homolog belong to the metazoan kingdom. Apart from *B. floridae* and *N. vectensis* all

MAST kinase homologues identified in this survey encode a protein with one DUF, one kinase and one PDZ domain (identified using the domain detection tool SMART - http://smart.embl-heidelberg.de). The Dop homolog in *B. floridae* was found to encode two DUF domains separated by 106 amino acids in the amino-terminal region. The homologue in *N. vectensis* lacks the region carboxy-terminal of the kinase domain.

Recently a homolog of the MAST kinases *in A. thaliana* has been suggested by Karpov and colleagues. (Karpov et al., 2010). Their publication shows conservation of the ATP binding motif and active site. This kinase has an extended amino-terminal region but no conserved DUF domain is found (PID = 13.4 %). Genes encoding the kinase domain of Dop might therefore have a broader conservation as compared to genes with the DUF/Kinase/PDZ structure. These genes might correspond to the human MAST-like kinases, which only contain the kinase domain. Conservation of the kinase domain might implicate shared kinase target proteins. However, because of their structural difference to Dop these kinases are beyond the scope of this thesis.

4.2.1.2. Novel *dop*[1] non-complementing mutations are alleles of *dop*

In a previous mutagenesis experiment additional *dop* mutant alleles, called *dop*[LH] alleles, were generated by testing for non-complementation of the *dop*[1] chromosome (L. Hauer and A. Müller, unpublished). Genomic sequencing showed that these fly lines did not show any point mutations in *ago*2 (Meyer et al., 2006 and this work), however sequencing of *CG6498* in six *dop*[LH] lines revealed single and unique point mutations in each of the alleles analysed (Fig. 6.2). *dop*[LH5], *dop*[LH9], *dop*[LH10] and *dop*[LH15] carry nonsense mutations causing a premature stop of translation. The introduced stop codon in *dop*[LH10] is situated after position 523 in the protein sequence. This might lead

to expression of a truncated protein without kinase and PDZ domain and only a fragment of the DUF domain. dop^{LH5} and dop^{LH9} might express larger fragments containing the DUF and the kinase domain. The mutation in dop^{LH15} is predicted to represent a truncated protein carrying only the DUF domain. dop^{LH15} carries an insertion of one nucleotide which leads to the shift to another reading frame.

Like dop^1, the allele dop^{LH7} shows a missense mutation, however it is localised in the DUF domain. The dop^1 mutation implies that the kinase domain is needed for the function of dop during cellularisation. In parallel, the molecular aberration in dop^{LH7} might indicate that the DUF domain provides a function for cellularisation as well.

Unlike the mutations described before, dop^{LH14} carries a mutation in untranslated region. The mutation found in dop^{LH14} mutants lies in the last base of the fifth intron and might affect the splice acceptor for exon 6. This mutation might lead to exon skipping of the sixth exon, which would be excluded from the mRNA transcript. This mutation might lead to the loss of amino acids 1007 to 1170 in the kinase domain (marked black in Fig. 6.2) or destabilise the whole protein.
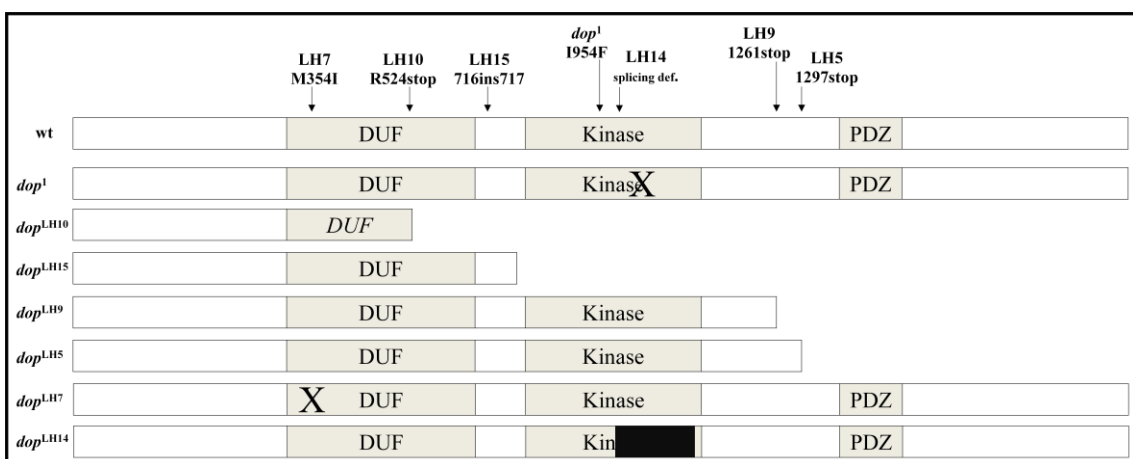
Fig. 6.2: *dop* **mutant fly lines carry mutations in *CG6498*.** The mutation found in the *dop*[1] allele leads to a missense mutation in a so far uncharacterised gene in *Drosophila* named *CG6498*. The gene encodes a 2139 amino acid protein, which contains three conserved domains: a domain of unknown function (DUF), a serine/threonine kinase domain and a PDZ domain (see text for functions). The mutation in *dop*[1] affects the kinase domain. Results of the genomic sequencing of six LH *dop* alleles are indicated. The domain organization of the different LH alleles indicate possible gene products created by: non-sense mutations (truncated protein in *dop*[LH5], *dop*[LH9], *dop*[LH10], *dop*[LH15]), missense mutations (marked by a X in *dop*[1], *dop*[LH7]), a frame shift mutation *dop*[LH15] (leads to formation of a stop codon close to the insertion site) and a splice site mutation (exon skipped in *dop*[LH14] marked by black bar).

4.2.1.3.   Detection of the Dop protein

This work represents the first attempt to determine the function of a MAST kinase using mutations in the *Drosophila dop* gene. As *dop* has not been investigated previously, molecular tools to dissect *dop* function had to be developed. The production of an antibody directed against amino-terminal peptide sequences allowed investigation of protein expression in *wild type* and *dop* mutant alleles. Antibodies were raised against amino-terminal peptides of Dop in rabbits (see material and methods). Two separately produced antibodies (αDop1302 and αDop1303) were used to detect Dop protein in wild type and mutant embryo lysate (Fig. 6.3). To identify the size of the Dop protein in Dalton a HA-tagged Dop protein was expressed in flies. Western blots using protein extracts of embryos that over-expressed Dop were incubated with either HA-antibody or Dop antibody (Fig. 6.3A). This comparison showed that the produced antibodies detect ectopically expressed Dop protein in two bands around 300kDa. This finding suggests post-translational modification as the theoretical weight of Dop is predicted to be 225.5kDa.

To further test the specificity of the produced antibody it was used against protein extracts from *dop* mutants (Fig. 6.3B). The antibody was able to detect endogenous Dop in wild type lysate but not in *dop*[LH10] mutants indicating that the antibody is specific for Dop. Comparison of endogenous Dop bands in *wt, dop*[1] and *dop*[LH10] also showed that Dop is expressed weakly in *dop*[1] mutants and is undetectable in *dop*[LH10]. A band corresponding to a truncated protein could not be seen in *dop*[LH10] (an additional band of 170kDa could only be detected with αDop1302; not with αDop1303 and is most likely resulting from the altered genetic background in *dop*[LH10]/*Df MR15* embryos). Therefore it is postulated that *dop*[1] is a loss-of-function mutation while

dop[LH10] can be considered as a protein null allele. This finding will be supported by the severity of cellularisation defects in *dop*[LH10] (see chapter 4.2.3).
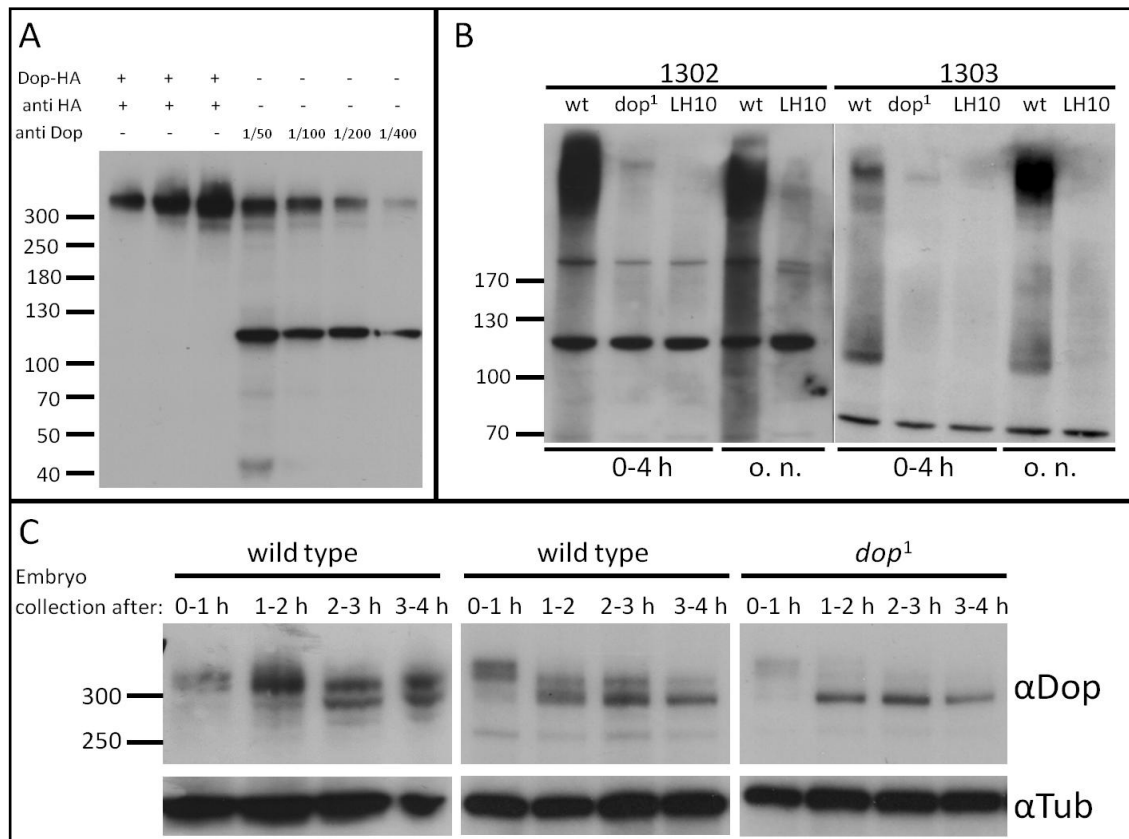
Fig. 6.3: Analysis of the Dop protein in embryonic lysates using peptide antibodies. (A) Overexpressed Dop protein runs at a band with apparent molecular weight of 350 kDa. Dop-HA was expressed in embryos Lanes 1 to 3 containing 3, 5 and 7 µl extract, were incubated with a HA-tag antibody. Lanes 4 to 7 contain 7 µl lysate and were incubated with the affinity purified αDop1303 antibody. (B) Detection of endogenous Dop protein wild type, *dop*[1] and *dop*[LH10] embryos. Embryos were collected after 0-4 hours or overnight. Wild type embryos show a strong signal, while *dop*[1] embryos retain only very weak expression. *dop*[LH10] embryos are lacking Dop expression. (C) Developmental western blot of Dop protein in timed embryonic extracts (using αDop1303). The band shift indicates posttranslational modification during the first hours of development. To show reproduceability different wild type blots are shown (left and middle). *dop*[1] embryos (right) show decreased levels of the higher molecular weight bands.

Some of the *dop*[LH] mutants might express truncated or non-functional Dop proteins. Mutations like *dop*[LH7], which carries a point mutation in the DUF domain, might be used as genuine tools to investigate specific functions of Dop domains. The presence of Dop was investigated in the *dop*[LH] alleles but difficulties were encountered as the severe developmental defects of most *dop*[LH] lines prevented collection of sufficient

amounts of protein. The data suggest that Dop is not expressed in dop^{LH5}, dop^{LH7} and dop^{LH15} but these experiments need to be reproduced with different genetic background to yield more protein (supplemental material). No strong evidence for truncated gene products were found in the dop^{LH} lines, suggesting that these mutations might result in nonsense mediated decay (Chang et al., 2007).

Problems with the detection of Dop in embryos might derive from changes in Dop regulation during the cell cycle. The early stages of embryonic development are characterised by rapid cell cycles that are synchronised and lack interphases. With onset of cellularisation cell cycles slow down and become unsynchronised. Dop protein shows a band shift between 350 kDa and 280 kDa that occurs during the first 4 hours after egg laying (Fig. 6.3C). After the first 2 hours embryos enter cellularisation normally. The band shift might indicate that Dop is differentially regulated during the cell cycle. Additional evidence that Dop is regulated differentially throughout the cell cycle is found by localisation studies (see 4.2.1.5).

Differential regulation of Dop might explain variations of Dop protein levels in embryonic extracts. The detection of endogenous Dop protein failed in many experiments. By using different lysis buffers and conditions it was found that the endogenous Dop protein band could only be detected if the embryos were boiled in loading buffer and instantly used for gel electrophoresis. Lysis protocols that required prolonged incubation always resulted in very poor detection of protein bands at the expected sizes. Also freezing of embryos or extracted protein interfered with the detection of Dop bands. These findings suggest that the endogenous Dop protein might be unstable under these conditions. Another possibility is that the peptide sequence the antibody was raised against is target for post-translational modification

in the Dop protein. Post-translational modification like phosphorylation and ubiquitination has been shown for MAST kinases and might interfere with the binding of the antibody to Dop.

4.2.1.4. Ectopically expressed Dop complements the lethality of dop^1 and dop^{LH10}

dop^1 and dop^{LH10} carry different mutations in the dop gene. The mutation in the dop^1 allele creates an isoleucine to phenylalanine missense mutation in the kinase region at position 954. This mutation is close to the D958 residue, which is predicted to function as proton acceptor. A similar mutation in RSK2 results in 90% reduction of kinase activity (Field et al., 2006). As a mutant protein is expressed in dop^1 mutants dop^1 is most likely a partial loss of function allele. dop^{LH10} is likely to be a null allele. To test the strengths of the different dop alleles and to gain additional proof that the cellularisation defect derives from loss of Dop function transgene rescue experiments were performed.

Using dop transcript-specific primers the cDNA of dop was amplified by PCR and cloned into an expression vector. The expression vector allowed generate transgenic flies, in which germ line transformation inducible expression of dop cDNA can be achieved (see material and methods). To test the possibility of complementation of the lethality in dop mutants, expression of transgenic dop was induced in dop^1 and dop^{LH10} embryos (Tab. 6.4). Expression of dop transgenes was induced using the Gal4/UAS system. The expression level of the dop transgene was varied by using two copies of a Gal4 transgene driven by a tubulin promoter (see description of Tab. 6.4 for exact genotypes). High expression levels of ectopic Dop did not rescue lethality of dop^1

mutant embryos, presumably because over expression of Dop-HA and Dop-GFP leads to a dominant developmental arrest in the syncytial division stages (see 4.2.3). However, lower expression levels of the *dop* transgene expression in the *dop* mutant genetic background showed increasing survival rates. Reduction of *dop* expression to 50 % led to 9.3 % survival while further reduction of expression by lowering the temperature from 25 to 20 degree resulted in 50.2 % survival in *dop*^{1} mutants. Similar results were achieved in the *dop*^{LH10} mutant background. It is to note that the wild type control embryos expressing Gal4 showed a lethality of 14.2 %. The rescued embryos developed into hatching larvae that developed into fertile flies (not shown). These data show that the defects in *dop*^{1} and *dop*^{LH10} mutants can be rescued at equal levels by adding back *dop* through transgenic expression. The experiments prove that *dop*^{1} and *dop*^{LH10} are loss of function mutations of *dop*. A reason for not reaching 100 % survival rates in the rescue might be the use of a promoter different from the endogenous *dop* promoter.

	control 25°C	dop1 rescue (high) 25°C	dop1 rescue (low) 25°C	LH10 rescue (low) 25°C	control 20°C	dop1 rescue (low) 20°C	LH10 rescue (low) 20°C	mat::Gal4 25°C
■ embryo lethality	894	409	1023	596	201	225	305	49
■ embryo survival	0	17	105	69	0	227	218	297
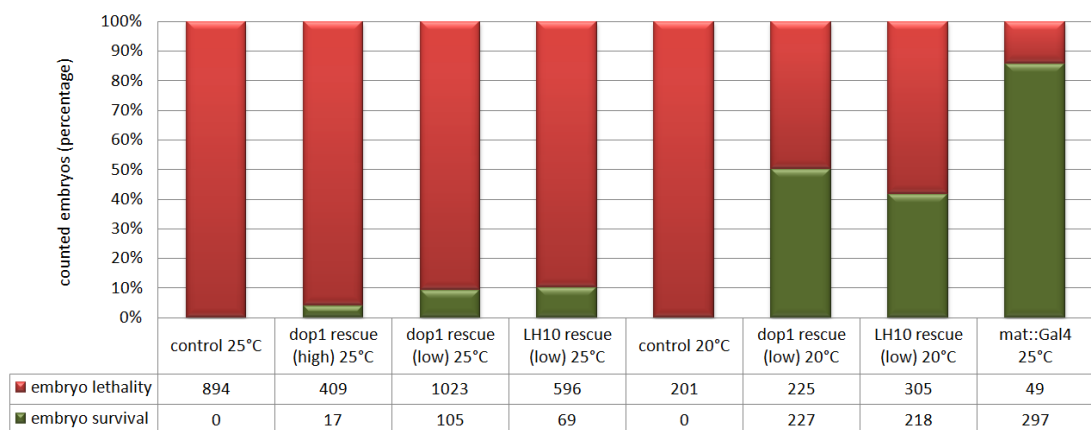
Tab. 6.4: Expression of a *dop* transgene rescues the lethality of *dop*^{1} and *dop*^{LH10} mutant embryos. Flies carrying the cloned *dop* gene were crossed against *dop*^{1} and *dop*^{LH10} mutant flies. The expression of the *dop* was induced by the Gal4/UAS system using either one or two gene copies of a maternally expressed Gal4 protein. Selected flies were cultivated on egg collection chambers and eggs were counted after four hours and again after 48 hours (numbers are displayed under the columns). Control embryos did not show any survival at 25 or 20°C. *Dop*^{1} and *dop*^{LH10} embryos showed a slight rescue effect, if transgenic *dop* was expressed; survival rates were higher when the expression level of the transgene was reduced. **Genotypes are (in column):** *mat15::Gal4/+;dop*^{LH10}/*MR15* **(1+5)**, UAS::*dop/mat15::Gal4;dop*^{1}/*Df(3L)XG9)*, *mat67::Gal4* **(2)**, UAS::*dop/ mat15::Gal4;dop*^{1} **(3+6)**, UAS::*dop/ mat15::Gal4;dop*^{LH10}/*MR15* **(4+7)**, *mat15::Gal4* **(8)**.

4.2.1.5. The localisation of Dop during early development

The mutant phenotype of *dop*[1] embryos indicates that *dop* is essential for cellularisation. It has been shown that many regulators of cellularisation are localised to specific compartments like the membrane, the cytoskeleton, nuclei or cytoplasmic vesicles. To investigate how Dop might control cellularisation the localisation of Dop protein in early embryos was analysed. First the localization of endogenous Dop protein was analysed using the Dop antibodies described above. The localisation pattern using these antibodies showed diffuse distribution (supplementary material). To determine the specificity of the staining, a control staining was performed using null mutant *dop*[LH10] embryos. This control also showed significant amounts of diffuse staining and therefore the specificity of the Dop antibodies for immune-fluorescence labelling is questionable. For this reason transgenic flies expressing Dop or Dop-fragments tagged with either HA or GFP tags proteins were created (see material and methods).

Expression of Dop-GFP in early embryos showed that Dop-GFP has a dynamic localisation pattern (Fig. 6.5). In the short interphases during syncytial division stage Dop-GFP localises to the cytoplasm but is excluded from the nuclei. At the onset of mitosis the GFP signal enters the nuclear space and becomes enriched in the region of the mitotic spindle (Fig. 6.5B, C). In metaphase Dop-GFP covers the mitotic spindle (Fig. 6.5D). In anaphase and telophase the signal accumulates at the central region of the mitotic spindle (Fig. 6.5E-G). As the new nuclei are surrounded by nuclear membrane in late telophase, Dop-GFP is excluded again from the nucleus. Isolated dots of signal are found in the nuclei after the nuclear membranes are re-established. The structures that these dots associated with could not be revealed. As the fluorescence of Dop-GFP

in the nucleus fades quickly the dots might derive from intra-nuclear protein degradation sites.

Co-localisation studies with Dop-GFP and markers for microtubules or the proteasome might give more insights into the localisation of Dop. These experiments could not be done due to time restrictions. However, the expression of Dop during syncytial cleavage cycles could be compared with the localisation pattern of a microtubule associated protein called Jupiter (Fig. 6.5K, L). Jupiter-GFP expression localises uniformly to microtubules and serves therefore as a good comparison to the Dop-GFP signal (Karpova et al., 2006). A direct comparison between the GFP-tagged proteins shows that Dop might localise to a fraction of microtubules only. Striking difference between Dop-GFP and general microtubule localisation can be seen in early
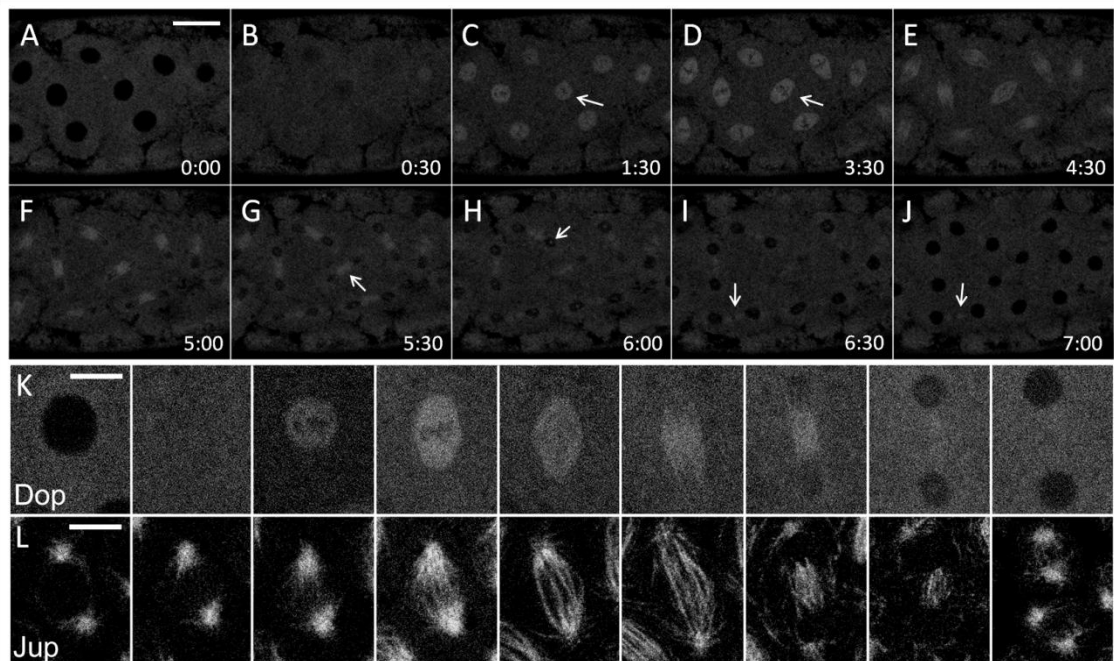
Fig. 6.5: Dop-GFP localises to the mitotic spindle during syncytial cell cycles. Time points of a video-timelapse analysis taken from an embryo expressing a *dop-GFP* transgene driven by *nanos::Gal4* (A-F). Dop-GFP localises diffusely in the cytoplasm during interphase (A). As the nuclear membrane breaks down during prophase the protein enters the nuclear space (B) and localises to the mitotic spindle (arrows in C and D). During telophase Dop-GFP becomes visible at the central spindle region (arrow in G, I-J) and in two bipolar dots (arrow in H). With the establishment of the new nuclear envelope Dop-GFP becomes excluded from the nuclear space (time is displayed in min:sec; scale bar: 50 μm). Characteristic time points from this movie were compared to the pattern of the microtubule marker Jupiter-GFP (K, L)(scale bar: 10 μm).

Metaphase and during Ana-/Telophase where Dop localises to the central spindle region exclusively. This finding might indicate a specific role for Dop in the structure of the mitotic spindle or Dop transport towards the plus ends of microtubules. However, localisation of Dop to other microtubule sub-populations or other cellular compartments might be overshadowed by the prominent cytoplasmic signal. This diffuse cytoplasmic signal might result from an excess amount of Dop-GFP protein in the embryo. As the Dop-GFP protein was expressed in wild type embryos endogenous Dop might also prevent Dop-GFP from localising in a more precise pattern. A possible way to test this hypothesis would be the expression of Dop-GFP in *dop* null mutant embryos. Another valid theory is that Dop-GFP does not co-localise to microtubules but becomes enriched within the nuclear membrane during chromosomal segregation. The nuclear membrane is not completely dispersed in metaphase and Dop-GFP protein might accumulate in the nucleus due to transport through the nuclear pore complexes (personal communication with J. Raff).

During cellularisation Dop-GFP localisation could be observed at microtubule baskets around the nuclei when overexpressed with stronger promoters only (*mat*α4-tub-*GAL-VP16* on chromosome II and III). However, strong expression of Dop-GFP led to early lethality in almost all observed embryos, so that a proper analysis could not be conducted (see chapter 4.2.3).

4.2.1.6. Localisation and function of Dop domains

To determine whether individual protein domains of Dop exhibit distinct subcellular binding specificities, the localisation of tagged DUF and PDZ domains was determined in the embryo. Ectopic expression of a protein corresponding to the DUF domain

localised to the membrane furrow (Fig. 6.6). During the syncytial cleavage cycles DUF-HA (HA is a 3 copy hemagglutinin-tag) localised to the pseudo cleavage furrows and during cellularisation it was found at the furrow canal in fixed embryos. Between the syncytial divisions DUF-HA localises to the furrow regions exclusively (Fig. 6.6A). During metaphase in syncytial divisions DUF could also be found in close proximity to the chromosomes (arrows in Fig. 6.6B). This localisation might also correspond to the central spindle. During the slow phase of cellularisation DUF-HA accumulates at the growing furrow (Fig. 6.6F). This signal decreases during the fast phase of cellularisation (Fig. 6.6H). The localisation pattern of the DUF domain was reproducible when different fixation methods were applied (Fig. 6.6A-H show formaldehyde fixations; I-K are heat fixed embryos). As the morphology of the furrows is affected in dop^1 mutants (see 6.2) these data suggest that Dop is regulating furrow structure by interacting with other localised proteins.
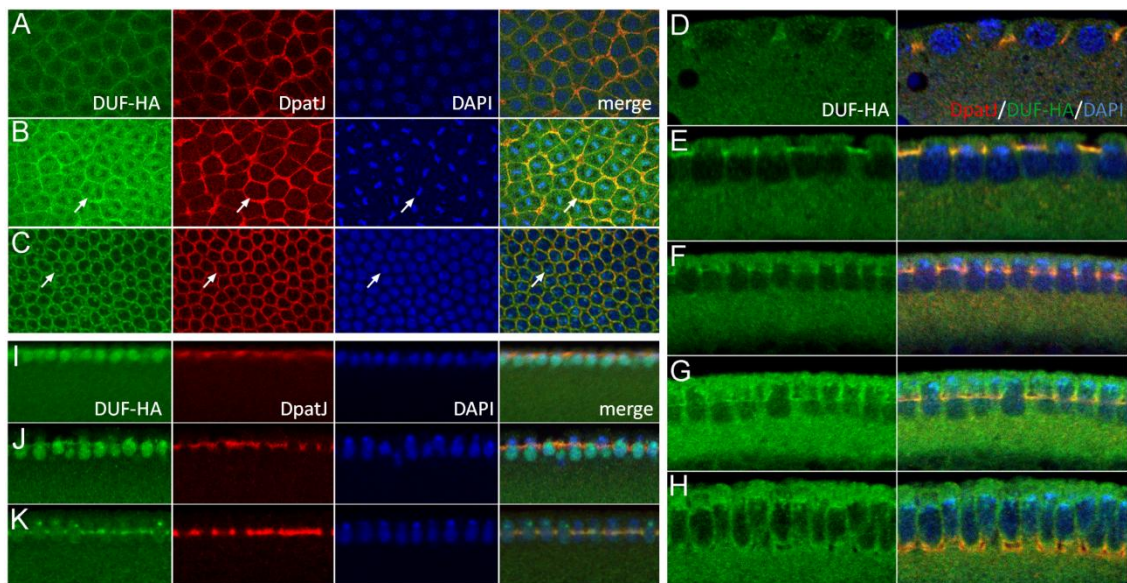
Fig. 6.6: DUF-HA localises to the furrow region. DUF-HA expression in early embryos using a mat::Gal4 driver line shows localisation to the pseudo cleavage furrows during syncytial division cycles and to the furrow canals during early cellularisation. The localisation of the DUF domain to the furrow region during interphase in formaldehyde fixed embryos (A). In metaphase DUF can be found at the metaphase plate, surrounding the chromosomes (B). At onset of cellularisation DUF-GFP localises to the furrow canal and to single dots in the nuclei (C). D-H show the localisation of DUF during cellularisation. In early cellularisation DUF is highly concentrated at the furrow while it becomes less enriched during the progression to the fast phase of cellularisation. Using a fixing method that extracts cytoplasmic proteins (heat fixation) DUF can also be seen at the furrow, however the nuclear staining becomes stronger (C). DUF-HA localisation is shown in green, DpatJ in red and DNA in blue.

The PDZ domain of Dop might be essential for Dop localisation. Proteins containing PDZ domains are often found in protein complexes associated with the control of cell polarity. PDZ domains bind conserved amino acid motifs usually located directly at the carboxy terminus of the target protein. Proteins harbouring PDZ domains often function as scaffolding proteins. An example of such a protein is Bazooka/Par-3, which carries 3 PDZ domains and is essential for the assembly of adherens junctions (Müller, 1996; Kuchinke et al., 1997). Many proteins containing PDZ domains localise directly to the lateral membrane or the furrow canal (reviewed in Bilder, 2001). Therefore it was expected that the Dop PDZ domain might localise to a membrane compartment. Surprisingly, expression of PDZ-HA and PDZ-GFP showed a punctual distribution of the protein. The signal was enriched in the basal region of the nuclei during cellularisation (Fig. 6.7A). As dop^1 mutants show a defect in lipid droplet transport the PDZ localisation pattern might relate to lipid droplets.

Two methods to distinguish whether PDZ-GFP binds lipid droplets were performed. By centrifugation experiments with early embryos the lipid droplets can be separated from nuclei and other cytosolic components (Tran and Welte, 2010). This fractionation method is very easy to perform and very robust. Conventional fractionation assays use lysis buffers and (usually) a sucrose matrix that can change the properties of protein bonds. The centrifugation of embryos leads to a comparable separation of proteins in completely native conditions. Centrifugation leads to fractionation of the embryo into three layers, a bright lipid droplet cap, a layer with nuclei and a layer with other cytosolic components (see 6.7D, E). Centrifugation of embryos expressing PDZ-GFP showed accumulation of GFP signal in the lipid droplet cap (Fig. 6.7C, D). The localisation of PDZ-GFP is comparable to the localisation of lipid droplets stained with an antibody against the lipid droplet marker Klarsicht in centrifuged embryos (Welte,

2002). This finding was underlined by sucrose-gradient centrifugation experiments using lysate of PDZ-HA expressing embryos that showed an enrichment of PDZ-GFP in the lipid droplet fraction (Fig. 6.7F).
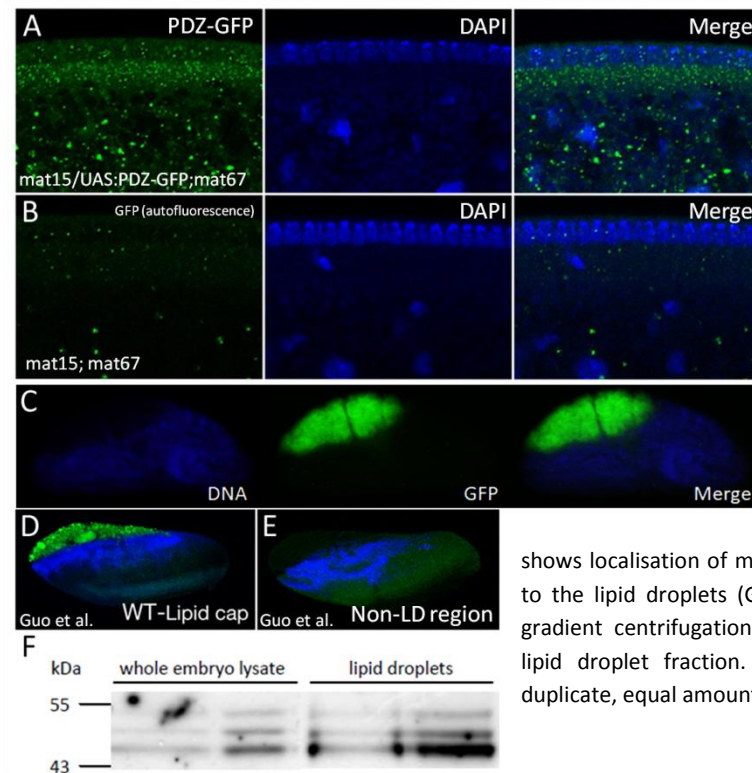
Fig. 6.7: PDZ-GFP binds to lipid droplets. Embryos expressing the PDZ-domain tagged with GFP were fixed and stained with a GFP antibody. The PDZ-GFP protein localises at the basal side of the nuclei (A). Wild type embryos fixed and stained with the same procedure do only show unspecific labelling (B). Embryo centrifugation leads to aggregation of Dop-GFP in the lipid droplet fraction (C). A comparison of this pattern to embryos published from the lab of M. Welte (Guo et al., 2005) is shown in D (lipid droplets shown by Klar staining; green). E shows localisation of mutant Klar protein which cannot localise to the lipid droplets (Guo et al., 2005). Conventional sucrose gradient centrifugation shows enrichment of PDZ-GFP in the lipid droplet fraction. The experiments were performed in duplicate, equal amounts of protein were used (F).

These experiments suggest that the PDZ domain might be regulating an interaction of Dop with lipid droplets. In a previously published proteomic study, Dop has been found associated with purified lipid droplets (Cermelli et al., 2006). Since lipid droplet transport is disrupted in dop^1 mutant embryos, an association of Dop with lipid droplets might be necessary to regulate the transport machinery attached to the lipid droplets (Welte, 2010).

To test the requirement of the Dop domains for Dop function during cellularisation a domain function analysis was performed. For this reason transgenes expressing *dop* versions with deficiencies for the DUF, the kinase and the PDZ domains were cloned and used to create transgenic flies (Fig. 6.8A). The expression of full length Dop,

Dop$^{\Delta DUF}$, Dop$^{\Delta Kinase}$, and Dop$^{\Delta PDZ}$ was induced in *dop* mutants (Fig. 6.8B). The expression of full length Dop resulted in survival of 62% of the embryos, while expression of the deletion mutants did not show a significant rescue of survival. This indicates that each of the conserved domains of Dop is essential for cellularisation. Dop$^{\Delta DUF}$ and Dop$^{\Delta PDZ}$ induced low level survival rates while Dop$^{\Delta Kinase}$ showed no surviving embryos. This finding demonstrates that the kinase domain is essential for the function of the protein. Furthermore, the study suggests that Dop localisation by the DUF and PDZ domains is needed for localised activity of the kinase. The use of the deficient proteins for localisation studies might further prove that Dop is regulated by its subcellular position. The DUF and PDZ domains might also be needed to bind and position substrates of the kinase domain.

	control	Dop full length	Dop$^{\Delta DUF}$	Dop$^{\Delta Kinase}$	Dop$^{\Delta PDZ}$
hatch	0.0 %	61.9 %	1.2 %	0.0 %	2.7 %
dead	100 %	38.1 %	98.8 %	100 %	97.3 %
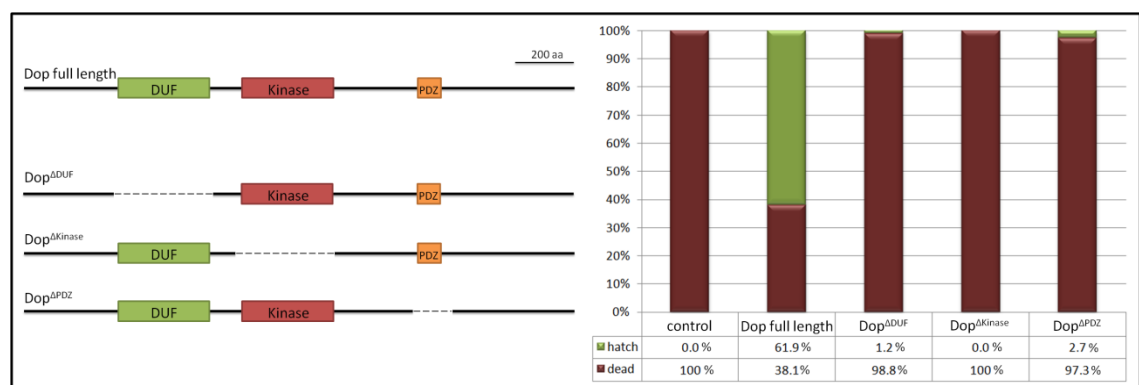
Tab. 6.8: Structure-function analysis using survival rates in *dop* mutant embryos. Full length Dop and the proteins expressed by the deficiency constructs are shown in A. These proteins were expressed in dop1/dopLH10 mutants (B). Expression of these constructs resulted in varying degrees of survival. The numbers of the counted eggs: control (566), full length (1019), Dop$^{\Delta DUF}$ (1130), Dop$^{\Delta Kinase}$ (747), Dop$^{\Delta PDZ}$ (1296).

The localisation analysis performed in this chapter suggest an association of Dop with microtubules, the membrane furrow and lipid droplets. The localisation of Dop is regulated in part by the conserved DUF and PDZ domains. The DUF domain localises to the furrow canal during syncytial divisions and cellularisation while the PDZ domain might bind to lipid droplets. Dop mutant embryos show defects in membrane furrow

organisation and disruption of lipid droplet transport. The functions of the DUF and PDZ domain might be needed to localise the kinase domain to substrate proteins. Lipid droplet transport and the membrane furrow structure also rely on microtubules. Association of MAST kinases to microtubules of the spermatid manchette has been shown previously to be dependent on microtubule-associated proteins (MAP) (Walden et al. 1993). Potential MAPs that interact with Dop could include Dynein and Kinesin transport complexes, a group of proteins addressed in the following chapter.

4.2.2. Developmental defects in *dop* mutant embryos

Cellularisation is a unique process leading to the formation of the polarised blastoderm epithelium. Loss of polarised structure in epithelial tissues has been shown to result in epithelial-to-mesechymal transition - one of the possible entry points into malignant behaviour of tumour cells (Humbert 2003; Bilder 2004). Dop mutant embryos show defects in the establishment of a polarised epithelium and might help to gain new insights into the control of cell polarity. In this part of the thesis, polarity establishment was investigated by microscopic analysis of the localisation and recruitment of polarity regulators in wild-type and *dop*[1] mutant embryos. Studying the developmental defects in *dop* mutants will provide hints for the function of Dop and of mammalian MAST kinases.

4.2.2.1. *dop*[1] mutant embryos mis-localise apical and baso-lateral polarity markers

To identify which cell-biological processes are affected in *dop*[1] mutants during cellularisation epithelial polarity markers were visualised. The experimental

approaches were microscopic analysis of immunolabelled embryos and live imaging of embryos expressing GFP-tagged proteins.

Antibody staining of the proteins Slow as molasses (Slam) and Discs Large (Dlg) was used to analyse membrane ingression in fixed embryos (Fig. 6.9). Slam is considered as a major regulator of furrow canal structure (Lecuit et al., 2002). Slam localises to the basal membrane region and regulates furrow canal structure by recruiting RhoGEF2. RhoGEF2 is needed for Rho1 activation and enables actin remodelling (Wenzl et al., 2010). Slam is also required for the recruitment of proteins like Armadillo (Arm/β-catenin), and cytoplasmic myosin (Lecuit, 2002; Stein et al., 2002). Dlg is a scaffold protein containing three PDZ domains and an inactive guanylate kinase domain. Dlg is necessary for the formation of apico/lateral septate junctions in epithelial cells (Woods et al., 1996). Absence of Dlg is also resulting in mis-arrangement of the apical junctions. Apart from regulating apico/basal polarity Dlg has been identified as a tumor suppressor as Dlg mutant imaginal disc cells show an enhanced level of cell proliferation (Woods et al., 1996) Using Slam and Dlg as membrane marker reveals the structure of the membrane and the progression of cellularisation.

Wild type cellularisation starts after the last syncytial division (Fig. 6.9A-F). Dlg and Slam localise to the lateral and basal membrane compartments respectively. Imaging of wild type embryos showed the membrane reaching into the embryo between the elongating nuclei as a pointed structure. The lateral membrane, identified by Dlg localisation, is ending in a tear shaped membrane fold, identified as the furrow canal by Slam staining. During mid cellularisation Dlg is localised to the basal junctions with a bias towards the apical membrane. At the end of cellularisation Dlg is also found in the apico/lateral septate junctions. Slam localises to the furrow canal exclusively. At onset
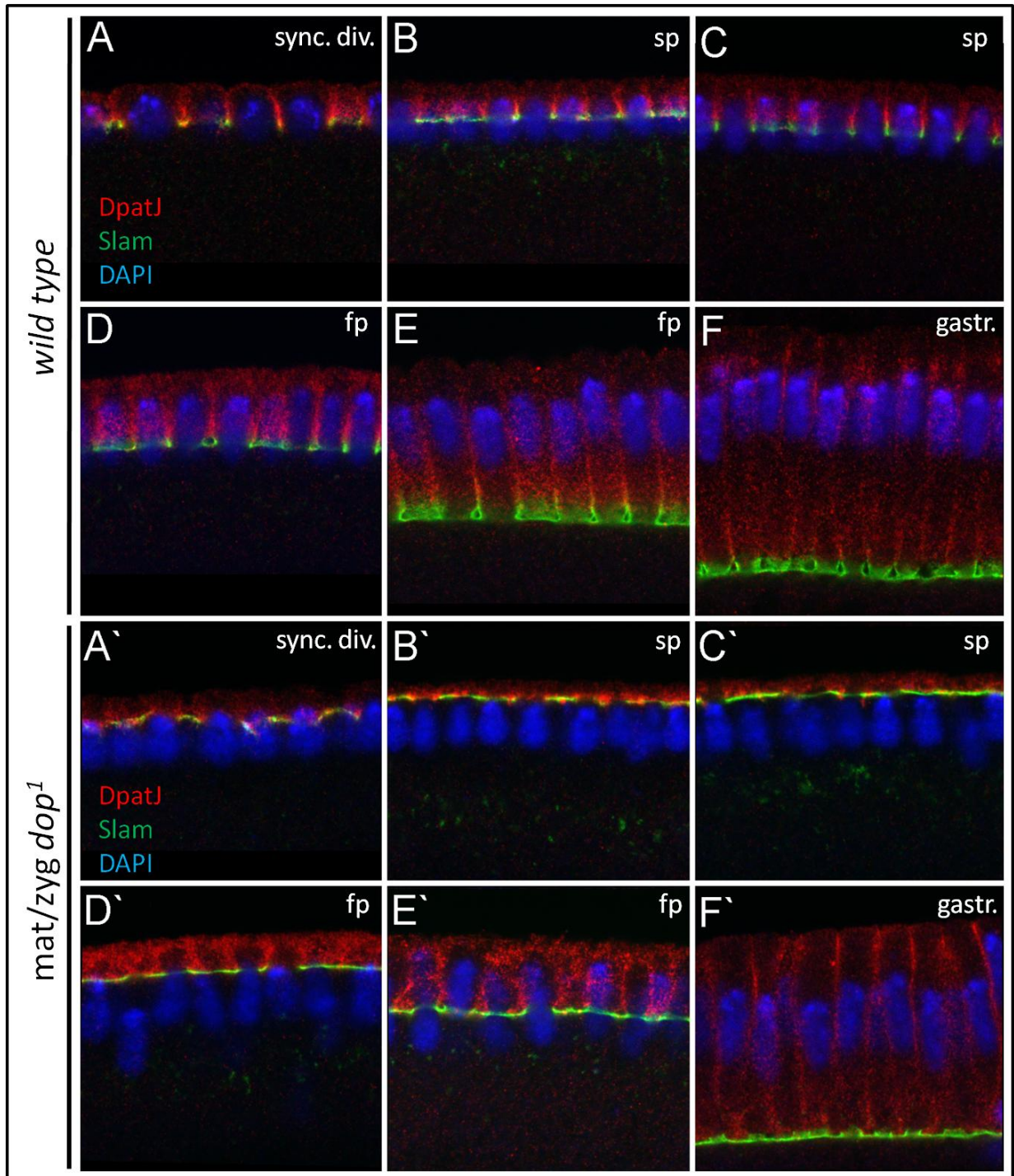
Fig. 6.9: Comparison of cellularisation in wild type and *dop*[1] mutants. Embryos stained with antibodies against Dlg (red) and Slam (green); nuclei stained with DAPI (blue). Wild type embryos were fixed using the heat fixation protocol (A-F). Wild type cellularisation progresses through a slow phase (B-D) and a fast phase (E-F). The Dlg protein is enriched at the baso/lateral membrane and does not overlap with the Slam signal at the furrow canal. *dop*[1] mutant embryos are shown in (A`-F`). These mutants do not show membrane growth during slow phase. The membrane growth during fast phase produces a disrupted membrane pattern. Slam staining shows enlarged furrow canals. Fixed embryos were staged by the extent of nuclear elongation, as described by (Lecuit et al., 2002). Developmental stages are indicated by: sync. div (syncytial divisions), sp/fp (slow or fast phase of cellularisation), gastr. (post-cellularisation).

of cellularisation Slam marks a small region of membrane between the nuclei and reveals a very compact furrow during early cellularisation (see Fig 6.9B, C) that expands slightly to form a tear shaped structure during fast phase of cellularisation (Fig 6.9D). At the end of cellularisation the furrow canals expand further until they fuse with each other and close the membrane around the nuclei (Fig. 6.9F). This process forms a polarised epithelium with the depth of 30 μm.

dop^1 mutant embryos show an irregular Slam localisation (Fig. 6.9A`-F`). At onset of cellularisation Slam does not focus between the nuclei but localises to a broad membrane region. During fast phase of cellularisation mutant Slam localisation suggests a furrow canal that is flat instead of having the normal tear shape (compare Fig 6.9D and D`). However, the furrow canal is still the leading edge of the invaginating membrane and accumulates actin in wild type proportions (data not shown and shown by Meyer, 2006) and the actin remodelling Rho1 (see Fig. 6.10M-P). It is to note that Rho1 localisation seems to be less restricted to the furrow canal and is also found in lateral regions of the membrane. Another furrow marker, dPatJ localised in the same way as Slam (data not shown).

Maternal/zygotic dop^1 embryos also show aberrant localisation of Dlg. Dlg localisation is not peaking at the basal junctions like in wild type, but is distributed over the whole lateral membrane (Fig. 6.9D`, E` and Fig. 6.10B). Dlg is highly scattered throughout the cytoplasm and is also found at high level at the furrow canal membrane. In wild type embryos the furrow canal region is a separated compartment that does not mix with the lateral membrane (Lecuit, 2002; Sokac et al., 2008). Dlg at the furrow canal migh indicate loss of the diffusion barrier between lateral and basal membrane compartments or misdirected vesicle insertion of vesicles containing Dlg at the furrow.
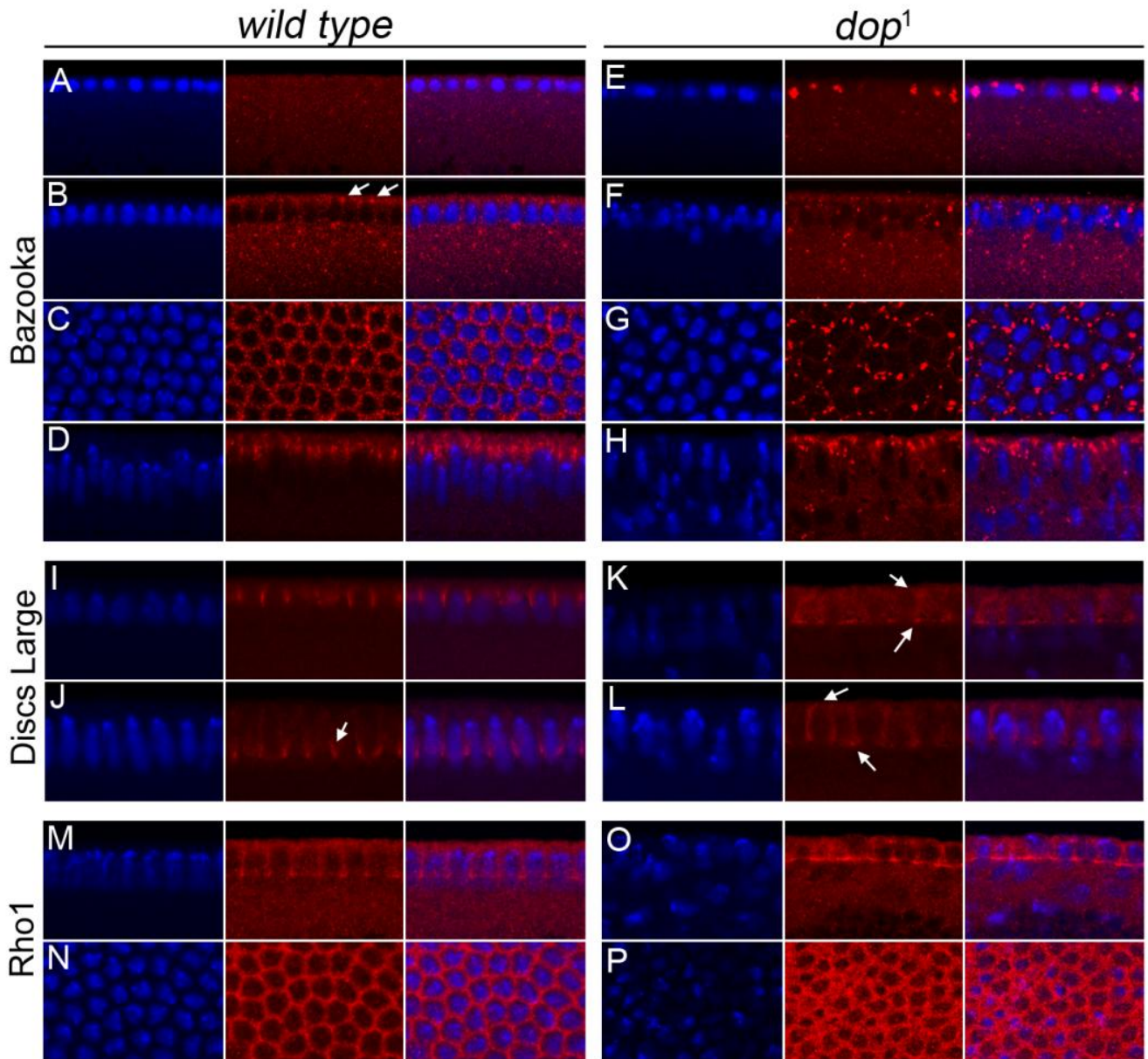
Fig. 6.10: *dop*[1] affects the localisation of apical, lateral and basal polarity markers. Wild type and *dop*[1] embryos have been fixed and stained with antibodies against Baz (A-H), Discs Large (I-L) and RhoA (M-P). Baz is hardly found at the apical membrane before late cellularisation in wild type embryos (A-C). During fast phase of cellularisation Baz clusters are found at the apical membrane (B, C). During gastrulation Baz becomes established at the apical adherens junctions. In *dop*[1] embryos Baz is found in large aggregates already before onset of cellularisation (E). During cellularisation no Baz is incorporated into the apical membrane (F, G). During gastrulation Baz is partially localised correctly (H). The baso/lateral marker Dlg localises to the basal junctions adjacent to the furrow canal. Dlg signal fades with a bias in apical direction but is sharply restricted from the basal membrane (I, J). In *dop*[1] embryos Dlg spreads over the membrane boundaries. Accumulation of Dlg can be found at the furrow and at the apical membrane (K, L). Rho1 is localised at the furrow canal. On top view of the embryo shows Rho1 localisation in a hexagonal pattern (M, N). In the mutants Rho1 staining is located at the furrow but can also be observed at the lateral membrane (O, P). Proteins (indicated for each panel on the left) labelled in red, nuclei in blue.

Baz acts as a scaffolding protein and binds many proteins to regulate the maintenance of the apical junction also called zonula adherens (Wieschaus et al., Müller et al. 1996). This cell-cell junction is established after cellularisation (Wieschaus, 1984 and Tepass, 1993) and *baz* mutant embryos do not show defects before gastrulation. However, Baz is necessary for the recruitment of E-cadherin into the spot adherens junctions during cellularisation (McGill et al., 2009). In wild type embryos apical clusters containing Baz protein can be found during late cellularisation at very precisely positioned apical cell-cell contacts sites (Fig. 6.10A-D). In dop^1 embryos the protein accumulates very early, even before onset of cellularisation in large protein aggregates (Fig. 6.10E-H). These Baz containing aggregates are not recruited to the membrane during later cellularisation implying that Baz might either be mis-regulated itself or its transport fails due to mis-regulation of its interaction partners. The localisation of Baz has been analysed closer using a different fixation protocol that maintains cytoplasmic structures (FA-fixation). This analysis showed accumulation of Baz in vesicle like structures (Fig. 6.11).

The localisation studies showed that the dop^1 mutation affects several aspects of cellularisation. The size of the furrow canal region, the integrity of the invaginating membrane, and the recruitment of cell-cell junction proteins are affected.
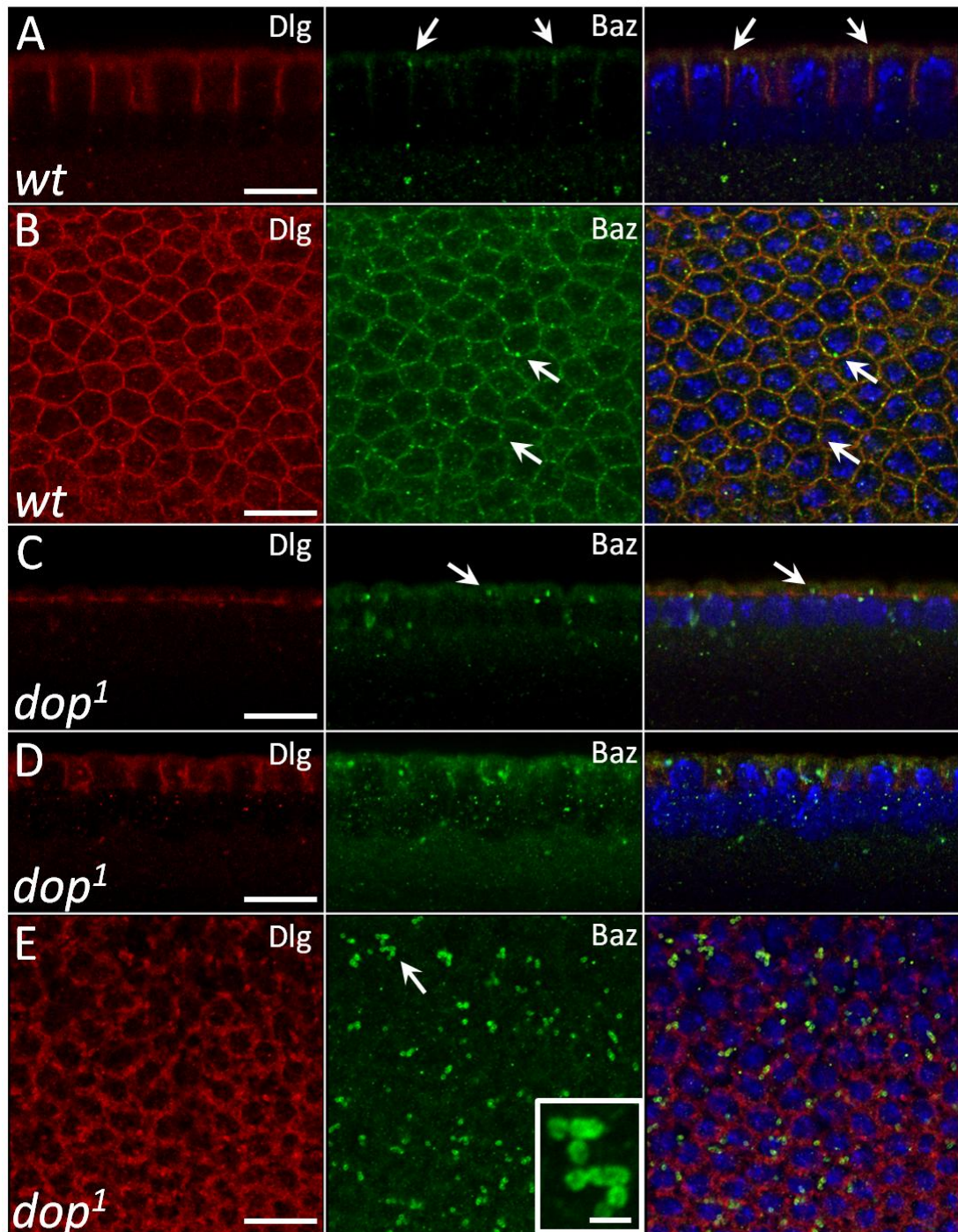
Fig. 6.11: Abnormal localisation of Baz in *dop*[1] mutant embryos. Embryos were FA fixed and stained against Baz (green). Nrt antibodies were used to stain the membrane (red). Transversal sections shown in A, C and D; en face view is shown in B and E. In wild type embryos Baz aggregates (green) are found in the apical SAJ at onset of the fast phase of cellularisation (A, B; arrows). In *dop*[1] mutants Baz accumulates in large cytoplasmic clusters (C-E). The shape of the Baz aggregates is shown in the inset (inset in E). Scale bar represents 20 μm; scale bar in inset represents 4 μm.

4.2.2.2. Dop controls the formation of the membrane furrow

The proper placement of the cytokinetic furrow is important for all cells proceeding through cellular division. The furrow canal of *Drosophila* embryos can be used as a

model to study furrow organisation (Sisson et al., 1999; Monzo et al., 2006). Antibody staining against Slam demonstrated a mis-arrangement of the furrow canal in dop^1 mutants. Slam is an early zygotic expressed furrow marker. Slam localisation to the membrane is necessary for recruitment of RhoGEF2 and therefore important for restructuring the furrow canal (Wenzl et al., 2010). Dop might control furrow formation by influencing the positioning of furrow determinants like Slam. The defect in furrow formation is the earliest defect in the development of dop^1 mutants. How the furrow is organised is not yet fully understood. Investigation of furrow formation might reveal the cause of the lethality in the *dop* mutants and might indicate a function for the Dop kinase as a new regulator of cytokinesis.

To look at furrow canal structure in more detail Slam staining was used as a marker for a quantitative evaluation of furrow size (Fig. 6.12). For this purpose embryos were carefully staged and the diameter of the furrow was measured throughout cellularisation. Wild type embryos showed distribution of Slam in a dispersed pattern (spread over 4.4 µm) before cellularisation. During the slow phase of cellularisation Slam localised in a very narrow region, resulting in a very compact furrow (1.7 µm) (Fig. 6.12C). In fast phase the furrow expanded slightly (2 µm). The contraction of the furrow at the end of cellularisation was not measured due to lack of embryos at the right stage. Measurement of furrow diameter in dop^1 embryos showed that Slam is not focussed into a narrow furrow region at slow phase. The overall size of the furrow canal was found to be about 3 times as large as in wild type (between 8-4 µm). In many places the furrow region expanded so far that a physical hindrance for the nuclei might result.
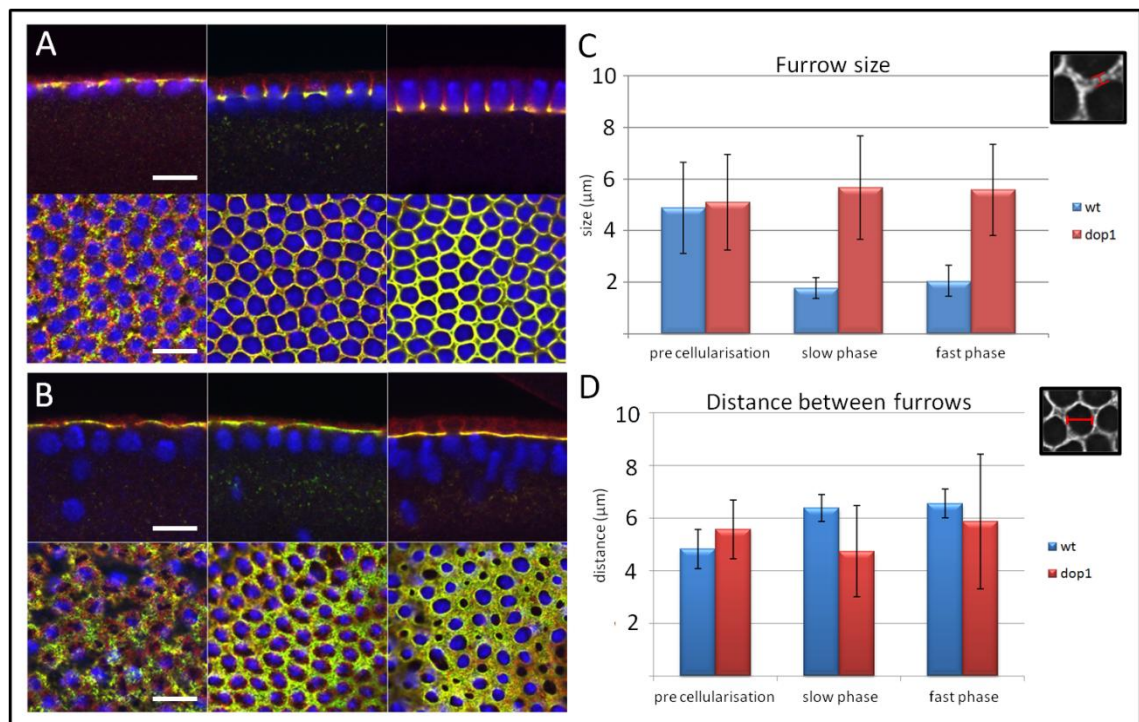
Fig. 6.12: The furrow canal region is expanded in *dop*[1] mutants. Immunofluorescence images of wt and *dop*[1] embryos during cellularisation. Staining against furrow markers DpatJ (red) and Slam (yellow) shows that the furrow canals are abnormally expanded in the mutants (A, B). Measurement of the diameter of the furrow region shows the enlargement of the furrow in *dop*[1] mutants. Measurement of the opening between the furrow canals shows huge deviation from the norm in *dop*[1] embryos (white bar = 20 µm).

When the membrane furrow grows it has to encompass the nuclei. Small furrows are necessary to prevent their collision with the nuclei. In *dop*[1] mutants the furrows are enlarged and prevent the membrane from passing the nuclei. To see whether the collision of the furrow with the membrane is a common defect in *dop*[1] mutants the size of the opening between the furrows was measured (Fig. 6.12D). In wild type the space between the furrows has a diameter of 5 µm before onset of cellularisation and about 6 µm during slow and fast phases of cellularisation. In *dop*[1] mutants the values were similar to wild type before onset of cellularisation. However, during cellularisation a precise diameter could not be determined because of a large variation of values. This is because an estimated 50-80 % of the furrow openings were very small, but the remaining regions showed enlarged openings. These findings suggest that the membrane tension created by the enlarged furrows might tear the cellular

compartments apart and thereby create larger regions between the furrows in some places. In conclusion it was found, that the furrow is expanded already at the onset of cellularisation. Because premature furrows are already established during the syncytial divisions it was interesting to see whether these furrows are misorganised as well. However in fixed embryos this could not be determined because of the rapid cell cycles that do not allow discrimination between forming and established furrows.

To observe the formation of the furrow in living embryos GFP-tagged DE-Cadherin (Cad-GFP) was expressed. Over-expression of Cad-GFP in the early embryo leads to accumulation of GFP signal at the forming furrow. Wild type and dop^1 embryos expressing Cad-GFP were analysed using a spinning disc confocal microscope. Time points were taken every 30 seconds and each time point a stack of 30 slices was scanned. The stacks were assembled to projections covering 10 µm of the membrane and underlying cytoplasm to detect the complete Cad-GFP signal. Embryos were imaged throughout the syncytial divisions and cellularisation. Cad-GFP localises diffusely in a spotted pattern before new furrows are formed. After every syncytial cell division the Cad-GFP spots were recruited towards the newly formed furrow. To measure the speed of the furrow formation the region in which Cad-GFP spots are localised was determined for every time point. An example of how the region was defined is shown in Fig. 6.13A. The measured distances were plotted against time (Fig. 6.13D). During the 11th − 13th cell cycle the recruitment of the Cad-GFP to the furrow lasted roughly 8 minutes until the diffuse Cad-GFP signal was concentrated in a furrow with a diameter of 1 µm. After the last syncytial division the recruitment of Cad-GFP lasted 14 minutes. At the end of the image acquisition the wild type embryo arrived at the end of slow phase cellularisation (min. 115; Fig. 6.13D). Imaging of a dop^1 mutant embryo showed comparable focussing during cell cycles 11th − 13th. However in cell

cycle 14 Cad-GFP was aggregated in an abnormally broad furrow measuring up to 4 μm diameter. The furrow region accumulated Cad-GFP in a tubular pattern with significant difference to the furrow in wild type (compare the last pictures in Fig. 6.13B and C).

The transport of Cad-GFP to the furrow shows how proteins are recruited to the emerging membrane furrow. The dop^1 mutant embryos showed no significant recruitment of Cad-GFP at onset of cellularisation. In conclusion, the formation of the furrow is most likely disturbed because furrow determinants are not recruited properly at onset of cellularisation. The regulation of furrow formation is differentially regulated during syncytial divisions and cellularisation. During the syncytial cell cycles maternal gene products regulate all processes in the embryo while cellularisation is dependent on zygotic gene expression. As the defect in furrow formation only occurs at onset of cellularisation the underlying mechanism must be dispensable for the syncytial divisions and might rely upon zygotic regulation. This finding offers an interesting view on Dop regulation.
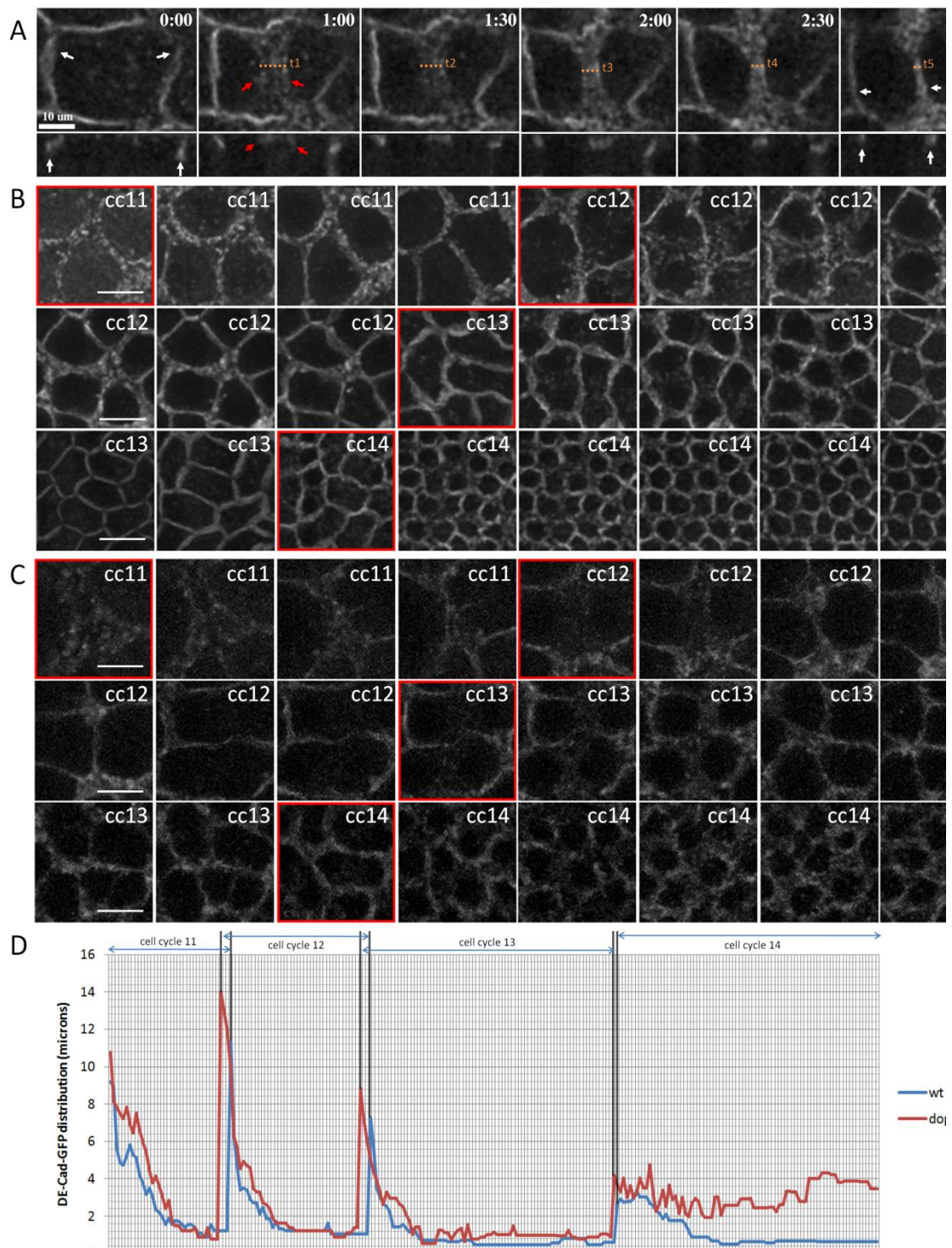
Fig. 6.13: The formation of cell boundaries is affected in *dop*[1] embryos. Live imaging of wild type and *dop*[1] embryos expressing Cad-GFP. Time points were taken every 30 seconds and each time point a stack of 30 slices was scanned (A). The stacks were assembled to projections (B wt) (C *dop*[1]). This data shows the recruitment of single Cad-GFP foci into the cellular boundaries after every syncytial division. The formation of new cellular junctions at the end of every cell division is marked by a red outline (in B, C) or asterisks (in D). The width of newly forming cellular junctions was measured (like indicated by the broken lines in A) and plotted against time (D). The decrease of width (in µm) relates to the speed of transport of DE-cadherin into the cellular boundaries. During syncytial divisions no difference of Cad-GFP focussing can be seen, however at onset of cellularisation DE-cadherin does not focus into the cellular junctions. Scale bar = 20 µm
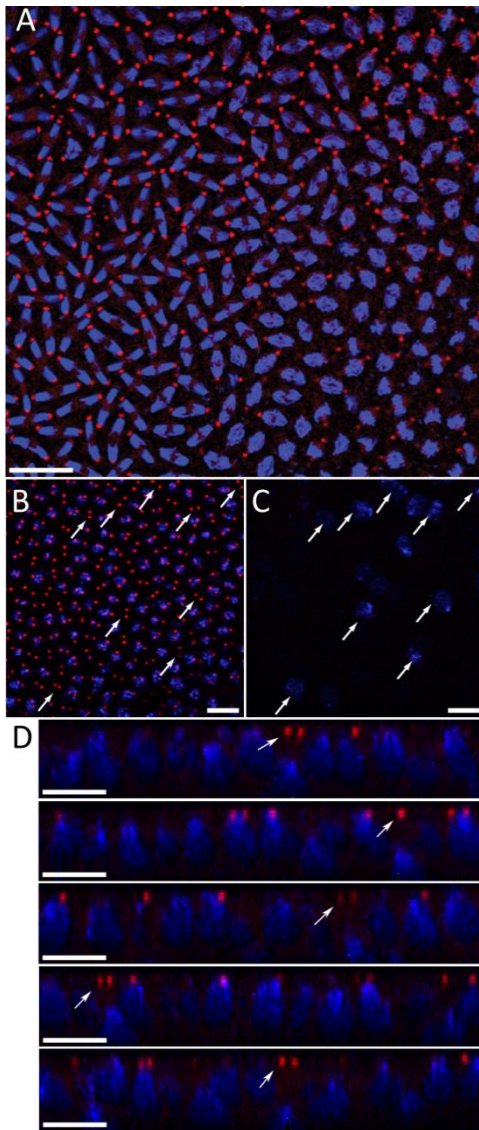
Fig. 6.14: Nuclei detach from the centrosomes in _dop_[1] mutant embryos. _dop_[1] embryos were fixed and hand peeled prior to incubation with a gamma-tubulin antibody. The centrosome location during syncytial divisions is shown (A). In _dop_[1] mutants nuclei detach from the membrane and from the centrosomes during early cellularisation. The centrosomes of dropped nuclei stay aligned with nuclei that did not detach (B, D arrows). Dropped nuclei are shown in (C). Scale bar represents 20 μm.

The position of the cytokinetic furrow has been shown to be dependent on the centrosomes and microtubule associated transport (Albertson et al., 2008; Foe and Dassow 2008; Foe et al., 2000; Glotzer, 2001; Rappaport 1961 and 1986; Vale et al., 2009). A possible function of the centrosomes is the establishment of a microtubule network that places microtubule plus ends in close distance to the furrow membrane. This organisation of microtubules might allow Kinesin and Dynein transport complexes to interact with the furrow membrane. The furrow defects in _dop_[1] mutant embryos might derive from mis-placement of the centrosomes. Therefore embryos have been fixed and stained with an antibody against gamma-tubulin, a marker for centrosomes. In wild type embryos the centrosomes locate between the nuclei and the membrane. During the rapid syncytial divisions the centrosomes can be found on opposing sites of the cytokinetic spindle. After segregation of the chromosomes the single centrosomes duplicate immediately. During the short S-phases each embryonic nucleus is therefore attached to two centrosomes. The centrosomes replicate also before cellularisation. During cellularisation the nuclei stay closely attached to the

centrosomes. In agreement with earlier studies no aberration from the norm was found in dop^1 mutants during syncytial cleavage cycles (Fig. 6.14A). During early cellularisation the dop^1 mutation causes detachment of the nuclei from the membrane. Figure 6.14B and C show nuclei arranged at the membrane (Fig 6.14B, 5 µm below the membrane) and detached nuclei (Fig. 6.14C, 20 µm below the membrane). It was found that DAPI stained nuclei that are detached from the membrane also loose attachment to the centrosomes (Fig. 6.14D). The centrosomes stay in close distance to the membrane and do not display any differences from the organisation in wild type embryos. This observation shows that the nuclear drop out defect in dop^1 mutants might originate from defects in the interaction between nuclei and microtubules which is needed to locate the nucleus in close distance to the centrosomes. The observed embryos also proved that the position of the centrosomes is not altered in the mutants and is therefore not the cause for the furrow defects.

4.2.2.3.   Dop dependent transport is needed for the localisation of Baz

dop^1 mutants show significant defects in microtubule associated transport. The first defects observed were in the transport of lipid droplets. Lipid droplet transport is differentially regulated during early embryonic development and occurs in two phases. Before cellularisation lipid droplets are transported into the centre of the embryo. This process has been shown to be dependent on Kinesin motor proteins. At the end of cellularisation before the cells are completely closed the lipid droplets are transported in an apical direction into the cells. The second phase of this transport is dependent on cytoplasmic dynein motors.

In fixed embryos the distribution of the polarity regulator Baz was found to be abnormal. Dynein dependent transport of Baz has been shown to be necessary for Baz localisation to the membrane previously (Harris and Peifer, 2005). One possibility to explain the phenotype in dop mutants therefore was that *dop* mutations affect Dynein dependent transport of Baz. To investigate the transport of Baz protein to the membrane a UAS::Baz-GFP transgene was expressed in early embryos using maternal Gal4 expression. Over-expression of Baz-GFP in wild type leads to incorporation of Baz-GFP into the lateral membrane and aggregation of Baz-GFP in cytosolic clusters (Fig. 6.15A; white arrows show Baz in the membrane, red arrows show the ectopic Baz clusters).

During cellularisation the Baz-GFP clusters move bidirectional along the apico/basal axis until they are incorporated into the growing membrane (Fig. 6.15). In wild type and dop^1 mutant embryos the movement of Baz-GFP clusters was analysed using time-lapse imaging and particle tracking software. Baz-GFP clusters of a size of 2 μm (10 pixels), which were visible for at least 2 minutes were tracked. In Fig. 6.14C the distance of movement of the Baz-GFP clusters along the apico/basal axis was plotted against time. Wild type clusters showed almost equal amounts of bidirectional movement with a net upwards movement of 3.9 μm. Most of the clusters could be tracked until their signal merged with the membrane signal (the movement of the membrane was tracked simultaneously; marked M). In dop^1 embryos the movement of
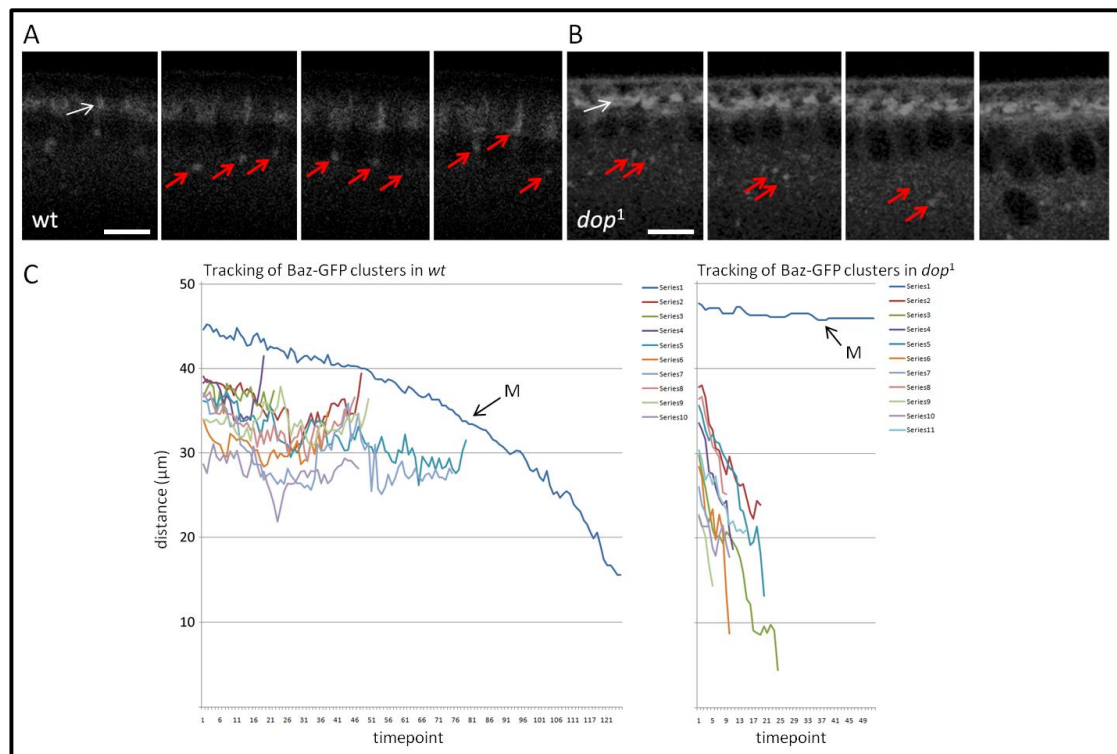
Fig. 6.15: The transport of Baz-GFP clusters is misdirected in *dop*[1] embryos. The transport of ectopically expressed Bazooka-GFP protein was monitored using confocal microscopy for life imaging. In wild type embryos Baz-GFP aggregates are transported along microtubules in a bi-directional manner. Using imageJ particle tracking software the movement of single aggregates was tracked and plotted against the movement of Baz-GFP incorporated into the membrane (M). Only particles of a minimal size of 10 pixels and visible for more than 5 time points were tracked. The graphical plot shows the net movement of the tracked particles towards the membrane (Series1-10 correspond to individual particles). The same analysis in *dop*[1] mutants shows that the net movement of the aggregates is directed away from the membrane. Aggregates were only measured at locations where the nuclei stayed at the membrane. Time points were taken every 20 seconds. Examples for measured aggregates are shown in (A).

the Baz-GFP clusters was directed towards basal regions almost exclusively (Fig. 6.15B). As a result a high amount of clusters were found in deeper regions of the embryo as compared to wild type. No Baz-GFP clusters were found to fuse with the apical membrane. In addition to the change in apico/basal movement Baz-GFP clusters were found to move in lateral direction through the embryo. These data show that the apico/basal transport of Baz is disturbed in *dop*[1] mutants. Since the localisation of Baz is dependent on Dynein and microtubules the transport defects might derive from mis-regulation of motor proteins and their complexes or break down of the microtubule structures. The regulation of Baz by phosphorylation represents a third possibility to explain defects in Baz recruitment.

Post-translational modification of Baz has been shown to regulate the localisation to junctional complexes and specific phosphorylation sites have been identified (Krahn et al., 2009). Three important phosphorylation sites in Baz are pS151 (phosphatidyl-serine 151), pS980 and pS1085. Phosphorylation of S151 and S1085 have been shown to be needed for correct Baz localisation in the follicle epithelium and the oocyte most likely by providing binding sites for 14-3-3 proteins (Benton and St. Johnston, 2003). Phosphorylation of S980 lowers Baz binding affinity to aPKC and over expression of a mutant S980A protein has been shown to disrupt the formation of cell-cell contact induced epithelial polarisation in MDCK cells (Suzuki, 2001, Nagai-Tamai, 2002). To check whether the phosphorylation of any of these sites is affected in dop^1 mutants, western blots using the available phosphospecific Baz antibodies were performed.

Baz protein in wild type and dop^1 embryonic extracts was investigated using phospho-specific Baz antibodies (Fig. 6.16). Protein samples enriched with embryos before (0-1h), during (1-2h and 2-3h) and after (3-4h) cellularisation were prepared and subjected to protein detection. Wild type and dop^1 embryonic extracts showed similar
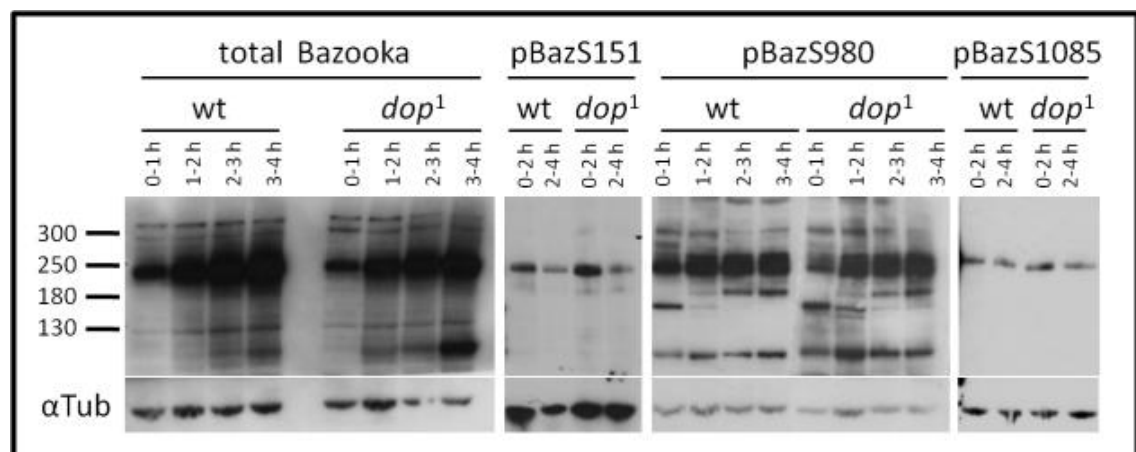
Fig. 6.16: Phosphorylation of three regulatory phosphorylation sites in Baz is not affected in dop^1 mutants. Western blots used for antibody detection of total Baz protein and Baz phosphorylated at S151, S980 and S1085. Embryos in different developmental stages were collected and used for protein extraction. The protein levels of total Baz were analysed using a monoclonal Baz antibody. The data are representative of triplicate experiments. Note that the Baz specific band size is below the 250 kDA marker.

levels of Baz expression. The phospho-specific antibodies against pS151 and pS1085 could detect single bands of Baz protein with equal intensity in wild type and dop^1 extracts. The pS980 antibody detected several bands and the banding pattern were generally similar between wild type and dop^1. Therefore no significant differences in phosphorylation of Baz could be found using phosphospecific antibodies against the three known phosphorylation sites of Baz.

4.2.2.4.   Dop mutations affect microtubule organisation

Intracellular transport is dependent on a functional microtubule network providing the tracks for the microtubule motors cytoplasmic Dynein and Kinesin. One reason for the transport defects seen in dop^1 mutants might be that the length or stability of the microtubules is affected. To assess the organisation of the microtubule bundles, the distribution of tubulin was imaged in early embryos. Tubulin was imaged in fixed embryos stained with a beta-tubulin antibody (Fig. 6.17). To prevent variations in staining due to different antibody amounts in the antibody dilutions, fixed wild type and dop^1 embryos were pooled prior to the tubulin staining. Before mixing the embryos the wild type embryos were incubated with a vasa antibody. Vasa is a marker of germ line cells and can be used to stain the pole cells. This marker was used to distinguish wild type from mutant embryos under the microscope (Fig. 6.17i, j). The imaging of wild type microtubules showed that microtubule bundles vary throughout early developmental stages. Before cellularisation the most abundant microtubules are found basal of the nuclei, reaching deep into the embryo. At onset of cellularisation the most prominent microtubule bundles are found in basket like structures around the nuclei and thinner bundles reaching the basal regions (Fig. 6.17B, C). In later
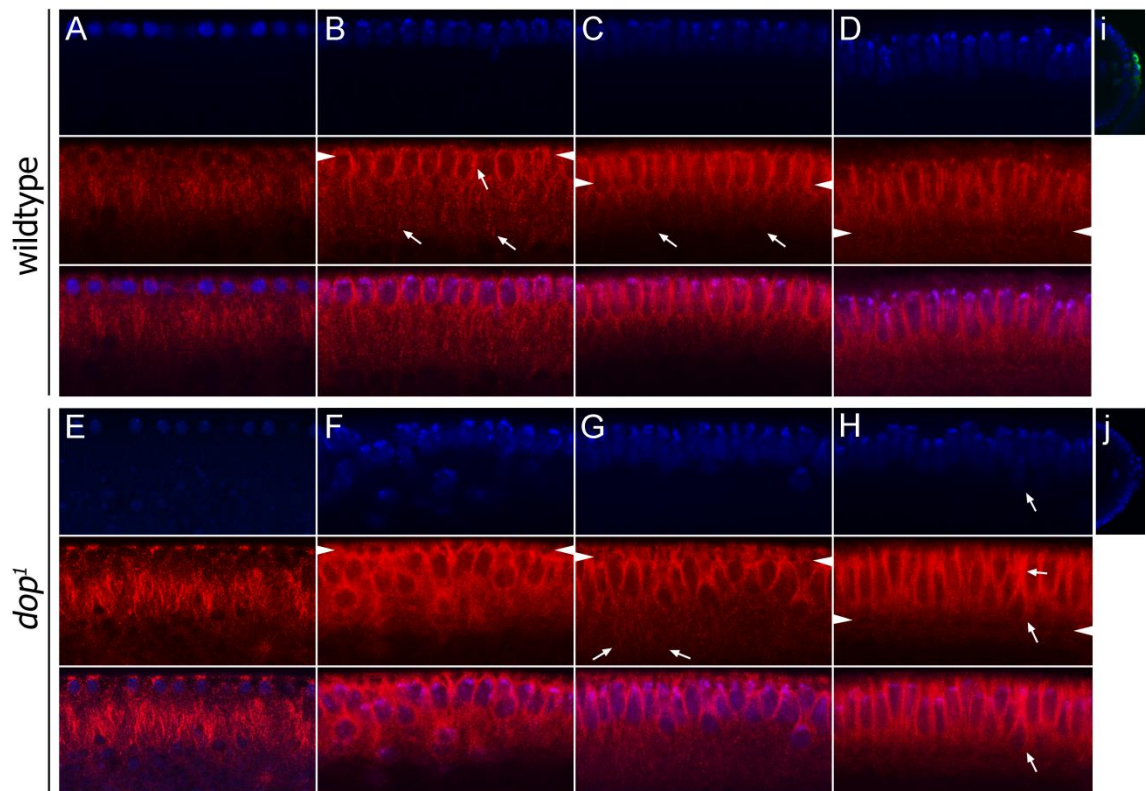
Fig. 6.17: Effects of the _dop_[1] mutation on microtubule bundle localization. Fixed wild-type and _dop_[1] embryos stained with a beta-tubulin antibody (red) and DAPI (blue). Embryos are shown in different stages: pre-cellularisation (A), slow (B), mid (C) and fast phase of cellularisation (D). Pre-cellularisation _dop_[1] embryos do not show any phenotype. During slow phase basket-like microtubule bundles surround the nucleus and thin filaments extend into the yolk (arrows in B). _dop_[1] mutant embryos at a comparable stage show an irregular orientation of microtubule bundles (F). Nuclei are surrounded by the thick basket like microtubules even if they detach from the plasma membrane. During mid cellularisation a similar pattern is observed (F, G). However _dop_[1] embryos with lower amount of nuclear detachment show a more wild type like organisation of the microtubule network (arrows in G). During fast phase wild-type and _dop_[1] mutant embryos show long microtubule bundles in the inner of the cellular compartments and less thin filaments. Wild type embryos could be distinguished from _dop_[1] embryos by previous vasa staining of the pole cells (i, j).

cellularisation stages the basal microtubules get less abundant while the basket microtubules are maintained (Fig. 6.17D). _dop_[1] mutant embryos show very varying conservation of the microtubule organisation seen in wild type embryos. In syncytial cleavage stages the microtubules do not show gross abnormalities when compared to wild type (Fig. 6.17E). During early cellularisation _dop_[1] embryos with severe nuclear drop out defects showed disruption of the microtubule organisation (Fig. 6.17F). While thick microtubule bundles were found surrounding the nuclei, the thinner bundles in the basal region were lost. However, this disruption is not observed in embryos with

less severe nuclear drop out defects (Fig. 6.17G). Areas less affected by nuclear drop out proceed through the fast phase of cellularisation without any defect in microtubule arrangement (Fig. 6.16H). Therefore the severe defects in microtubule organisation might be a secondary effect as consequence of the mis-localisation of the nuclei.

As the fixation of microtubules structures in the embryo does not allow observation of microtubule dynamics life imaging was conducted using expression of GFP-Tubulin (Fig. 6.18). Wild type embryos expressing GFP-Tubulin show a similar distribution and length of microtubules as dop^1 embryos. Differences were observed in the frequency and amount of microtubule bending in apical or basal direction of the embryo. While the microtubules in wild type extend straight from the membrane towards the centre of the embryo, dop^1 microtubules seem to be much more flexible. In the mutants excessive bending along the basal microtubules can be observed. Furthermore the basket microtubules show strong bending as the membrane furrow passes the nuclei suggesting that the microtubules are deformed by the sterical hindrance of the enlarged furrow canal. These observations indicate that the rigidity of the microtubule bundles might be lowered in dop^1 mutants. As the dop^1 allele is presumably an incomplete loss of function allele, microtubules were investigated in null mutant dop^{LH10} embryos (dop^{LH10}/$Df(3L)MR15$). Strikingly the investigation of dop^{LH10} embryos shows even stronger effects on microtubule rigidity as most microtubules are not arranged in an apico/basal manner but drift randomly towards anterior or posterior ends of the embryo. This collapse of microtubule arrays coincides with irregularities in the interphase between the peripheral cytoplasm (bright) and the inner yolk (dark) (see asterisks in Fig. 6.18). Irregularities between peripheral cytoplasm and the central yolk mass have also been observed in light microscopic investigation of *dop* mutants.

The precise organisation of this interphase in wild type embryos might be controlled by the rigid microtubule matrix build by the radial microtubules.
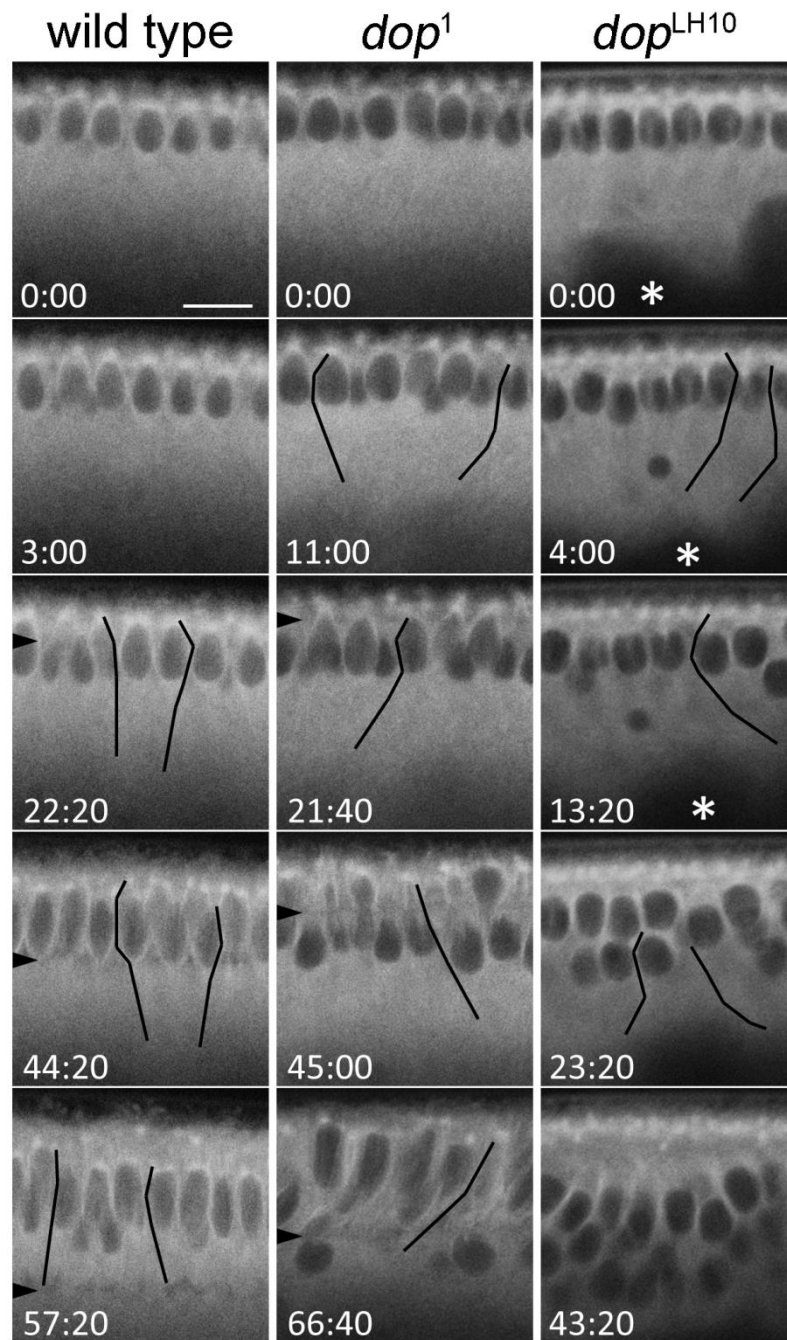
Fig. 6.18: *dop* alleles affect microtubule rigidity. Embryos expressing GFP-tubulin show the formation of microtubule bundles during cellularisation. Pictures from a wild type embryo movie show the apico/basal orientation of the microtubules. Examples of microtubules spotted in the movies are shown (black lines). In *dop*[1] embryos the orientation of bundles shifts from anterior to posterior (left to right) and bending of the microtubules around the nuclei occurs as the membrane furrow passes (black arrowheads). *dop*[LH10] embryos show severe bending of the microtubules and the interphase between yolk and cytoplasm is deformed. Note that *dop*[LH10] embryos show no membrane growth. Time is displayed in min:sec. Scale bar shows 20 µm (white).

4.2.2.5. Evidence for Dop interactions with microtubule associated transport

Microtubule associated motor complexes are grouped in two functionally different families: Dynein and Kinesin. Cytoplasmic Dynein is a multi-protein complex consisting of several light chains, two intermediate chains, two intermediate-light chains and two heavy chains, which generally provides transport towards the minus ends of microtubules. The light and intermediate chains of Dynein have been shown to regulate cargo binding and activity of the motor function provided by the heavy chains. The functions of Dynein are also regulated by a plethora of other proteins through mechanisms including phosphorylation events. Cytoplasmic Dynein has been shown to be necessary for Baz localisation, nuclear localisation and lipid clouding; strikingly, these processes are disrupted in dop^1 mutants. Therefore, it seemed likely that Dop might regulate Dynein functions.

Adult flies that are homozygous mutant for *dop* develop a wing phenotype that is indistinguishable from the mutant phenotype of a gene associated with Dynein function called *short wing* (*sw*) (Fig. 6.19). dop^1 homozygous flies hatched at 25° C show a varying wing phenotype, affecting posterior regions of the wing first while, in flies with more severe defects, the whole wing becomes deformed. This defect is represented in a higher percentage in many of the LH alleles (will be analysed in Langlands et al.; unpublished). Literature analysis showed that *sw* encodes Dynein intermediate chain (DIC) in *Drosophila* and sw^1 mutants display an identical wing phenotype. DIC is part of the cytoplasmic Dynein protein complex and has been shown to facilitate interaction of Dynein to the Dynactin complex by binding its p150[Glued] subunit. Moreover DIC has been shown to be phosphorylated in its Dynactin

interaction domain; a regulatory process that prevents its binding to Dynactin (Vaughan et al., 2001).
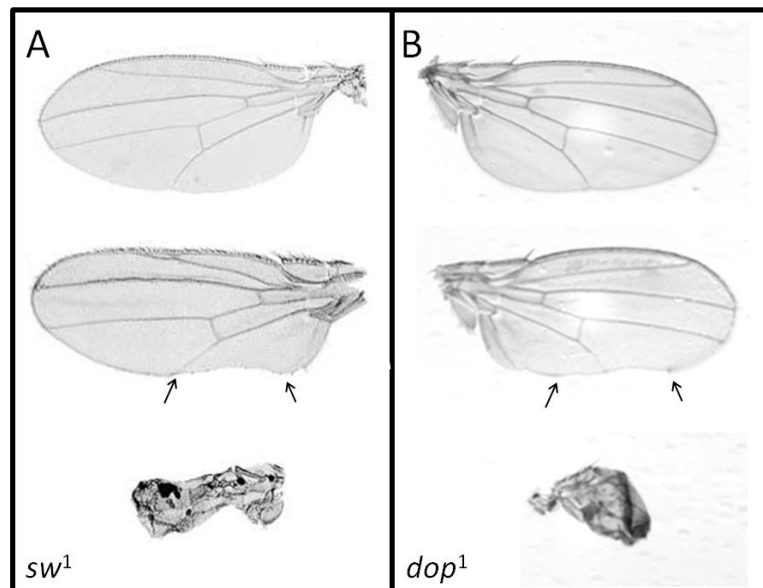
Fig. 6.19: Similar wing defects caused by dop^1 **and** sw^1**.** Fixed wings of sw^1 (A) and dop^1 (B) homozygote mutants show a similar range of wing phenotypes. Light defects lead to loss of posterior wing regions (arrows) or vein pattern defects. More severe wing defects cause loss of expanded wing regions with malformation of the whole wing.

To assess DIC phosphorylation a DIC antibody was used to detect phosphorylation dependent band shift in western blots with lysate from wild type and dop^1 embryos (Fig. 6.20). Conventional western blotting showed single bands of DIC in wild type and dop^1 extracts. While no band shift could be detected, this experiment shows that the protein level of DIC in wild type and dop^1 mutants are equal. To improve the level of protein separation and to enable the detection of differently charged DIC polypeptides 2D gel electrophoresis was performed (Fig. 6.20). This method revealed three to four DIC positive spots arranged at a similar height and a smear of DIC towards the acidic side of these dots. The pattern of these 2D spots is similar to 2D gel electrophoresis pattern of human DIC (Pfister et al., 1994; Vaughan et al., 2001). To identify protein bands that contain phosphorylated DIC wild type protein extract was incubated with phosphatase. Phosphatase treatment induced a shift of the smear band on the basic

side towards the more acidic region. The specificity of the phosphatase treatment was controlled using the same protocol with addition of phosphatase inhibitors. In dop^1 extracts the intensity of the phosphatase sensitive protein fraction was significantly reduced but not completely. This observation is supporting the theory that the dop^1 mutation might affect the kinase activity of Dop. Mis-regulation of DIC might provide an important explanation for the molecular basis behind many of the defects observed during cellularisation in dop^1 embryos.
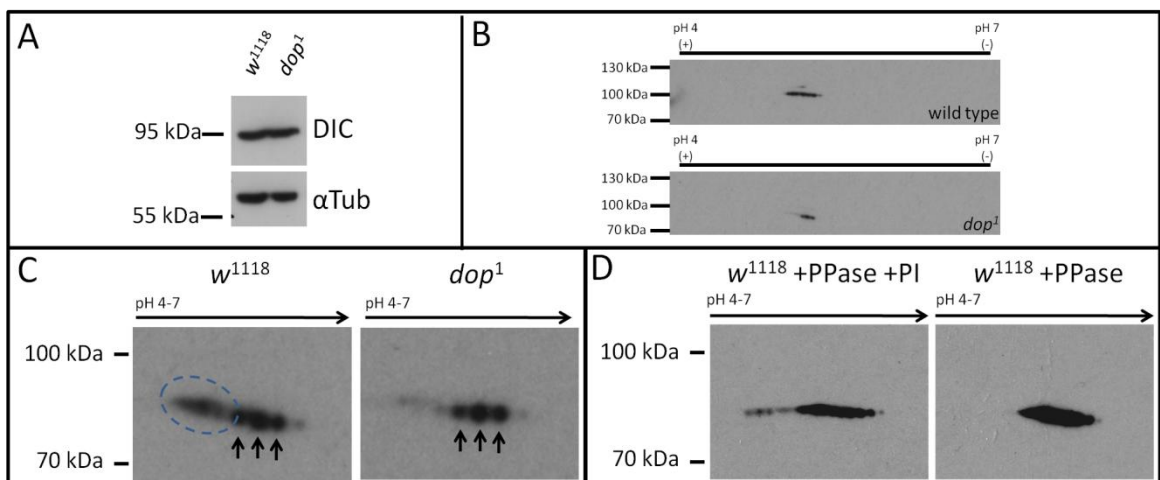
Fig. 6.20: Dynein intermediate chain phosphorylation states are different in wt and dop^1. Wild type and dop^1 0-4h embryonic extracts were used for western blotting. (A) shows a conventional western blot using a DIC antibody. Expression levels of DIC are equal in wt and dop^1. (B) shows separation of DIC by 2D gel electrophoresis. Black bars indicate the position of the gel strips used for isoelectric focussing (IEF) between ph 4 and pH 7. (C) and (D) show magnifications of the DIC migration pattern. (C) Round dots of DIC are marked with arrows. Additionally a smear of protein can be detected (dotted circle). This smear is drastically reduced in dop^1 mutant protein extract. (D) Phosphatase treatment of protein extracts prior to gel electrophoresis shows that the acidic fraction of the DIC protein are phosphatase sensitive (w^{1118}+PPase). The left picture shows a mock treatment with deactivated phosphatase and phosphatase inhibitors (w^{1118}+PPase+PI).

Further repetitions of the 2DGE experiment showed some variability in the arrangement of the protein and phospho-protein spots (Supplemental material). These findings might indicate that the used assay is not very robust or that phosphorylation of DIC might change in a stage-dependent fashion or throughout different phases of the cell cycle. Therefore, the variation in the DIC pattern might depend on the developmental stages of the embryos used for protein extraction. A second cause for the variations might originate from technical problems with the isoelectric focussing of

the proteins. It is also noteworthy that these experiments do not prove direct phosphorylation of DIC by Dop. *In vitro* kinase assays were under way to test the possibility of Dop phosphorylating DIC directly but these experiments could not be finished within the submission deadline of this thesis.

4.2.2.6. Interactions of Dynein and Kinesin mediated transport pathways

It has been shown that microtubule associated transport occurs in a bidirectional fashion (Welte, 2004). This bidirectional movement is administrated by Dynein and Kinesin motors, which attach to the cargo simultaneously. The regulation of the activity of Dynein and Kinesin motors is not well understood. It is known that the activity of the two microtubule motor classes is interdependent as Kinesin functions are compromised in Dynein- or Dynactin mutants (Gross et al., 2002). Previous data indicated that Dynein functions are compromised in dop^1 embryos. Therefore, the lack of Dynein activity in the dop^1 mutants might affect Kinesin motor localisation or function. The Kinesin family contains mostly microtubule plus-end directed motors. Although Kinesins have been shown to be necessary for the transport of apical junction proteins (Chen, 2003) and mRNA localisation their role in the process of cellularisation is not investigated.

A method to test whether Kinesin is affected in dop^1 mutants is to look at its localisation. A transgenic construct containing the Kinesin heavy chain motor domain fused to beta-Galactosidase (encoded by the *lacZ* gene) was expressed in wild type and dop^1 embryo. Wild type and mutant embryos were collected and pooled to prevent signal differences caused by fixation or staining procedures. The detection of the beta-Gal tag showed an even distribution of Kinesin throughout cellularising wild type embryos (Fig. 6.21A, C). In dop^1 embryos Kinesin-lacZ accumulated at the basal region

below the furrow canals and around nuclei in the centre of the embryo (Fig. 6.20B, D).

The intensity of the fluorescence in the apical region (above the furrow canal) and the

basal region (below the furrow canal) was measured to show the level of accumulation

(Fig. 6.21E). While in wild type the fluorescence intensity is almost equal in apical and

basal regions, dop^1 embryos show an enrichment of basal Kinesin-lacZ by the factor

1.8. It is to note that the signal intensity in dop^1 embryos was much higher than in wild

type embryos. These experiments indicate that Kinesin motor proteins on dop^1

embryos are aberrantly distributed along the microtubules. The aberrant localisation

of Kinesin-lacZ might derive from the lack of Dynein dependent transport of Kinesin

molecules towards the microtubule minus ends. Further understanding of the

interplay between Dyniein and Kinesin motors and the function of Dop might help

understand these observations.
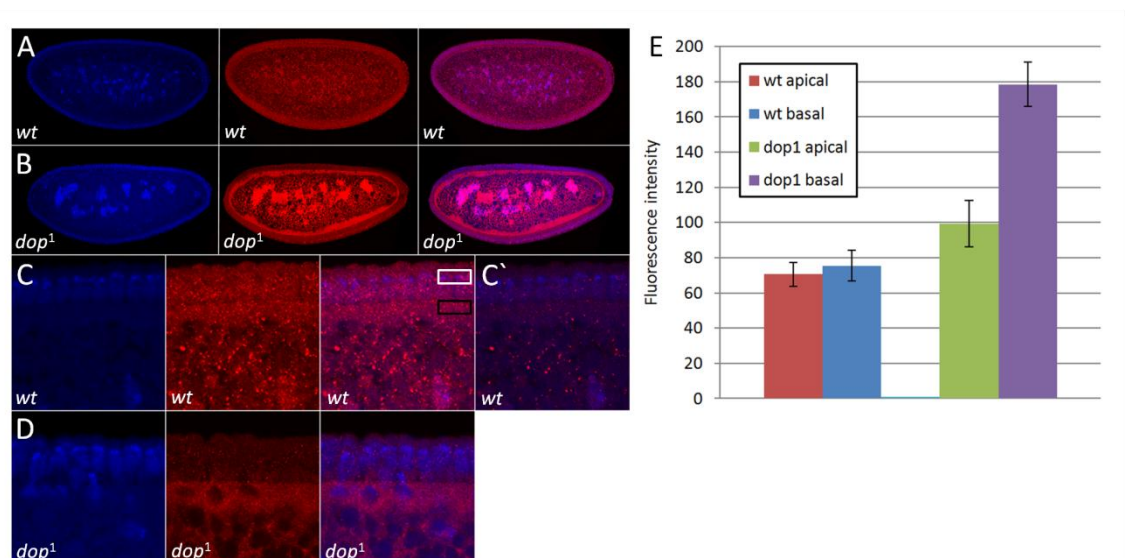
Fig. 6.21: Expression of a *kinesin-lacZ* reporter gene in wild type and *dop*^{1} mutants. Kinesin-lacZ was expressed in wild type (A, C) and *dop*^{1} mutants (B, D). The localisation of Kinesin-lacZ was detected using a beta-Gal antibody (red) and DNA was stained with DAPI (blue). The wild type embryos showed a significantly lower amount of signal (images in C` and D have been taken with identical microscope settings). The fluorescence intensity has been measured in the apical region and in the basal region of the forming cells (example shown in C; white box=apical, black box=basal).

To investigate the role of Kinesin during cellularisation germ line clones carrying a null mutation of the *kinesin light chain* gene (*klc*^{8ex94}) were generated. Embryos lacking maternal and zygotic *klc* were collected, fixed and stained with an antibody against the membrane marker Neurotactin to investigate membrane formation during cellularisation (Fig. 6.22). This experiment showed that *klc* null mutant embryos are defective in cellularisation. Among the mutant embryos only embryos during syncytial divisions and cellularisation stages but no later stages were found indicating a severe defect in cellularisation. The DAPI staining of the embryonic DNA did not reveal severe defects in syncytial divisions but did show massive nuclear drop out during cellularisation. In *klc* mutants Neurotactin was localised at the lateral membrane and massively concentrated at the basal furrows during cellularisation (arrows in Fig. 6.22B and E) Also 100% of the nuclei detach from the membrane. In comparison *dop*^{1} embryos show incomplete nuclear drop out (Fig. 6.22C) a very diffuse Neurotactin
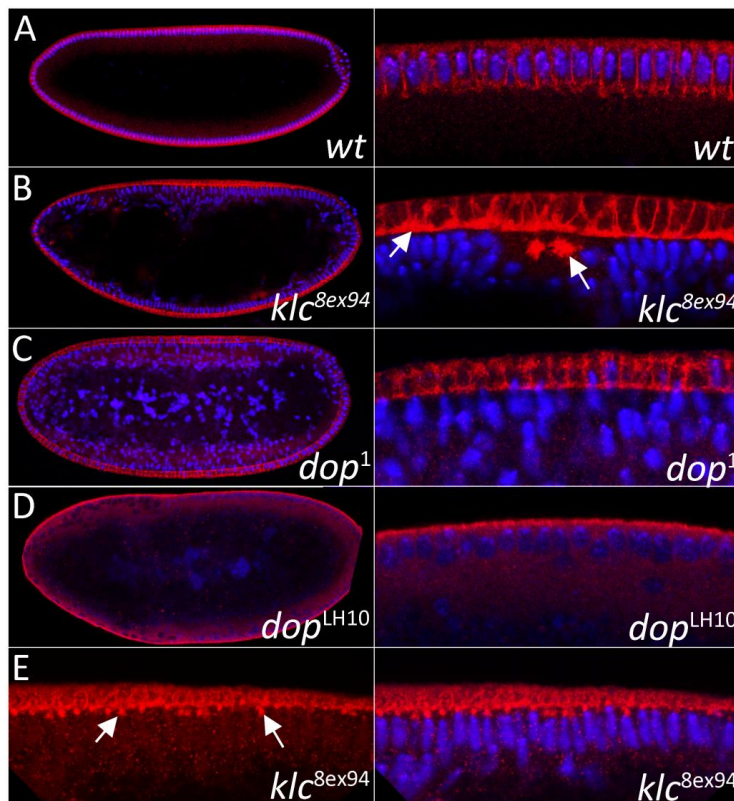
Fig. 6.22: *klc* **null mutants exhibit a severe nuclear drop out phenotype.** This figure shows a comparison of wild type (A), *klc*^{8ex94} germ line clones (B, E), *dop*^{1} (C) and *dop*^{LH10} (D) embryos at cellularisation stage. The membrane is stained using a Neurotactin antibody (red) and nuclei with DAPI (blue). *klc* mutants have low levels of membrane growth and complete nuclear drop out. Neurotactin staining shows accumulation of membrane material at the furrow canal region (arrow in B) and formation of membrane aggregates on the apical side of the nuclei (arrows in E). *dop*^{1} embryos show diffuse membrane growth, altered furrow structure and a varying percentage of nuclear drop out (C). *dop*^{LH10} embryos lack membrane growth. Most nuclei detach from the membrane before cellularisation starts and no nuclear elongation is observed (D). A-D shows whole embryos on the left; higher magnifications on the right.

localisation, enlarged furrow canals and a large amount of Neurotactin in the apical region of the cells. The same analysis in dop^{LH10} null mutant embryos showed no membrane growth at all (Fig.6.22D). The embryonic nuclei were found to detach from the cortex at onset of cellularisation.

The comparison to *dop* mutant phenotypes shows that maternal/zygotic *klc* mutants exhibit defects in membrane organisation and nuclear anchoring. dop^1 and dop^{LH10} embryos also show defects in membrane structure and nuclear anchoring but the characteristics of these defects differ from the *klc* mutants. This analysis indicates that Dop and Klc regulate similar processes during cellularisation. A deeper investigation of the transport of vesicles and lipid droplets in the klc^{8ex94} mutants might reveal functions for plus-end directed transport during cellularisation.

4.2.3. An outlook on Dop functions beyond cellularisation

4.2.3.1. dop^{LH10} represents a stronger allele than dop^1

The dop^1 mutation leads to a very specific defect in membrane growth, as it merely affects the slow phase and spares the fast phase of cellularisation. This work showed that dop^1 mutant flies carry a point mutation in the kinase domain of a multi domain kinase with homology to mammalian MAST kinases. This mutation seems to affect protein levels as only a low amount of Dop is found in embryonic extracts. As a low amount of Dop protein is still present in dop^1 mutants certain functions of Dop might be retained. The dop^{LH10} allele is a null allele and might therefore have a more severe phenotype than dop^1. In order to compare the phenotypes of dop^1 and dop^{LH10} mutants, *dop* null mutant flies were created and their embryos were analysed. To create zygotic null mutant flies the dop^{LH10} flies were crossed with flies carrying the

MR15 deficiency. The hatching rate of hemizygous *dop*^{LH10} flies was considerably lower than hatching rates of *dop*^{1} hemizygous flies and sufficient numbers of flies could only be collected at low incubation temperature (20 °C instead of 25 °C). The adult flies showed stronger wing defects than observed in *dop*^{1} mutants and also displayed a defect in leg development (supplemental material). Microscopic analysis of the mat/zyg *dop*^{LH10} embryos showed that *dop*^{LH10} embryos do not cellularise and show no elongation of the nuclei (Fig. 6.23A-D). In contrast to *dop*^{1} embryos, which lack membrane growth in the slow phase of cellularisation, *dop*^{LH10} embryos did not show any membrane formation between the nuclei.

The same observation was made in living embryos monitored with bright field microscopy. Here it was observed that the nuclei detach from the membrane immediately at onset of cellularisation (for movie data see attached CD). Figure 6.22E shows kymographs of movies from wild type, *dop*^{1} and *dop*^{LH10} embryos. The kymographs in Fig. 6.23F show the positions of nuclei, membrane and cytoplasm cleared of lipid droplets in an overlay of coloured lines (red = membrane, yellow = nuclei, green = cleared cytoplasm). Tracking of the position of the membrane front shows that the membrane in *dop*^{LH10} embryos grows only residually while membrane growth occurs normally in wild type and slightly delayed during slow phase in *dop*^{1} embryos. The region cleared of lipid droplets is smaller in *dop*^{LH10} mutants and retracts even further after the nuclei detach from the membrane. These results indicate that Dop is necessary for membrane growth in general and provides further evidence for the model that *dop*^{1} causes incomplete loss of function. A noticeable effect of the *dop*^{LH10} mutation is the rapid streaming of yolk (see supplemental material). In wild type embryos the central yolk mass is relatively static. In *dop*^{LH10} mutants the yolk shows turbulent movement throughout the syncytial division cycles and during

cellularisation. The cytoplasmic streaming might drag the nuclei away from the membrane (see nuclear shape in Fig. 6.23D). The rapid movement of the yolk in the embryo might in part result from low microtubule rigidity (see chapter 4.2.2.4). An alternative explanation for the disturbance in the cytoplasm might derive from irregularities of the syncytial divisions (see below). During the syncytial divisions the cellular boundaries defined by the cleavage furrows expand due to the extension of the microtubule spindle. Uncontrolled or unsynchrone expansion and retraction in the cellular boundaries might lead to acceleration of yolk particles and induce yolk streaming.
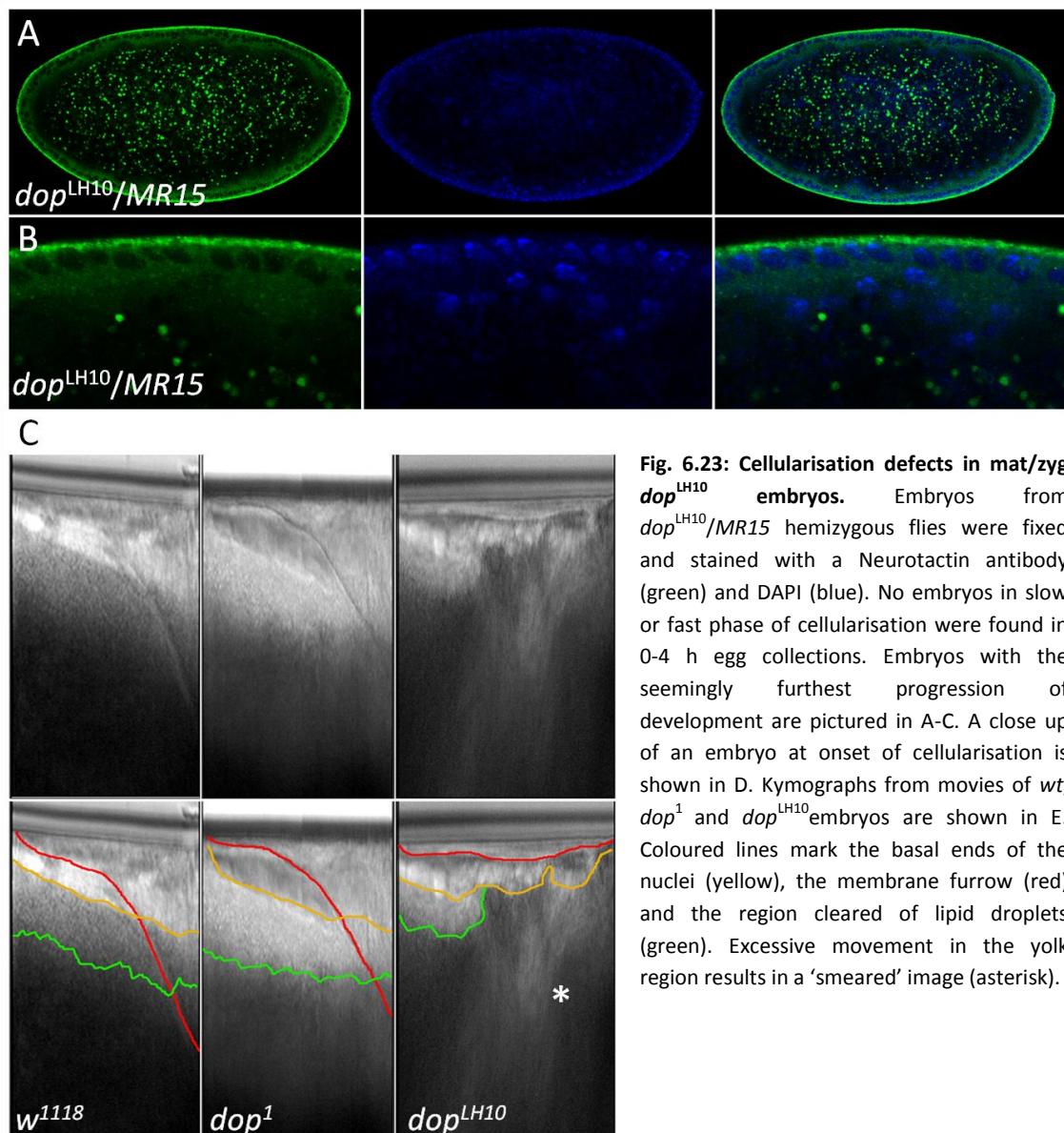
Fig. 6.23: Cellularisation defects in mat/zyg dop^{LH10} embryos. Embryos from $dop^{LH10}/MR15$ hemizygous flies were fixed and stained with a Neurotactin antibody (green) and DAPI (blue). No embryos in slow or fast phase of cellularisation were found in 0-4 h egg collections. Embryos with the seemingly furthest progression of development are pictured in A-C. A close up of an embryo at onset of cellularisation is shown in D. Kymographs from movies of *wt*, dop^1 and dop^{LH10} embryos are shown in E. Coloured lines mark the basal ends of the nuclei (yellow), the membrane furrow (red) and the region cleared of lipid droplets (green). Excessive movement in the yolk region results in a 'smeared' image (asterisk).

To investigate syncytial divisions Tubulin-GFP was expressed in wild type and dop^{LH10} embryos. Imaging of Tubulin-GFP revealed the mitotic spindle and could therefore be used as a marker for division timing. Embryos during the syncytial divisions 10-14 were examined. In wild type embryos syncytial divisions occurred periodically and are initiated from anterior and posterior ends of the egg. In wild type embryos expressing Tubulin-GFP no nuclear drop out was detected (data not shown). In dop^{LH10} embryos nuclear drop out prior to cellularisation and disruption of division cycle timing were observed (Fig. 6.24). The embryo displayed nuclear dissociation from the cortex during cell cycle 13 (arrow heads) and detachment of microtubule spindles (arrows in D, E, G, H).

The regulation of the cell cycle seemed to be affected as well. In wild type embryos the syncytial divisions are synchronous and proceed in waves starting at the anterior and posterior poles (not shown). In the dop^{LH10} mutant the divisions start from a random positions (Fig. 6.24A) and spread in an undirected manner (areas containing mitotic spindles are indicated by white lines). These findings show that dop null mutant embryos display more severe defects than dop^{1} mutants and provide preliminary data showing that Dop might be involved in the control of syncytial divisions.

Additional evidence that Dop might be involved in syncytial cleavages was found by analyses of phenotypes induced by overexpression of Dop protein. Overexpression of Dop-GFP in wild type embryos resulted in 100% lethality and "messy" embryos (shown in Fig. 6.25B). These embryos did not show arrangement of nuclei at the outer membrane and contained large vesicle-like structures. The same defect was induced by overexpression of a Dop protein with a different molecular tag (Dop-HA; Fig.6.25A) and untagged Dop protein (not shown) suggesting that protein tags at the carboxy-

terminus of Dop did not cause the lethality. Embryos expressing Dop-HA were fixed and stained using DAPI and anti HA antibody (Fig. 6.25A). The DAPI staining revealed that Dop overexpressing embryos contained only a few nuclei while wild type embryo collections of identical age (0-4 h after egg laying) generally include high amounts of cellularisation stage embryos and blastoderm stage embryos. Therefore overexpression of Dop might slow or block the early syncytial cell cycles.
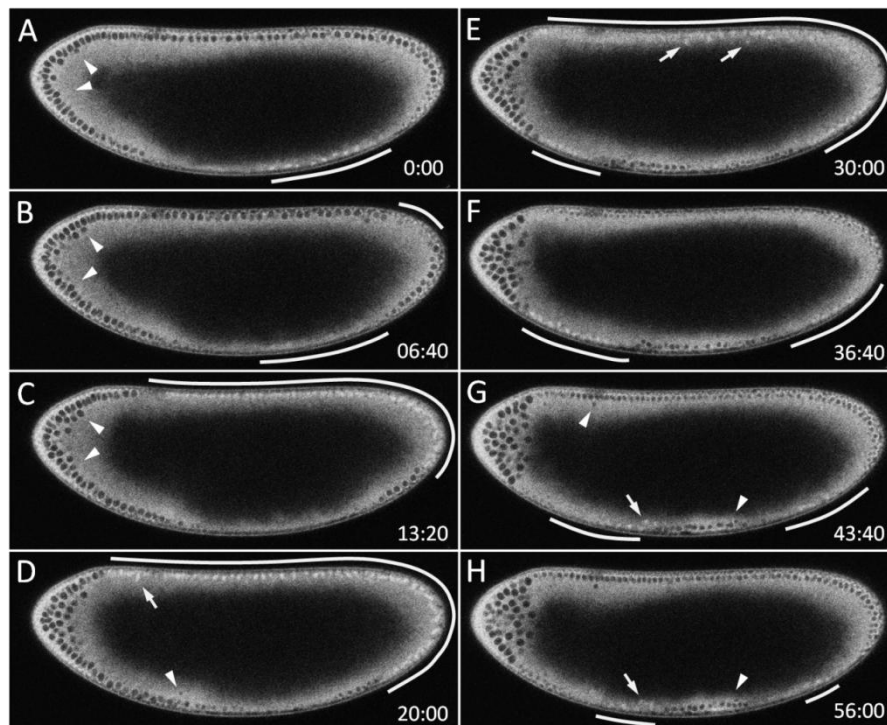
Fig. 6.24: Defects during syncytial division cycles in *dop*^{LH10} embryos. Live imaging of tubulin-GFP expression in a *dop* mat/zyg null mutant embryo. An embryo with nuclei progressing from the 13th to the 14th cell cycle is shown (A: most nuclei are in cell cycle 13; mitotic spindles in progression to cell cycle 14 are marked by a white outline). Nuclei that detach from the membrane are indicated by arrow heads; detached spindles are indicated by arrows. Time is displayed in min:sec.

To express Dop protein in levels that allow survival of the embryos a Gal4 driver with lower expression level was used. The expression of Dop-GFP by Gal4 driven by the *nanos* promoter (*nos*::*gal4*) showed survival rates around 76 % (Fig. 6.25C). Having identified a promoter that allowed expression of Dop proteins at non-lethal levels a structure function analysis was performed. This analysis was based on the expression

of the deficiency constructs encoding the proteins Dop$^{\Delta DUF}$, Dop$^{\Delta Kin}$ and Dop$^{\Delta PDZ}$. The expression of the Dop$^{\Delta DUF}$ and Dop$^{\Delta Kin}$ proteins did show slightly higher survival rates compared to expression of full length Dop (Dop$^{\Delta DUF}$: 87 %; Dop$^{\Delta Kin}$: 84 %). Surprisingly the expression of Dop$^{\Delta PDZ}$ resulted in 100 % lethality. Microscopic analysis of embryos expressing Dop$^{\Delta PDZ}$ showed embryos identical to those found after high-level expression of Dop. This analysis shows that the deletion of the PDZ domain might create dominant negative effects or result in over-activation of the deficient protein. The PDZ domain might function intrinsically by affecting the structure of the Dop protein or extrinsically by recruiting Dop regulators and Dop targets. The identification of binding partners of the PDZ domain is therefore a promising aim for future work.
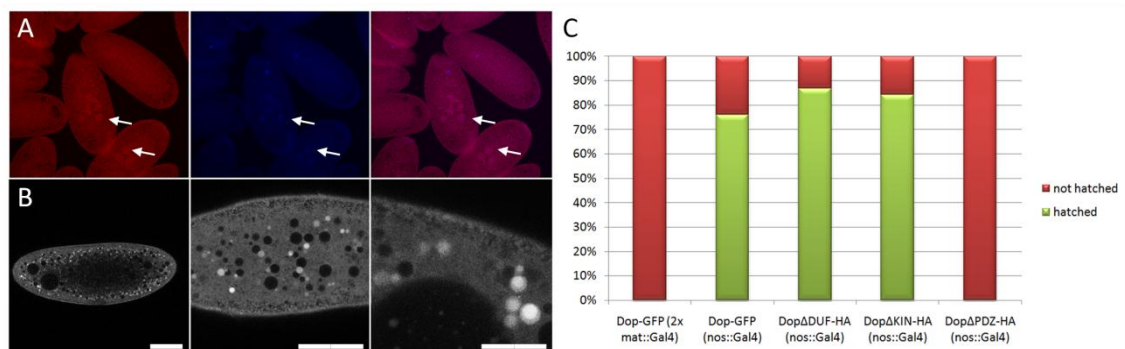
Fig. 6.25: Effects of *dop* overexpression and structure-function analysis. *dop* transgene expression was induced using strong promoters (2x *matTub::gal4*) or a weak promoter (*nos::gal4*). High expression levels of Dop-HA led to accumulation of embryos in early developmental stages (A shows representative embryos with only few central nuclei; arrows)(Dop-HA red, DNA blue). Live imaging of embryos expressing high level Dop-GFP showed abnormal aggregation of vesicles and absence of nuclei (B)(scale bars represent 100 µm (B left, middle) and 50 µm (B right). Survival rates of embryos expressing *dop* transgenes (C).

4.2.3.2. Possible interaction of Dop and the RNA silencing regulator Smaug

The experiments documented in this thesis show that the *dop* alleles are not affecting the *ago2* gene but the *Drosophila* homolog of MAST kinase. However previous publications showed that over-expression of an *ago2* transgene results in partial complementation of the lethal defects caused by the *dop* alleles *dop*[1] and *dop*[46] (Meyer

et al., 2006). Furthermore expression of *ago1* also complements the *dop*[1] mutation while reduction of silencing function (by introduction a mutation in *ago1*) makes the phenotype more severe (Meyer, 2007). These genetic interactions implicate an association between *dop* function and RNA silencing. Gene expression profiling in wild type and *dop*[1] embryos showed that *dop* – directly or indirectly – regulates mRNA stability (Gehlen, Smibert and Müller, unpublished). Comparison of mRNA levels in wild type and *dop*[1] showed elevated levels of *smaug* mRNA. Smaug regulates RNA silencing by degradation of transcripts during the MZT. Smaug protein is provided maternally and is degraded during early interphase 14, when zygotic transcription increases dramatically. In unfertilized eggs, which do not initiate zygotic transcription, Smaug protein accumulates with normal kinetics but then persists at high levels (from Tadros et al. 2007). To see whether the zygotic activation of Smaug degradation is altered in *dop*[1] mutants Smaug protein was detected in staged embryo collections (Fig. 6.26A). In wild type lysate Smaug is present up to 2 h after egg deposition while no Smaug was found at 2-3 or 3-4 h after egg laying. In *dop*[1] embryos Smaug protein is present in the early stages but is not degraded in later developmental stages. This result suggests that Dop might regulate Smaug degradation. To investigate whether Dop and Smaug
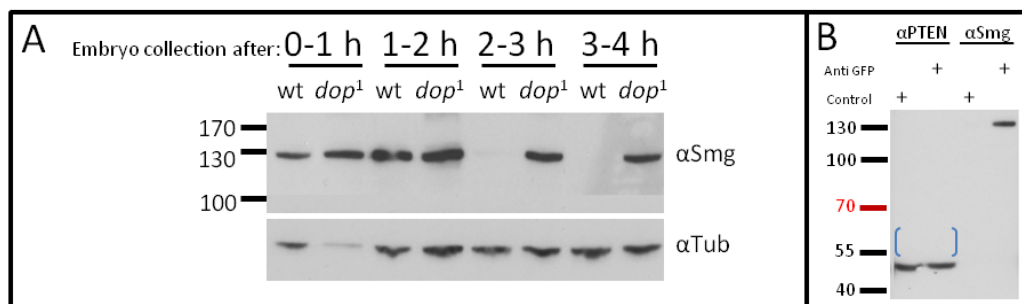
Fig. 6.26: Dop binds Smaug and is needed for Smaug degradation. Presence of Smaug protein in embryo lysates harvested at different time points (A). Smaug protein is present in wild type lysate between the hours 0-2 after egg laying but not after 2-3 and 3-4 h. In *dop*[1] mutants Smaug protein is maintained trough all measured time points. Immunoprecipitation of Dop-GFP leads to co-precipitation of Smaug protein. PTEN is not bound by Dop-GFP (brackets mark expected band size, protein bands below 55 kDa correspond to the IgG heavy chains.

might interact directly, Dop-GFP was expressed in embryos and used for co-immunoprecipitation experiments (Fig. 6.26B). The co-precipitating proteins were probed by gel electrophoresis and Western blotting. Antibodies were used to detect Dop-binding proteins. This experiment showed that Dop binds to Smaug directly as a band of 130 kDa could be detected in the Dop precipitate but not in a control fraction (using wild type embryonic extract instead of extract of Dop-GFP expressing embryos). Parallel detection of the published MAST kinase interactor PTEN did not show binding to Dop. This experiment indicates that Dop and Smaug are components of the same protein complex. Whether an interaction between Dop and Smaug is necessary to degrade Smaug protein or if the interaction is eventually important for the function of Smaug in regulation of the MZT has to be examined in future experiments.

Chapter IV: Discussion

5. Discussion

The *dop*[1] allele induces developmental defects and was previously published to be an allele of *ago2*. As the hypomorphic alleles of *ago2* which are commonly used did not prove an essential function in development *dop*[1] seemed to offer a highly interesting tool to gain further insights into *ago2* functions. However, the way the *dop*[1] allele affects *ago2* function has been enigmatic so far. The *ago2* gene in *dop*[1] mutant flies encodes an Ago2 protein that lacks one repeat of the amino-terminal GRR region and the function of these repeats is not understood. In this work the analysis of GRR conservation and function of different GRR haplotypes in development and RNAi argued against a significant function of the GRRs for early embryonic development. These experiments raised doubts on the finding that *dop*[1] is allelic to *ago2*. Indeed novel *ago2* null alleles were identified that are able to complement the developmental defects induced by *dop*[1]. The complementation analysis showed that *dop*[1] is not an allele of *ago2* and subsequent genomic mapping and sequencing revealed that the *dop*[1] allele arises from a mutation of a distinct gene. This gene encodes the *Drosophila* homolog of mammalian MAST kinases and its function has not been investigated prior to this work. Most importantly, phenotypic characterisation of *dop*[1] mutant embryos showed an accumulation of defects in Dynein-dependent processes. Furthermore an effect of *dop*[1] mutants on the Dynein subunit DIC and was found arguing that the Dop kinase might affect Dynein mediated transport by regulating DIC phosphorylation.

5.1. Relationship of *dop*[1] and *ago2*

5.1.1. Relevance of the GRR region of Ago2

The *Drosophila* Ago2 protein contains the functional domains PAZ and PIWI with high similarity to mammalian Ago proteins. In addition to the conserved region *Drosophila ago2* encodes an amino-terminal extension containing two groups of imperfect glutamine-rich repeats (GRRs). *dop*[1] mutants carry a variation in the GRR region of Ago2 and affect the cellularisation of early embryos. Therefore it was proposed that the GRR haplotype is important for Ago2 function and that Ago2 plays a significant role in development. This work shows that GRR variations are a common phenomenon within wild type species and different populations of a species and are unlikely to cause the defects found in *dop* mutants.

How the GRRs affect silencing is an important question. A possible paradigm comes from the analysis of *Trypanosoma brucei* Ago1: Here, the amino-terminal 68 amino acids contain ten arginine-glycine rich motifs (Shi et al., 2004). This so-called RGG domain is involved in the association of TbAgo1 with poly-ribosomes, an association required for an efficient RNAi response in this organism. Variations in RGG repeat number affects the strength of RNAi responses (Shi et al., 2009). Intriguingly, the TbAgo1 RGG domain and the GRRs of arthropod Ago2s are all characterised by low sequence complexity and are likely to be intrinsically unstructured (Hain et al., submitted). As intrinsically unstructured domains have been proposed as protein interaction domains (Dunker et al., 2005) and changes in the number of glutamine-rich repeats can modulate interaction strength (Liu and Lindquist, 1999; Parham et al., 2001), RGG or GRR variation might modulate the affinity of the Argonaute protein to particular targets. Indeed, mutant versions of TbAgo1 show progressively stronger

RNAi responses, the more copies of the RGG motif are present (Shi et al., 2009). Future experiments might compare the strength of RNA silencing and viral defence in flies with different numbers of GRRs or in the absence of GRRs.

5.1.2. The function of *ago2*^{short}

The *ago2* gene locus in *Drosophila* encodes two long isoforms and a short isoform. The long isoforms are largely identical and differ only in the first 9 amino acids. Both long isoforms contain the amino-terminal GRRs and the functional PAZ and PIWI domains. The short isoform is transcribed from 5 prime of the third exon which allowed specific primer design for quantitative rt-PCR. Qrt-PCR analysis on samples from adult flies showed that the shorter transcript is expressed approximately 30 % less than the long isoforms. Although it has not been possible to verify protein production from this transcript a methionine is found in exon 3, preceded by a perfect match to the optimal *Drosophila* translational initiation consensus (caaaATG) (Cavener, 1987). Usage of this start would theoretically yield a protein product encoding the known functional domains of Ago2, but lacking the GRRs. A truncated Ago2 protein lacking GRRs was recently shown to support full biochemical reconstitution of the RISC indicating that the N-terminal region does not contain domains that are essential for core RNAi (Liu et al., 2009). In the lack of the amino-terminal sequence, Ago2^{short} is reminiscent of the mammalian Argonautes. Surprisingly in this study no significant effect of Ago2^{short} on RNAi could be found using a DIAP1^{RNAi} reporter assay in the eye. Analysis of combinations of different *ago2* alleles showed that the long *ago2* isoforms and not the short isoform alone conduct RNAi in the eye. In absence of Ago2^{long}, Ago2^{short} did not show any functions towards RNAi. However in the presence of low levels of the long

isoform the Ago2^{short} did show a weak effect on RNAi response. Therefore the functional RNAi response of Ago2^{short} might rely on the presence of the long isoform and its GRRs. Alternatively, Ago2^{short} might not primarily interact with siRNA but function in another RNA silencing pathway. The function of Ago2^{short} and Ago2^{long} in different pathways could depend on the GRRs which might allow Ago2^{long} to interact specifically with siRNAs. The investigation of Ago2 alleles deficient for the long and short isoform might bring new insights about the function of *ago2^{short}*.

5.1.3. The genetic relationship between *ago2* and *dop*

One of the difficulties associated with the mapping of *dop^1* was the unavailability of *ago2* null alleles. The widely used mutant alleles *ago2^{414}* and *ago2^{51B}* have been considered as null alleles so far. However, previous studies showed that these alleles still express the short isoform of *ago2* and therefore might retain certain functions of *ago2* (Meyer, 2007; Hain et al. submitted). This work identified the mutant fly lines *ago2^{321}* and *ago2^{454}* as novel alleles of *ago2* that prevent expression of the *ago2^{short}* isoform. These putative null alleles of *ago2* complemented the developmental defects of *dop^1* which led to the final conclusion that *dop^1* is not an allele of *ago2*.

The novel *ago2* null alleles provided interesting insights into the *ago2* gene locus. Genomic sequencing showed that the deletions caused by the mobilisation of the P-element start 34 bp downstream of the first transcriptional start site (TSS1). *ago2^{321}* contains a deletion similar in size to the hypomorphic *ago2^{414}* allele. Both alleles *ago2^{321}* and *ago2^{414}* do not delete the coding region for *ago2^{short}*. This raises the question why *ago2^{414}* but not *ago2^{321}* retains expression of the short isoform. In contrast to *ago2^{414}*, *ago2^{321}* retains a fragment of the P-element downstream of TSS1.

A possible hypothesis is that the TSS1 in *ago2*[414] triggers expression of *ago2*[short] while the fragment of the P-element in *ago2*[321] is blocking promoter read-through. Further evidence for promoter read-through comes from the mapping of the deletion in *ago2*[454]. *ago2*[454] shares the upstream breakpoint with *ago2*[321], but its deletion is much larger removing the PAZ and PIWI domains up to the last two exons. Northern blot analysis shows expression of a 600 bp fragment in *ago2*[454] which might correspond to the last two exons transcribed by promoter read-through from TSS1.

Homozygous *ago2*[321] and *ago2*[454] stocks were viable, but unlike *ago2*[51B] and *ago2*[414], they exhibited low fertility in both males and females. 55% of embryos obtained from *ago2*[321] homozygous mothers did not hatch, while *ago2*[454] homozygous females did not lay any eggs. 50% ovaries from *ago2*[321] and 90% ovaries from *ago2*[454] homozygotes are rudimentary. Surprisingly, none of the phenotypes seen in *ago2*[321] or *ago2*[454] homozygotes except male sterility were seen in *ago2*[321]/*ago2*[454] trans-heterozygotes. Moreover, *ago2*[321]/*Df* or *ago2*[454]/*Df* hemizygotes (using the molecularly defined deficiencies *Df(3L)ED218* and *Df(3L)BSC5580*) displayed none of the above-mentioned phenotypes. Therefore, the fertility phenotypes observed in *ago2*[321] and *ago2*[454] homozygotes are likely attributable to background mutations. An exciting prospect for the future is to determine whether these alleles corroborate or extend the phenotypes that were previously reported for *ago2*[414] or *ago2*[51B] alleles. Such phenotypes include defective heterochromatin formation (Fagegaltier et al. 2009), defective neuromuscular junction and egg chamber development (Pepper et al., 2009) and defects in embryonic syncytial divisions and pole cell formation (Deshpande et al., 2005).

5.1.4. Interaction between *dop* and RNA silencing

The *dop^1* mutation can be partially complemented by the ectopic expression of either *ago1* or *ago2*. These findings provided the mis-leading evidence for *dop^1* being an allele of *ago2*. In retrospect these experiments might indicate an interaction between the Argonautes and Dop. In the following three possible ways of interaction between Dop and Ago2 are suggested:

Dop and Ago2 might interact directly. Evidence for the regulation of human Ago2 by phosphorylation could be shown previously (Zeng et al., 2008). Using *in vivo* labelling as well as MS approaches hAgo2 was found to be phosphorylated at serine 387. This phosphorylation was dependent on the MAPK-activated protein kinase-2 (MAPKAP2) and a phospho-deficient mutant hAgo2 protein showed decreased localisation to the P-bodies (processing bodies). P-bodies have been implicated in RNA metabolism as well as miRNA-guided gene silencing (Eulalio et al. 2007). MAPKs are members of signalling pathways that transfer extracellular signals from the cell membrane to the nucleus allowing the cell to respond to extracellular stimuli. Such signalling pathways are very often affected in various types of cancer leading to constitutive gene activation. The regulation of Ago2 by phosphorylation is not studied in *Drosophila* but might be a promising endeavour in future projects. Molecular tools like phosphospecific antibodies for Ago2 might allow the assessment of Ago2 phosphorylation in *dop^1* mutants.

A second possibility is that Dop might influence RNA silencing in an Argonaute-independent mechanism. Smaug is a major regulator of maternal mRNA destabilisation in *Drosophila* as it is essential for the destruction of maternal transcripts during the MZT (reviewed in Tadros and Lipshitz, 2005; Tadros et al., 2007). Failure of Smaug

dependent transcript destruction leads to defects in cellularisation and dissociation of the nuclei from the membrane (Dahanukar et al., 1999; Benoit et al., 2009). The results presented in this thesis show direct interaction between Dop and Smaug by immunoprecipitation of a tagged Dop protein. This interaction might be needed for proper timing of Smaug activity. In wild type embryos Smaug is provided maternally but becomes rapidly degraded with onset of the zygotic gene transcription (Tadros et al., 2007). In dop^1 mutants Smaug protein is stabilised indicating that Dop might interact with zygotic factors for Smaug degradation. Future investigation of the interaction of these proteins might show whether Dop is controlling Smaug functions during MZT. Smaug and the Ago proteins act on the degradation of mRNA levels during MZT. Both proteins have been shown to degrade a subset of RNAs and these subsets might overlap in part (Tadros and Lipshitz, 2009). Accordingly the roles of Ago2 and Smaug during MZT might be partially redundant and given that *dop* mutations lead to loss of Smaug activity Ago overexpression might complement the defects partially. Maternal overexpression of Ago2 in Smaug mutants would show if the Ago2 mediated RNA silencing pathway can partially complement defects in Smaug dependent degradation. However, the observation of the interaction between Dop and Smaug is interesting as the regulation of Smaug during MZT is not understood.

Finally, an indirect interaction between the dop^1 defects and Argonaute overexpression might be possible without Dop regulating RNA silencing. An example: Ago2 regulates the mRNA levels of *fmr1* (*fragile X mental retardation 1*) in development (Pepper et al., 2009). FMRP (the protein expressed from the *fmr1* gene) controls transport and translation of mRNA and has been shown to regulate synaptic plasticity, oogenesis and cellularisation in *Drosophila* (Monzo et al., 2006; Pepper et al.

2009). Interaction of FMRP with the microtubule associated protein MAP1B (*futsch* in *Drosophila*) leads to destabilisation of MTs. In cellularising *fmr⁻* mutant embryos *futsch* is significantly upregulated (Lu et al., 2004). In conclusion, experimental overexpression of *ago2* might lead to reduction of FMRP and successively to stabilisation of MAP1B and microtubules. Stabilisation of microtubules might reduce the lethality of *dop¹* embryos as these mutants seem to suffer from lowered microtubule stability. Future analysis of Dop interactors might offer other explanations for the interaction with Ago2.

5.2. Dop as a regulator of early embryonic development

By genetic mapping of the *dop¹* allele and several other *dop¹* non-complementing alleles this work identified a formerly uncharacterised gene as a regulator of cellularisation. The identified gene was named *dop* and phenotypic characterisation of different mutant *dop* alleles showed defects at onset of cellularisation. Two types of mutant *dop* alleles have been identified in this study. The *dop¹* mutation is a loss of function mutation that leads to the expression of a mutant protein while the *dop^{LH10}* mutation abolishes expression of the Dop protein and is considered a null mutation. The *dop¹* mutation affects an amino acid in the kinase domain of Dop and therefore might result in loss or reduction of kinase activity or substrate binding. A detailed investigation of the *dop¹* mutation and its mutant phenotype showed that *dop¹* specifically affects the slow phase of membrane growth during cellularisation while the growth during fast phase is unaffected. The slow phase-specific defect of *dop¹* allowed investigation of polarity establishment and microtubule associated vesicle transport and the defects in these processes share a common characteristic: their dependence

on Dynein mediated transport. Phenotypic and biochemical evidence suggests that Dop affects Dynein by regulating the phosphorylation of the Dynein subunit DIC.

5.2.1.   Interaction of Dop and Dynein mediated transport

Investigation of *dop*[1] mutant embryos showed defects in processes that are dependent on Dynein function. Lipid droplet transport takes course in two phases; an early Kinesin-mediated phase and a later Dynein-dependent phase (Gross et al., 2000). In *dop*[1] embryos only the Dynein dependent phase is disturbed indicating a Dynein specific effect of the *dop* mutation (Meyer et al., 2008). Further evidence for compromised Dynein functions was found in the nuclear detachment from the centrosomes. Failure to tether the nucleus towards the membrane anchored centrosomes might be the molecular reason for the name-giving 'drop out' defect in *dop*[1] mutants. Nuclear positioning has been shown to be dependent on Dynein and the Dynactin complex in several studies*. Finally, the recruitment of the apical polarity marker Baz fails in *dop*[1] mutants. Baz transport along the microtubule network was tracked using Baz-GFP overexpression and this analysis showed that Baz-GFP clusters did not move towards microtubule plus ends in *dop*[1] mutants. The imaging of Baz-GFP also indicated that the mislocalisation of Baz is only dependent on transport defects rather than failure to anchor Baz at the membrane as high amounts of overexpressed Baz-GFP were found at the apical membrane of the mutants. While no endogenous

---

*Nuclear movement is not well understood but has been found to be Dynein dependent in filamentous fungi (Xiang et al., 1993; Alberti-Segui et al., 2001; Morris, 2000), mouse neurons (Umeshima et al., 2007), insect and arthropod photoreceptors (Whited et al., 2004; Tsujikawa et al., 2007). The activity of the Dynein motors is thought to provide force to pull the nucleus towards the centrosomes. Interestingly the SUN and KASH domain containing proteins Klaroid and Klarsicht are anchored in the inner and outer nuclear membrane respectively and directly establish a connection to Dynein (Razafski and Hodzic, 2009). *klaroid* and *klarsicht* mutants also display a lipid droplet transport defect as seen in *dop*[1] mutants which might indicate that lipid droplet transport is regulated in a similar way as nuclear positioning.

Baz was found at the membrane in dop^1 mutants the overexpressed protein might have reached the apical membrane because of the unnaturally high protein levels of Baz-GFP. Baz transport to the apical membrane domain was shown to be dependent on Dynein (Harris and Peifer, 2005). The endogenous Baz in dop^1 mutants accumulates in vesicle shaped structures in the cytoplasm. A failure of Baz transport might lead to accumulation of Baz in the early endosome. The early endosome is proposed to be involved in Dynein dependent transport of vesicles and protein to the outer membrane. Co-labelling of Baz and endosome markers like Rab11 or Nuf might reveal if Baz is recruited to the membrane via this transport pathway.

The transport defects in dop^1 embryos might rely on failure of mutant Dop protein to regulate Dynein. We identified a wing phenotype in *dop* mutants, which has similarity to loss of function of the Dynein intermediate light chain (DIC) gene *short wing*. DIC is a subunit of Dynein that has been shown to regulate the interaction between Dynein and the Dynactin complex. Dynactin (Dynein activator complex) is a multi subunit protein complex that aids in bidirectional transport by binding to Dynein and Kinesin motors and linking them to cargo like organelles or vesicles (King and Schroer, 2000). Dynactin also enhances the processivity of Dynein. The p150[Glued] protein is the largest subunit of Dynactin and is essential for Dynactin function and regulation. The mammalian DIC is phosphorylated at serine 84 and this phosphorylation inhibits DIC binding to p150[Glued] (Vaughan et al., 2001). In this work initial evidence that Dop might regulate the phosphorylation state of DIC has been introduced by 2D gel electrophoresis. It was shown that DIC separates into at least 6 different protein spots when run on a protein gel. Some of those spots correspond to the 13 predicted isoforms encoded by the *short wing* gene and two of the spots were found to be

sensitive to phosphatase treatment. One of the phosphatase sensitive spots was found

to be reduced in intensity in extract from *dop¹* mutants.
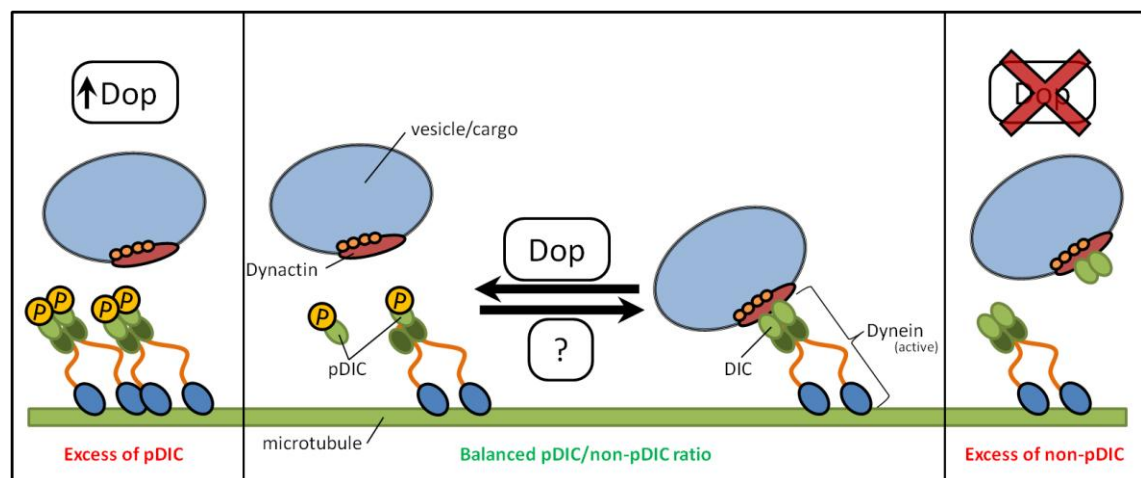
Fig. 7.1: Dop regulation of Dynein/Dynactin interaction. Phosphorylation of DIC by Dop might constitute a control mechanism to prevent binding of unassembled DIC to the cargo-associated Dynactin complex (middle). Loss of function (in *dop¹* or *dop*[LH10]) might lead to binding of unassembled DIC to Dynactin and thereby lead to sequestration of the Dynactin/cargo complex. An increased activity of the Dop kinase (e.g. by overexpression) might result in an excessive level of DIC phosphorylation which also prevents interaction between the motor and the cargo.

A model based on the hypothesis that Dop is necessary for DIC phosphorylation would

explain the defects during cellularisation. The biological significance of the DIC

phosphorylation has not been studied yet. A possible function for DIC phosphorylation

is to prevent unassembled DIC from binding to Dynactin (see Fig. 7.1). This hypothesis

might explain the defects in *dop¹* mutants. In *dop¹* mutants reduction of DIC

phosphorylation during cellularisation might lead to the binding of unassembled DIC to

p150[Glued] and therefore block Dynactin from binding to Dynein motors. This model is

consistent with the finding that overexpression of Dop induces severe defects, because

increased Dop activity might lead to phosphorylation of all DIC molecules and thereby

inhibit Dynein mediated transport completely. The ectopic aggregation of vesicles and

the abnormal structure of the furrow canal observed in *dop¹* mutants might result

from inappropriately deposited cargo vesicles sequestered from the microtubule

transport machinery or general failure of microtubule associated transport (Fig. 7.2).

Additionally, membrane transport towards the recycling endosome (RE) might fail and deplete the internal membrane pool that is needed for continous supply of membrane material during cellularisation. Therefore it would be a good idea to investigate the RE in *dop* mutant embryos.
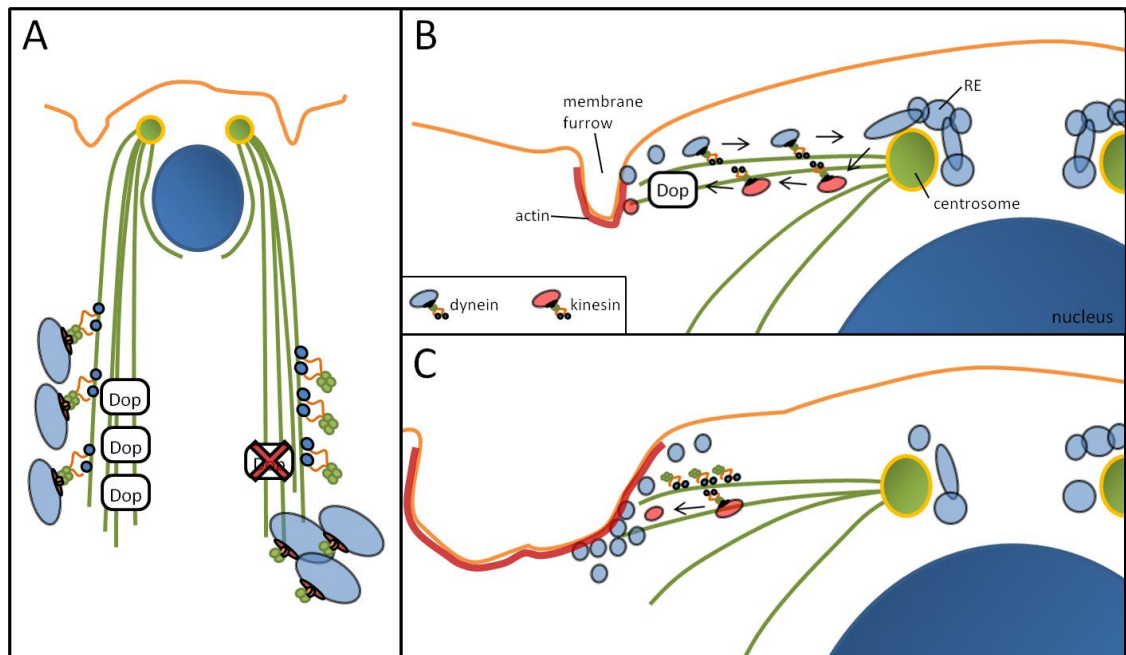
Fig. 7.2: Cell-biological consequences of Dop loss-of-function. Lack of DIC phosphorylation might in general lead to failure of attaching cargo vesicles to Dynein motors. This can be seen during the lipid droplet transport in the early embryo (A). In wild type circumstances lipid droplets are transported into the apical region during lipid clouding. The lack of Dop activity in *dop*[1] mutants leads to accumulation of droplets in the basal area of the cells. A similar mechanism might be involved into the formation of the membrane furrow (B and C). The size of the furrow might be controlled by simultaneous endocytosis and exocytosis directed by vesicle transport using Kinesin and Dynein motors. While the Kinesin motors deliver membrane material and furrow components such as actin to the furrow, Dynein motors might be needed to reduce the accumulating membrane material at the furrow and feed it back to the RE. Lack of Dynein-dependent transport might result in accumulation of membrane material at the furrow and induce unnatural furrow size.

Despite the 2DGE result seems to be very plausible several repetitions of this experiment did show very varying outcomes. A reason for varying phosphorylation levels of DIC might be that the phosphorylation changes relative to the phase of the cell cycle. Protein samples for this experiment were extracted from timed embryo collections, which allowed selection for syncytial stages and cellularisation stages but not specific stages of the cell cycle. Therefore the used protein samples might contain highly varying amounts of phosphorylated and unphosphorylated DIC. Further

experiments will be required using tightly staged embryos to address this problem. To verify the regulation of DIC phosphorylation by Dop the following experiments should be performed: (1) A direct phosphorylation of DIC by Dop could be tested by an *in vitro* phosphatase assay. This assay will surpass the influences of the cell cycle and interference of other regulators of DIC phosphorylation. (2) If the phosphorylation of DIC is regulated indirectly by Dop the protein can still be extracted from embryos. Low amounts of protein can be extracted from embryos with identical cell cycle stages. These embryos have to be monitored under the microscope and immediately lysed when the requested point in the cell cycle is reached. The use of dop^{LH10} mutants instead of dop^1 mutants would also be recommended, as it is not clear whether the dop^1 mutation is completely preventing the kinase activity of Dop.

If DIC turns out to be a direct or indirect target of Dop further investigation of the function of DIC phosphorylation should be carried out. Dop might regulate the assembly of the Dynein/Dynactin complex. A possible method to analyse Dynein/Dynactin assembly is by immunoaffinity purification *or* sucrose density gradient fractionisation using antibodies against the components of the Dynein and Dynactin complexes (like shown in El Kadi et al., 2010). This approach will show whether loss of Dop changes the association of the transport complex subunits. Multiple components of the Dynein complex are targets of phosphorylation and recent publications suggest there might be a phosphorylation code that facilitates the assembly of Dynein and regulates its motor and transport functions (Song et al. 2007). The phosphorylation changes of DIC in wild type and *dop* mutant background could be uncovered using modern phosphoproteomic methods, which might help identifying the phosphorylation site that regulates DIC. Identification of regulatory phosphorylation sites in DIC will allow creating phosphospecific antibodies and

phosphorylation defective transgenes. It will be exciting to see whether directed mutagenesis of phosphorylation sites in DIC can influence developmental processes and thereby help to understand the complex regulation of microtubule associated transport.

Other strategies have to be employed if DIC can not be confirmed as a direct or indirect Dop target. Without knowing the kinase substrates of Dop it is not possible to say how Dop is tied in with the many regulators of microtubule associated transport. An ongoing proteomic screen for Dop phosphorylation targets by heavy isotope labelling *in vivo* might reveal whether Dop specifically regulates proteins associated with Dynein or if Dop regulates transport on a global level (Langlands *et al.*, unpublished). Identification of phosphorylation sites might also help to reveal the consensus sequence for the Dop kinase domain and allow further prediction of Dop kinase substrates. The *Drosophila* model organism offers good ways to quantitatively monitor how mutations affect Dynein functions, such as the transport of the lipid droplets and modulation of mutant phenotypes like the wing defect described for *dop* and *sw* (DIC) mutants or the rough eye defect induced by *glued* mutations. Using phenotypic readout to investigate genetic interactions between *dop* and genes of putative Dop targets might help to dissect the Dop dependant regulation of Dynein mediated transport.

5.2.2. Additional effects of loss of Dynein functions

The misregulation of DIC phosphorylation might affect other transport mechanisms which might have secondary effects on the cellularisation phenotype. Genetic studies of Dynein, Kinesin and p150[Glued] function showed that these protein complexes are

interdependent in the regulation of microtubule associated transport and bind each other directly (Martin et al., 1999; Ligon et al., 2004; Shubeita et al., 2008; Hendricks et al., 2010). In this work the localisation of a Kinesin heavy chain reporter showed diffuse localisation in wild type embryos and aggregation at the microtubule plus ends in dop^1 embryos.

The results of the localisation analysis are difficult to explain without additional experiments as it was expected that the Kinesin reporter would accumulate at the basally arranged microtubule plus ends in wild type embryos. An analogy for this finding was reported for Dynein functions in *Drosophila* oocytes (Brendza et al., 2002; Palacios and St Johnston, 2002). In late stages of oogenesis the microtubules are arranged with their plus-ends facing the posterior pole and the minus-ends facing the anterior pole of the oocyte. Likewise, minus end-directed motors like Dynein should transport cargo to the apical side. Suprisingly, cytoplasmic Dynein accumulated at the posterior pole of the oocyte. This paradox was resolved by the finding that the posterior localisation of Dynein is dependent on Kinesin heavy chain. These studies showed that Dynein can be a cargo of Kinesin. Accordingly, the Kinesin-lacZ localisation in wild type embryos indicates that Kinesin motors are dispersed after reaching the plus ends of microtubules and this effect might result from immediate apical transport of the Kinesin-lacZ in a Dynein dependent manner. The basal accumulation of Kinesin-lacZ in dop^1 mutants might therefore derive from a lack of Dynein activity. To test this hypothesis the localisation of Kinesin-lacZ could be investigated in embryos with suppressed Dynein function.

The mislocalisation of the ectopically expressed Kinesin-lacZ in dop^1 mutants indicates that endogenous Kinesin is mislocalised as well. A depletion of kinesin motors at the

minus ends of microtubules might result in loss of transport towards microtubule plus ends, a process that would be needed for the transport of membrane material towards the growing membrane furrow (see Fig. 7.2B, C). Therefore the phenotype of *dop*[1] embryos might derive from multifactorial defects in the microtubule associated transport machinery. Only an analysis of direct interactors of Dop will help to explain the cause of the cellularisation defect.

5.2.3. *dop* mutations affect microtubule stability

The *dop*[1] and *dop*[LH10] alleles affect the shape of microtubules during cellularisation. Unlike in wild type, life imaging of the *dop* mutant embryos showed that microtubule bundles are easily deformed by the forces produced by the furrow canal and by the streaming yolk particles. The strong bending of microtubules might result from loss of flexural rigidity. A range of experiments to test microtubule rigidity has been established applying micromanipulation to measure the force needed for deformation of purified microtubules (Kikumoto et al., 2005). In future experiments the rigidity of microtubules could be measured in presence or absence of Dop to prove if Dop is involved in the regulation of microtubule rigidity.

A loss of microtubule rigidity in Dop mutants might explain the broadening of the furrow canal observed in *dop*[1] and *dop*[LH10] embryos. The organisation of the microtubule skeleton during cytokinesis has been shown to be important for the directed transport of furrow determinants like actin and the Rho activator Pebble towards the furrow region (Ai and Skop, 2009). Destabilisation of microtubule asters by injection of Nocodazole was shown to induce broadening of the cytokinetic furrow

in sea urchin zygotes (Foe and von Dassow, 2008; Odell and Foe, 2008). Similar to cytokinetic furrows the furrow canal might be regulated by the precise position of microtubule plus ends. Dop might contribute to furrow formation by regulating the stabilisation of microtubule plus ends at the furrow and by controlling the microtubule dependent transport of vesicles and proteins to the furrow. The DUF domain of Dop might be needed for the localised activity of Dop at the furrow canal, stabilising microtubules in the furrow region specifically.

A possible mechanism for how Dop might control microtubule stability is indicated by the localisation of the Dop homolog MAST2. MAST2 was shown to bind microtubules indirectly in a MAP (microtubule associated protein) dependent manner (Walden et al., 1993). This finding suggests that MAST kinases bind MAPs and might regulate their functions or affect their binding to microtubules. Several studies showed that microtubule associated proteins (MAPs) can enhance the rigidity of microtubules (Kurachi et al., 1995; Mickey and Howard, 1995; Felgner et al., 1996; Felgner et al., 1997). Dop might be involved in tethering MAPs to microtubules and thereby affect microtubule stability. An interaction between Dop and MAPs might also regulate microtubule associated transport. Although the functions of MAPs in regulating Dynein and Kinesin motors are not well investigated, studies of the MAP Tau showed the possibility of regulatory interactions between MAPs and microtubule associated transport (Dixit et al., 2008). The identification of MAPs as phosphorylation targets of Dop might provide interesting insights for localised control of Dynein and Kinesin dependent transport.

This work provides evidence that Dop-GFP localises to microtubules during syncytial cleavage cycles and cellularisation. Therefore Dop might not only affect microtubule

rigidity during cellularisation but also at the mitotic spindle. Misregulation of microtubule stability might induce serious defects in cellular division and although no cell cycle or spindle defects have been found in *dop*[1] mutants there might be defects in *dop* null mutants and in *dop* overexpressing embryos. Further evidence for a role for Dop in cellular divisions was found by a genome wide screen for kinases in cell cycle regulation which showed that RNAi against the *dop* gene leads to cell cycle arrest in G2 and metaphase and also chromosome alignment defects (Bettencourt-Dias et al., 2004). However, these results must be interpreted carefully as there were no follow up studies of this finding so far and high throughput RNAi screens are not always reliable. The detailed investigation of cell cycle timing and structure of the spindle in *dop* null mutant embryos will show whether Dop plays a significant role in the cell cycle.

5.2.4. *dop* in the regulation of apico/basal polarity

Analysis of *dop*[1] mutant embryos showed that Dop is involved into the establishment of polarity complexes along the apico/basal membrane (Fig.7.3). During wild type cellularisation the membrane is separated into lateral and basal membrane regions by the localisation of polarity proteins. The basal furrow canal is an isolated membrane domain as neither membrane lipids nor membrane associated proteins mix with the lateral domain (Lecuit and Wieschaus, 2000). The Dlg protein is a protein of the lateral membrane and is absent from the furrow canal. In *dop*[1] embryos Dlg crossed the membrane boundaries as it was found at the furrow canal and also spread far into apico-lateral regions of the membrane. Also the localisation of RhoA which is restricted to the furrow canal in wild type was found in lateral and apical membrane regions. There might be several reasons for polarity proteins crossing membrane compartment

borders. The formation of polarity complexes is dependent on microtubules and microtubule associated transport. As *dop* mutations disturb microtubule stability and microtubule associated transport the polarity defects might be a result of secondary nature. However, Dop might also regulate polarity in other ways, for example by interacting with membrane bound proteins directly.
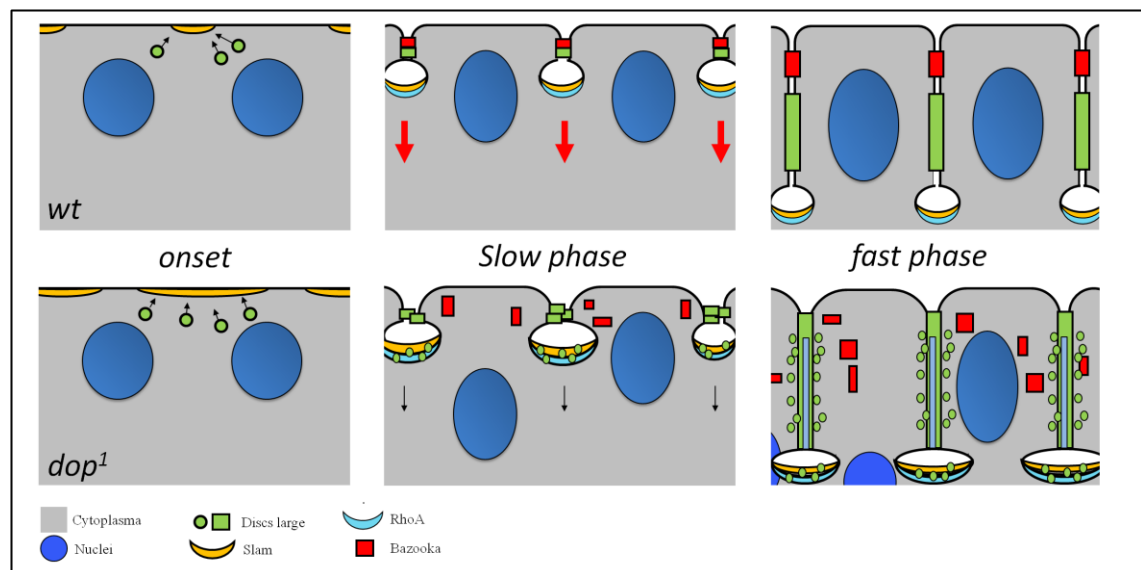
Fig. 7.3: Polarity defects in *dop*[1] embryos. At onset of cellularisation furrow markers arrange between the nuclei. While wild type embryos establish a narrow furrow region the furrow is enlarged in *dop*[1] mutants. During cellularisation lateral and basal polarity proteins are separated in different membrane regions. This strict separation is failing in *dop*[1] mutants as Dlg protein diffuses into the furrow canal and RhoA diffuses into the lateral region. Furthermore the formation of apical polarity complexes is inhibited as Baz cannot arrange at the membrane but accumulates in the apical cytoplasm. Further abnormalities are found in the structure of the lateral membrane. Staining of several lateral marker proteins show a diffuse outline of the lateral membrane, indicating that vesicles containing these markers are not properly inserted into the membrane.

A membrane associated protein that might interact with Dop is α-actinin, an actin bundling protein that also functions in the binding of trans-membrane proteins and receptors with the actin network. Some of its interactors are Cadherins, αCatenin and Dlg. α-actinin is needed for the tight control of actin assembly during cytokinesis (Mukhina et al., 2007). Mammalian α-actinin-4 was also suggested to play a role during endocytosis (Geiger and Singer 1979; Kim et al., 2002; Lanzetti et al., 2004). In a mass spectrometry fingerprint analysis α-actinin was found to bind to the PDZ-domain of

Dop (data not shown). Although this finding has to be confirmed by further experiments, the possible interaction of these proteins is very interesting. Lack of Dop binding to α-actinin might result in failure to regulate the connection between microtubules and Actin at distinct membrane sites and result in mislocalised recruitment of polarity regulators. Dlg staining in the mutants shows a disrupted/spotted pattern of the lateral membrane indicating that the lateral membrane is surrounded by membrane vesicles. These vesicles might not reach the membrane correctly and successively insert at random positions. A detailed analysis of vesicle trafficking by using GFP-labelled markers for Golgi- or RE-mediated vesicle transport towards specific membrane regions might confirm this theory.

The function of Dop in the regulation of epithelial polarity and cell junctions uncovers an interesting link between the human MAST3 and inflammatory bowel disease (IBD). In genetic linkage studies MAST3 mutations were found in patients that suffer from IBD (Labbe et al.; 2008). IBD is characterised by inflammation with defects in barrier and secretory function of the intestinal epithelium mucosal surface (Henderson, 2010). In mature epithelia cell-cell junctions provide an epithelial barrier function. Localisation studies in mucosal biopsies from IBD patients have revealed disruption of key Tight-junction (occludin, JAM1, ZO1, claudin 1) and adherens-junction (E-cadherin, beta-catenin) proteins from intercellular junctions (Ivanov et al., 2004). The effect of Dop on epithelial proteins shown in this work indicates that loss of MAST3 function might weaken the barrier function of epithelial tissues by failure to recruit polarity complex proteins.

5.2.5. The regulation of Dop

Investigation of the Dop protein and its localisation suggest that Dop function is regulated during different developmental stages. The predicted size for Dop is around 225 kDa (http://expasy.org/tools/pi_tool.html) but in embryonic lysates Dop protein is found in several protein bands around 300 kDa and the intensity of these bands varies throughout development. This finding suggests posttranslational modification in a developmental context. The observed band shift might be a result of phosphorylation. A likely role for phosphorylation of Dop might be the stabilisation of the protein. dop^1 mutant embryos carry a nonsynonymous mutation in the kinase domain and only low levels of Dop are found in these mutants. It is possible that the mutation in dop^1 affects autophosphorylation and that this elevates Dop stability or prevents its degradation. The regulation of Dop by phosphorylation should be investigated in other mutant fly lines displaying early developmental defects. Dop band shift might be affected in mutants of the cell cycle control like *grapes* or the machinery that controls initiation of cellularisation like the *zelda* or *smaug*.

Identification of the modification of Dop protein is important as it would allow insight into Dop regulation during development. The state of Dop changes as the Dop protein band shifts significantly after the first one to two hours of development. In embryo populations used for protein extraction the first two hours contain mostly embryos in the syncytial division stage, while older embryo collections contain cellularisation and blastoderm stages. Therefore, the band shift of Dop indicates that Dop is modified at onset of cellularisation. Additionally, the phenotypes of the *dop* mutants suggest that Dop might be specifically activated during cellularisation as the most severe defect in mat/zyg dop^1 and dop^{LH10} mutants is the cellularisation defect. In contrast, zygotic *dop*

mutants that have the wild type maternal *dop* contribution in early embryonic development develop almost normally. Homozygous *dop*^LH10 flies can survive for 6 to 8 weeks which is comparable to wild type flies. Interestingly, these mutants are much weaker than wild type flies as they are not able to hold on to vertical surfaces and are prone to get stuck in the fly food. The weakness of the flies might indicate a neuronal defect which could be explained by the interaction of mammalian MAST kinases with β2-syntrophin of the Dystrophin complex in motoneurons (Lumeng et al., 1999).

The regulation of the Dop kinase might also affect its localisation. Dop localisation is influenced by its accessory domains. The expression of the DUF domain in syncytial embryos showed localisation to the pseudo-cleavage furrow and a cell cycle dependent translocation towards the mitotic spindle. Therefore Dop might actively be involved into function of the mitotic spindle or into transport processes along the spindle microtubules. In future experiments the localisation of Dop or overexpressed Dop domains might be analysed in mutants that affect cellularisation and syncytial divisions. This analysis might provide more detail about the interactions of Dop and how it is localised.

5.2.6. Dop and the MAST kinases

Dop encodes the sole *Drosophila* homologue of the MAST kinase family. Phylogenetic analysis showed that the DUF/Kinase/PDZ domain structure of the MAST kinases is conserved in metazoan organisms. The most ancient organism known encoding a MAST gene is *Amphimedon queenslandica*, a sponge with an epithelial-like cell layer that also expresses other polarity regulators such as the tumor suppressor Dlg

(Srivastava et al., 2010). Therefore the evolutionary conserved role for MAST kinases might be associated with epithelial morphogenesis. The conserved protein domains of Dop show a very high homology to the domains of mammalian MAST kinases. Mammalian MAST2 (MAST205) is the first identified member of the MAST kinase family and was found associated with the microtubules of the spermatid manchette (Walden and Cowan, 1993). The spermatid manchette is a microtubule structure involved into the maturation and elongation of the sperm tail. *Drosophila* species are known to have the longest sperm tails of all animals and provide a good model to study sperm maturation. However, the studies of Dop do not suggest an important function in sperm development as *dop* mutant males are fertile.

Functional studies of MAST kinases are rarely published to date. This situation could change soon as MAST kinases have recently been implicated in various human diseases. Investigation of *dop* mutant flies might allow assessing the roles of MAST kinases in human diseases. Common haplotypes of MAST2 have been found to elevate the risk of breast cancer (Wang et al., 2009). The finding that Dop overexpression slows the syncytial divisions implies that MAST kinases might affect the cell cycle or the proper execution of mitosis. Further studies of Dop function in early syncytial cell cylces and in tissue culture may show whether the loss of Dop induces significant defects in cell cycle control. MAST3 has been found to suppress neuronal growth (Loh et al., 2007). The misregulation of synaptic integrity, loss of connectivity and axodendritic degeneration is a cause for neurodegenerative diseases. *Drosophila* is a well recognised model organism to study neurodegenerative diseases like Alzheimer`s or Parkinson`s disease (Jeibmann and Paulus, 2009; Moloney et al., 2010). The toolkit to investigate these diseases in the fly ranges from the assessment of phenotypes like

longevity and behaviour to the dissection of precisely conserved molecular mechanisms. MAST3 has also been found to be involved into inflammatory bowel diseases (IBD) such as Crohns`s disease or ulcerative colitis. The authors suggest that MAST3 plays a role in these diseases by modulating TLR4 signalling (Labbè et al., 2008). The findings made in this study offer an alternative and interesting view on MAST3 function in IBD by regulating epithelial boundaries (see 7.2.4). These examples show that future studies of Dop might help understanding the human diseases caused by mutations in MAST kinases. Cross species gene expression of Dop and MAST kinases might show whether the functions of these kinases are conserved.

Conclusion:

The aim of my PhD project was to investigate the molecular mechanism for the developmental defects induced by the dop^1 allele. Previously published data for dop^1 mutant flies showed a genetic aberration in the *ago2* gene. In the work presented here I show that the found aberration of *ago2* does not affect development and that loss of *ago2* function is not associated with the developmental defects observed in dop^1 mutants. In addition the identification of novel *ago2* null mutations proves that the current developmental roles for *ago2* have to be re-evaluated.

By deficiency mapping and genomic sequencing I identified an additional molecular aberration in dop^1 mutants. The mutation lies in the *dop* gene (formerly named *CG6498*) which encodes the *Drosophila* homolog of the MAST kinase family proteins and loss of dop function is responsible for the developmental defects in dop^1 mutants.

Phenotypic analysis of dop^1 embryos showed severe effects on the membrane transport during cellularisation and mislocalisation of apico/basal polarity markers. Further investigation of the mechanisms for the transport of membrane material and polarity regulators suggested that the dop^1 phenotype results from mis-regulation of microtubule dependent transport. Accordingly variations in the phosphorylation pattern of the Dynein intermediate chain were found in wild type and dop^1 embryos. The function of Dop as an activator of Dynein-mediated transport is very interesting as Dop itself seems to be highly regulated and restricted to specific developmental stages and cell types. Therefore, Dop might define one member of a complex group of transport regulators, each responsible for the control of distinct steps of microtubule associated transport.

An interaction of Dop with other proteins is very likely. I could confirm interaction of Dop with the RNA binding protein Smaug and phenotypic characteristics of dop mutants also point towards an interaction with the secretory pathway through proteins like Nuf, Rab11 or

Dynamin which could not be excluded in this work. Biochemical identification of direct interaction partners and phosphorylation targets seems highly promising in the further task to understand the role of the Dop kinase.

Reference List

Abbott, L. A. and J. E. Natzle. "Epithelial polarity and cell separation in the neoplastic l(1)dlg-1 mutant of Drosophila." Mech.Dev. 37.1-2 (1992): 43-56.

Ai, E. and A. R. Skop. "Endosomal recycling regulation during cytokinesis." Commun.Integr.Biol. 2.5 (2009): 444-47.

Albertson, R., et al. "Vesicles and actin are targeted to the cleavage furrow via furrow microtubules and the central spindle." J.Cell Biol. 181.5 (2008): 777-90.

Amano, M., et al. "Phosphorylation and activation of myosin by Rho-associated kinase (Rho-kinase)." J.Biol.Chem. 271.34 (1996): 20246-49.

Ang, A. L., et al. "Recycling endosomes can serve as intermediates during transport from the Golgi to the plasma membrane of MDCK cells." J.Cell Biol. 167.3 (2004): 531-43.

Bashirullah, A., R. L. Cooperstock, and H. D. Lipshitz. "Spatial and temporal control of RNA stability." Proc.Natl.Acad.Sci.U.S.A 98.13 (2001): 7025-28.

Baulcombe, D. C. "Gene silencing: RNA makes RNA makes no protein." Curr.Biol. 9.16 (1999): R599-R601.

Benoit, B., et al. "An essential role for the RNA-binding protein Smaug during the Drosophila maternal-to-zygotic transition." Development 136.6 (2009): 923-32.

Benton, R. and Johnston D. St. "Drosophila PAR-1 and 14-3-3 inhibit Bazooka/PAR-3 to establish complementary cortical domains in polarized cells." Cell 115.6 (2003): 691-704.

Bernstein, E., et al. "Role for a bidentate ribonuclease in the initiation step of RNA interference." Nature 409.6818 (2001): 363-66.

Beronja, S. and U. Tepass. "Cellular morphogenesis: slow-as-molasses accelerates polarized membrane growth." Dev.Cell 2.4 (2002): 382-84.

Bettencourt-Dias, M., et al. "Genome-wide survey of protein kinases required for cell cycle progression." Nature 432.7020 (2004): 980-87.

Bilder, D. "Epithelial polarity and proliferation control: links from the Drosophila neoplastic tumor suppressors." Genes Dev. 18.16 (2004): 1909-25.

Bilder, D., M. Li, and N. Perrimon. "Cooperative regulation of cell polarity and growth by Drosophila tumor suppressors." Science 289.5476 (2000): 113-16.

Bischof, J., et al. "An optimized transgenesis system for Drosophila using germ-line-specific phiC31 integrases." Proc.Natl.Acad.Sci.U.S.A 104.9 (2007): 3312-17.

Brand, A. H. and N. Perrimon. "Targeted gene expression as a means of altering cell fates and generating dominant phenotypes." Development 118.2 (1993): 401-15.

Brendza, R. P., et al. "Posterior localization of dynein and dorsal-ventral axis formation depend on kinesin in Drosophila oocytes." Curr.Biol. 12.17 (2002): 1541-45.

Bushati, N., et al. "Temporal reciprocity of miRNAs and their targets during the maternal-to-zygotic transition in Drosophila." Curr.Biol. 18.7 (2008): 501-06.

Cao, J., et al. "Nuf, a Rab11 effector, maintains cytokinetic furrow integrity by promoting local actin polymerization." J.Cell Biol. 182.2 (2008): 301-13.

Carmell, M. A., et al. "The Argonaute family: tentacles that reach into RNAi, developmental control, stem cell maintenance, and tumorigenesis." Genes Dev. 16.21 (2002): 2733-42.

Cavener, D. R. "Comparison of the consensus sequence flanking translational start sites in Drosophila and vertebrates." Nucleic Acids Res. 15.4 (1987): 1353-61.

Cermelli, S., et al. "The lipid-droplet proteome reveals that droplets are a protein-storage depot." Curr.Biol. 16.18 (2006): 1783-95.

Chen, M. S., et al. "Multiple forms of dynamin are encoded by shibire, a Drosophila gene involved in endocytosis." Nature 351.6327 (1991): 583-86.

Chen, X., et al. "p120 catenin associates with kinesin and facilitates the transport of cadherin-catenin complexes to intercellular junctions." J.Cell Biol. 163.3 (2003): 547-57.

Cohen, R. S. "Microtubule motors: LSD2 trips the toggle." Curr.Biol. 15.17 (2005): R651-R653.

Cortese, M. S., et al. "Uncovering the unfoldome: enriching cell extracts for unstructured proteins by acid treatment." J.Proteome.Res. 4.5 (2005): 1610-18.

Dahanukar, A., J. A. Walker, and R. P. Wharton. "Smaug, a novel RNA-binding protein that operates a translational switch in Drosophila." Mol.Cell 4.2 (1999): 209-18.

De, Renzis S., et al. "Unmasking activation of the zygotic genome using chromosomal deletions in the Drosophila embryo." PLoS.Biol. 5.5 (2007): e117.

Deshpande, G., G. Calhoun, and P. Schedl. "Drosophila argonaute-2 is required early in embryogenesis for the assembly of centric/centromeric heterochromatin, nuclear division, nuclear migration, and germ-cell formation." Genes Dev. 19.14 (2005): 1680-85.

Dillman, J. F., III and K. K. Pfister. "Differential phosphorylation in vivo of cytoplasmic dynein associated with anterogradely moving organelles." J.Cell Biol. 127.6 Pt 1 (1994): 1671-81.

Dixit, R., et al. "Differential regulation of dynein and kinesin motor proteins by tau." Science 319.5866 (2008): 1086-89.

Dollar, G., et al. "Rab11 polarization of the Drosophila oocyte: a novel link between membrane trafficking, microtubule organization, and oskar mRNA localization and translation." Development 129.2 (2002): 517-26.

Edgar, B. A., C. P. Kiehle, and G. Schubiger. "Cell cycle control by the nucleo-cytoplasmic ratio in early Drosophila development." Cell 44.2 (1986): 365-72.

Eulalio, A., et al. "P-body formation is a consequence, not the cause, of RNA-mediated gene silencing." Mol.Cell Biol. 27.11 (2007): 3970-81.

Fagegaltier, D., et al. "The endogenous siRNA pathway is involved in heterochromatin formation in Drosophila." Proc.Natl.Acad.Sci.U.S.A 106.50 (2009): 21258-63.

Felgner, H., et al. "Domains of neuronal microtubule-associated proteins and flexural rigidity of microtubules." J.Cell Biol. 138.5 (1997): 1067-75.

Felgner, H., R. Frank, and M. Schliwa. "Flexural rigidity of microtubules measured with the use of optical tweezers." J.Cell Sci. 109 (Pt 2) (1996): 509-16.

Fire, A., et al. "Potent and specific genetic interference by double-stranded RNA in Caenorhabditis elegans." Nature 391.6669 (1998): 806-11.

Foe, V. E., C. M. Field, and G. M. Odell. "Microtubules and mitotic cycle phase modulate spatiotemporal distributions of F-actin and myosin II in Drosophila syncytial blastoderm embryos." Development 127.9 (2000): 1767-87.

Forstemann, K., et al. "Drosophila microRNAs are sorted into functionally distinct argonaute complexes after production by dicer-1." Cell 130.2 (2007): 287-97.

Galewsky, S. and R. A. Schulz. "Drop out: a third chromosome maternal-effect locus required for formation of the Drosophila cellular blastoderm." Mol.Reprod.Dev. 32.4 (1992): 331-38.

Geiger, B. and S. J. Singer. "The participation of alpha-actinin in the capping of cell membrane components." Cell 16.1 (1979): 213-22.

Ghildiyal, M., et al. "Endogenous siRNAs derived from transposons and mRNAs in Drosophila somatic cells." Science 320.5879 (2008): 1077-81.

Ghildiyal, M., et al. "Sorting of Drosophila small silencing RNAs partitions microRNA* strands into the RNA interference pathway." RNA. 16.1 (2010): 43-56.

Gindhart, J. G., Jr., et al. "Kinesin light chains are essential for axonal transport in Drosophila." J.Cell Biol. 141.2 (1998): 443-54.

Giraldez, A. J., et al. "Zebrafish MiR-430 promotes deadenylation and clearance of maternal mRNAs." Science 312.5770 (2006): 75-79.

Glotzer, J. B., et al. "Cytoplasmic flows localize injected oskar RNA in Drosophila oocytes." Curr.Biol. 7.5 (1997): 326-37.

Glotzer, M. "Animal cell cytokinesis." Annu.Rev.Cell Dev.Biol. 17 (2001): 351-86.

Grant, D., et al. "Probable mechanisms underlying interallelic complementation and temperature-sensitivity of mutations at the shibire locus of Drosophila melanogaster." Genetics 149.2 (1998): 1019-30.

Gross, S. P., et al. "Interactions and regulation of molecular motors in Xenopus melanophores." J.Cell Biol. 156.5 (2002): 855-65.

Gross, S. P., et al. "Coordination of opposite-polarity microtubule motors." J.Cell Biol. 156.4 (2002): 715-24.

---. "Dynein-mediated cargo transport in vivo. A switch controls travel distance." J.Cell Biol. 148.5 (2000): 945-56.

Grosshans, J., H. A. Muller, and E. Wieschaus. "Control of cleavage cycles in Drosophila embryos by fruhstart." Dev.Cell 5.2 (2003): 285-94.

Grosshans, J., et al. "RhoGEF2 and the formin Dia control the formation of the furrow canal by directed actin assembly during Drosophila cellularisation." Development 132.5 (2005): 1009-20.

Guo, Y., S. Jangi, and M. A. Welte. "Organelle-specific control of intracellular transport: distinctly targeted isoforms of the regulator Klar." Mol.Biol.Cell 16.3 (2005): 1406-16.

Hanks, S. K. "Genomic analysis of the eukaryotic protein kinase superfamily: a perspective." Genome Biol. 4.5 (2003): 111.

Hanks, S. K. and T. Hunter. "Protein kinases 6. The eukaryotic protein kinase superfamily: kinase (catalytic) domain structure and classification." FASEB J. 9.8 (1995): 576-96.

Hanks, S. K., A. M. Quinn, and T. Hunter. "The protein kinase family: conserved features and deduced phylogeny of the catalytic domains." Science 241.4861 (1988): 42-52.

Harris, T. J. and M. Peifer. "Adherens junction-dependent and -independent steps in the establishment of epithelial cell polarity in Drosophila." J.Cell Biol. 167.1 (2004): 135-47.

---. "aPKC controls microtubule organization to balance adherens junction symmetry and planar polarity during development." Dev.Cell 12.5 (2007): 727-38.

---. "The positioning and segregation of apical cues during epithelial polarity establishment in Drosophila." J.Cell Biol. 170.5 (2005): 813-23.

Harrison, M. M., M. R. Botchan, and T. W. Cline. "Grainyhead and Zelda compete for binding to the promoters of the earliest-expressed Drosophila genes." Dev.Biol. 345.2 (2010): 248-55.

Henderson, P., et al. "Function of the intestinal epithelium and its dysregulation in inflammatory bowel disease." Inflamm.Bowel.Dis. (2010).

Hendricks, A. G., et al. "Motor Coordination via a Tug-of-War Mechanism Drives Bidirectional Vesicle Transport." Curr.Biol. (2010).

Hermiston, M. L. and J. I. Gordon. "Inflammatory bowel disease and adenomas in mice expressing a dominant negative N-cadherin." Science 270.5239 (1995): 1203-07.

Huh, J. R., M. Guo, and B. A. Hay. "Compensatory proliferation induced by cell death in the Drosophila wing disc requires activity of the apical cell death caspase Dronc in a nonapoptotic role." Curr.Biol. 14.14 (2004): 1262-66.

Humbert, P., S. Russell, and H. Richardson. "Dlg, Scribble and Lgl in cell polarity, cell proliferation and cancer." Bioessays 25.6 (2003): 542-53.

Ishizaki, T., et al. "Coordination of microtubules and the actin cytoskeleton by the Rho effector mDia1." Nat.Cell Biol. 3.1 (2001): 8-14.

Ivanov, A. I., A. Nusrat, and C. A. Parkos. "The epithelium in inflammatory bowel disease: potential role of endocytosis of junctional proteins in barrier disruption." Novartis.Found.Symp. 263 (2004): 115-24.

Iwasaki, S., T. Kawamata, and Y. Tomari. "Drosophila argonaute1 and argonaute2 employ distinct mechanisms for translational repression." Mol.Cell 34.1 (2009): 58-67.

Iwasaki, S. and Y. Tomari. "Argonaute-mediated translational repression (and activation)." Fly.(Austin.) 3.3 (2009): 204-06.

Jeibmann, A. and W. Paulus. "Drosophila melanogaster as a model organism of brain diseases." Int.J.Mol.Sci. 10.2 (2009): 407-40.

Johnson, L. N., et al. "The Eleventh Datta Lecture. The structural basis for substrate recognition and control by protein kinases." FEBS Lett. 430.1-2 (1998): 1-11.

Karpov, P. A., et al. "[Bioinformatic search of plant protein kinases, participating in microtubule protein phosphorylation and cell division regulation]." Tsitol.Genet. 43.3 (2009): 63-79.

Karpova, N., et al. "Jupiter, a new Drosophila protein associated with microtubules." Cell Motil.Cytoskeleton 63.5 (2006): 301-12.

Karr, T. L. and B. M. Alberts. "Organization of the cytoskeleton in early Drosophila embryos." J.Cell Biol. 102.4 (1986): 1494-509.

Kataoka, Y., M. Takeichi, and T. Uemura. "Developmental roles and molecular characterization of a Drosophila homologue of Arabidopsis Argonaute1, the founder of a novel gene superfamily." Genes Cells 6.4 (2001): 313-25.

Kikumoto, M., et al. "Flexural rigidity of individual microtubules measured by a buckling force with optical traps." Biophys.J. 90.5 (2006): 1687-96.

Kim, J. H., et al. "Ca(2+)-dependent inhibition of Na+/H+ exchanger 3 (NHE3) requires an NHE3-E3KARP-alpha-actinin-4 complex for oligomerization and endocytosis." J.Biol.Chem. 277.26 (2002): 23714-24.

King, S. J. and T. A. Schroer. "Dynactin increases the processivity of the cytoplasmic dynein motor." Nat.Cell Biol. 2.1 (2000): 20-24.

Koch, R., et al. "Systematic functional analysis of Bicaudal-D serine phosphorylation and intragenic suppression of a female sterile allele of BicD." PLoS.One. 4.2 (2009): e4552.

Krahn, M. P., D. Egger-Adam, and A. Wodarz. "PP2A antagonizes phosphorylation of Bazooka by PAR-1 to control apical-basal polarity in dividing embryonic neuroblasts." Dev.Cell 16.6 (2009): 901-08.

Kurachi, M., M. Hoshi, and H. Tashiro. "Buckling of a single microtubule by optical trapping forces: direct measurement of microtubule rigidity." Cell Motil.Cytoskeleton 30.3 (1995): 221-28.

Labbe, C., et al. "MAST3: a novel IBD risk factor that modulates TLR4 signaling." Genes Immun. 9.7 (2008): 602-12.

Lanzetti, L., et al. "Rab5 is a signalling GTPase involved in actin remodelling by receptor tyrosine kinases." Nature 429.6989 (2004): 309-14.

Leaman, D., et al. "Antisense-mediated depletion reveals essential and specific functions of microRNAs in Drosophila development." Cell 121.7 (2005): 1097-108.

Lecuit, T. "Junctions and vesicular trafficking during Drosophila cellularization." J.Cell Sci. 117.Pt 16 (2004): 3427-33.

Lecuit, T. and E. Wieschaus. "Polarized insertion of new membrane from a cytoplasmic reservoir during cleavage of the Drosophila embryo." J.Cell Biol. 150.4 (2000): 849-60.

Lecuyer, E., et al. "Global analysis of mRNA localization reveals a prominent role in organizing cellular architecture and function." Cell 131.1 (2007): 174-87.

Liang, H. L., et al. "The zinc-finger protein Zelda is a key activator of the early zygotic genome in Drosophila." Nature 456.7220 (2008): 400-03.

Ligon, L. A., et al. "A direct interaction between cytoplasmic dynein and kinesin I may coordinate motor activity." J.Biol.Chem. 279.18 (2004): 19201-08.

Lingel, A., et al. "Structure and nucleic-acid binding of the Drosophila Argonaute 2 PAZ domain." Nature 426.6965 (2003): 465-69.

Liu, J., et al. "Argonaute2 is the catalytic engine of mammalian RNAi." Science 305.5689 (2004): 1437-41.

Liu, J. J. and S. Lindquist. "Oligopeptide-repeat expansions modulate 'protein-only' inheritance in yeast." Nature 400.6744 (1999): 573-76.

Liu, Y., et al. "C3PO, an endoribonuclease that promotes RNAi by facilitating RISC activation." Science 325.5941 (2009): 750-53.

Lock, J. G., et al. "E-cadherin transport from the trans-Golgi network in tubulovesicular carriers is selectively regulated by golgin-97." Traffic. 6.12 (2005): 1142-56.

Lock, J. G. and J. L. Stow. "Rab11 in recycling endosomes regulates the sorting and basolateral transport of E-cadherin." Mol.Biol.Cell 16.4 (2005): 1744-55.

Loh, S. H., et al. "Identification of new kinase clusters required for neurite outgrowth and retraction by a loss-of-function RNA interference screen." Cell Death.Differ. 15.2 (2008): 283-98.

Lu, R., et al. "The fragile X protein controls microtubule-associated protein 1B translation and microtubule stability in brain neuron development." Proc.Natl.Acad.Sci.U.S.A 101.42 (2004): 15201-06.

Lu, X., et al. "Coupling of zygotic transcription to mitotic control at the Drosophila mid-blastula transition." Development 136.12 (2009): 2101-10.

Lumeng, C., et al. "Interactions between beta 2-syntrophin and a family of microtubule-associated serine/threonine kinases." Nat.Neurosci. 2.7 (1999): 611-17.

Lykke-Andersen, K., et al. "Maternal Argonaute 2 is essential for early mouse development at the maternal-zygotic transition." Mol.Biol.Cell 19.10 (2008): 4383-92.

Mani, S. A., et al. "The epithelial-mesenchymal transition generates cells with properties of stem cells." Cell 133.4 (2008): 704-15.

Manning, G., et al. "The protein kinase complement of the human genome." Science 298.5600 (2002): 1912-34.

Martin, M., et al. "Cytoplasmic dynein, the dynactin complex, and kinesin are interdependent and essential for fast axonal transport." Mol.Biol.Cell 10.11 (1999): 3717-28.

Mavrakis, M., et al. "Fluorescence imaging techniques for studying Drosophila embryo development." Curr.Protoc.Cell Biol. Chapter 4 (2008): Unit.

Mavrakis, M., R. Rikhy, and J. Lippincott-Schwartz. "Cells within a cell: Insights into cellular architecture and polarization from the organization of the early fly embryo." Commun.Integr.Biol. 2.4 (2009): 313-14.

---. "Plasma membrane polarity and compartmentalization are established before cellularization in the fly embryo." Dev.Cell 16.1 (2009): 93-104.

Mazumdar, A. and M. Mazumdar. "How one becomes many: blastoderm cellularization in Drosophila melanogaster." Bioessays 24.11 (2002): 1012-22.

McCleland, M. L., A. W. Shermoen, and P. H. O'Farrell. "DNA replication times the cell cycle and contributes to the mid-blastula transition in Drosophila embryos." J.Cell Biol. 187.1 (2009): 7-14.

McGill, M. A., R. F. McKinley, and T. J. Harris. "Independent cadherin-catenin and Bazooka clusters interact to assemble adherens junctions." J.Cell Biol. 185.5 (2009): 787-96.

Meister, G., et al. "Human Argonaute2 mediates RNA cleavage targeted by miRNAs and siRNAs." Mol.Cell 15.2 (2004): 185-97.

Merrill, P. T., D. Sweeton, and E. Wieschaus. "Requirements for autosomal gene activity during precellular stages of Drosophila melanogaster." Development 104.3 (1988): 495-509.

Meyer, W. J., et al. "Overlapping functions of argonaute proteins in patterning and morphogenesis of Drosophila embryos." PLoS.Genet. 2.8 (2006): e134.

Miyoshi, K., et al. "Slicer function of Drosophila Argonautes and its involvement in RISC formation." Genes Dev. 19.23 (2005): 2837-48.

Moloney, A., et al. "Alzheimer's disease: insights from Drosophila melanogaster models." Trends Biochem.Sci. 35.4 (2010): 228-35.

Monzo, K., et al. "Fragile X mental retardation protein controls trailer hitch expression and cleavage furrow formation in Drosophila embryos." Proc.Natl.Acad.Sci.U.S.A 103.48 (2006): 18160-65.

Morrison, D. K., M. S. Murakami, and V. Cleghon. "Protein kinases and phosphatases in the Drosophila genome." J.Cell Biol. 150.2 (2000): F57-F62.

Mukhina, S., Y. L. Wang, and M. Murata-Hori. "Alpha-actinin is required for tightly regulated remodeling of the actin cortical network during cytokinesis." Dev.Cell 13.4 (2007): 554-65.

Muller, H. A. "Genetic control of epithelial cell polarity: lessons from Drosophila." Dev.Dyn. 218.1 (2000): 52-67.

---. "Of mice, frogs and flies: generation of membrane asymmetries in early development." Dev.Growth Differ. 43.4 (2001): 327-42.

Muller, H. A. and E. Wieschaus. "armadillo, bazooka, and stardust are critical for early stages in formation of the zonula adherens and maintenance of the polarized blastoderm epithelium in Drosophila." J.Cell Biol. 134.1 (1996): 149-63.

Murray, J. W. and A. W. Wolkoff. "Assay of Rab4-dependent trafficking on microtubules." Methods Enzymol. 403 (2005): 92-107.

Nagai-Tamai, Y., et al. "Regulated protein-protein interaction between aPKC and PAR-3 plays an essential role in the polarization of epithelial cells." Genes Cells 7.11 (2002): 1161-71.

Newport, J. and M. Kirschner. "A major developmental transition in early Xenopus embryos: I. characterization and timing of cellular changes at the midblastula stage." Cell 30.3 (1982): 675-86.

Odell, G. M. and V. E. Foe. "An agent-based model contrasts opposite effects of dynamic and stable microtubules on cleavage furrow positioning." J.Cell Biol. 183.3 (2008): 471-83.

Okamura, K., et al. "Distinct roles for Argonaute proteins in small RNA-directed RNA cleavage pathways." Genes Dev. 18.14 (2004): 1655-66.

Okazaki, N., et al. "Protocadherin LKC, a new candidate for a tumor suppressor of colon and liver cancers, its association with contact inhibition of cell proliferation." Carcinogenesis 23.7 (2002): 1139-48.

Padash, Barmchi M., S. Rogers, and U. Hacker. "DRhoGEF2 regulates actin organization and contractility in the Drosophila blastoderm embryo." J.Cell Biol. 168.4 (2005): 575-85.

Palacios, I. M. and Johnston D. St. "Kinesin light chain-independent function of the Kinesin heavy chain in cytoplasmic streaming and posterior localisation in the Drosophila oocyte." Development 129.23 (2002): 5473-85.

Palazzo, A. F., et al. "mDia mediates Rho-regulated formation and orientation of stable microtubules." Nat.Cell Biol. 3.8 (2001): 723-29.

Papoulas, O., T. S. Hays, and J. C. Sisson. "The golgin Lava lamp mediates dynein-based Golgi movements during Drosophila cellularization." Nat.Cell Biol. 7.6 (2005): 612-18.

Parham, S. N., C. G. Resende, and M. F. Tuite. "Oligopeptide repeats in the yeast protein Sup35p stabilize intermolecular prion interactions." EMBO J. 20.9 (2001): 2111-19.

Pastor-Pareja, J. C., et al. "Invasive cell behavior during Drosophila imaginal disc eversion is mediated by the JNK signaling cascade." Dev.Cell 7.3 (2004): 387-99.

Pearce, L. R., D. Komander, and D. R. Alessi. "The nuts and bolts of AGC protein kinases." Nat.Rev.Mol.Cell Biol. 11.1 (2010): 9-22.

Peifer, M. and E. Wieschaus. "The segment polarity gene armadillo encodes a functionally modular protein that is the Drosophila homolog of human plakoglobin." Cell 63.6 (1990): 1167-76.

Pelissier, A., J. P. Chauvin, and T. Lecuit. "Trafficking through Rab11 endosomes is required for cellularization during Drosophila embryogenesis." Curr.Biol. 13.21 (2003): 1848-57.

Pepper, A. S., et al. "Argonaute2 suppresses Drosophila fragile X expression preventing neurogenesis and oogenesis defects." PLoS.One. 4.10 (2009): e7618.

Rand, T. A., et al. "Biochemical identification of Argonaute 2 as the sole protein required for RNA-induced silencing complex activity." Proc.Natl.Acad.Sci.U.S.A 101.40 (2004): 14385-89.

Rappaport, R. "Establishment of the mechanism of cytokinesis in animal cells." Int.Rev.Cytol. 105 (1986): 245-81.

Riggs, B., et al. "The concentration of Nuf, a Rab11 effector, at the microtubule-organizing center is cell cycle regulated, dynein-dependent, and coincides with furrow formation." Mol.Biol.Cell 18.9 (2007): 3313-22.

Riggs, B., et al. "Actin cytoskeleton remodeling during early Drosophila furrow formation requires recycling endosomal components Nuclear-fallout and Rab11." J.Cell Biol. 163.1 (2003): 143-54.

Rivas, F. V., et al. "Purified Argonaute2 and an siRNA form recombinant human RISC." Nat.Struct.Mol.Biol. 12.4 (2005): 340-49.

Robinson, J. T., et al. "Cytoplasmic dynein is required for the nuclear attachment and migration of centrosomes during mitosis in Drosophila." J.Cell Biol. 146.3 (1999): 597-608.

Rose, L. S. and E. Wieschaus. "The Drosophila cellularization gene nullo produces a blastoderm-specific transcript whose levels respond to the nucleocytoplasmic ratio." Genes Dev. 6.7 (1992): 1255-68.

Rothwell, W. F., et al. "The Drosophila centrosomal protein Nuf is required for recruiting Dah, a membrane associated protein, to furrows in the early embryo." J.Cell Sci. 112 (Pt 17) (1999): 2885-93.

Royou, A., et al. "Reassessing the role and dynamics of nonmuscle myosin II during furrow formation in early Drosophila embryos." Mol.Biol.Cell 15.2 (2004): 838-50.

Sanchez-Soriano, N., et al. "Are dendrites in Drosophila homologous to vertebrate dendrites?" Dev.Biol. 288.1 (2005): 126-38.

Sanger, J. M., J. S. Dome, and J. W. Sanger. "Unusual cleavage furrows in vertebrate tissue culture cells: insights into the mechanisms of cytokinesis." Cell Motil.Cytoskeleton 39.2 (1998): 95-106.

Schejter, E. D., et al. "Role of the zygotic genome in the restructuring of the actin cytoskeleton at the cycle-14 transition during Drosophila embryogenesis." Cold Spring Harb.Symp.Quant.Biol. 57 (1992): 653-59.

Schejter, E. D. and E. Wieschaus. "Functional elements of the cytoskeleton in the early Drosophila embryo." Annu.Rev.Cell Biol. 9 (1993): 67-99.

Schweisguth, F., J. A. Lepesant, and A. Vincent. "The serendipity alpha gene encodes a membrane-associated protein required for the cellularization of the Drosophila embryo." Genes Dev. 4.6 (1990): 922-31.

Semotok, J. L., et al. "Smaug recruits the CCR4/POP2/NOT deadenylase complex to trigger maternal transcript localization in the early Drosophila embryo." Curr.Biol. 15.4 (2005): 284-94.

Shan, X. J., et al. "Ontogenetic development of digestive enzymes and effect of starvation in miiuy croaker Miichthys miiuy larvae." Fish.Physiol Biochem. 35.3 (2009): 385-98.

Shi, H., et al. "RNA interference in Trypanosoma brucei: role of the n-terminal RGG domain and the polyribosome association of argonaute." J.Biol.Chem. 284.52 (2009): 36511-20.

Shubeita, G. T., et al. "Consequences of motor copy number on the intracellular transport of kinesin-1-driven lipid droplets." Cell 135.6 (2008): 1098-107.

Sibon, O. C., V. A. Stevenson, and W. E. Theurkauf. "DNA-replication checkpoint control at the Drosophila midblastula transition." Nature 388.6637 (1997): 93-97.

Sisson, J. C., et al. "Lava lamp, a novel peripheral golgi protein, is required for Drosophila melanogaster cellularization." J.Cell Biol. 151.4 (2000): 905-18.

Sisson, J. C., W. F. Rothwell, and W. Sullivan. "Cytokinesis: lessons from rappaport and the Drosophila blastoderm embryo." Cell Biol.Int. 23.12 (1999): 871-76.

Smibert, C. A., et al. "smaug protein represses translation of unlocalized nanos mRNA in the Drosophila embryo." Genes Dev. 10.20 (1996): 2600-09.

Sommi, P., et al. "A mitotic kinesin-6, Pav-KLP, mediates interdependent cortical reorganization and spindle dynamics in Drosophila embryos." J.Cell Sci. 123.Pt 11 (2010): 1862-72.

Song, J. J., et al. "The crystal structure of the Argonaute2 PAZ domain reveals an RNA binding motif in RNAi effector complexes." Nat.Struct.Biol. 10.12 (2003): 1026-32.

Song, Y., et al. "Potential role for phosphorylation in differential regulation of the assembly of dynein light chains." J.Biol.Chem. 282.23 (2007): 17272-79.

Spradling, A. C., et al. "The Berkeley Drosophila Genome Project gene disruption project: Single P-element insertions mutating 25% of vital Drosophila genes." Genetics 153.1 (1999): 135-77.

Srivastava, M., et al. "The Amphimedon queenslandica genome and the evolution of animal complexity." Nature 466.7307 (2010): 720-26.

Stein, J. A., et al. "Slow as molasses is required for polarized membrane growth and germ cell migration in Drosophila." Development 129.16 (2002): 3925-34.

Sullivan, W. and W. E. Theurkauf. "The cytoskeleton and morphogenesis of the early Drosophila embryo." Curr.Opin.Cell Biol. 7.1 (1995): 18-22.

Suzuki, A., et al. "Atypical protein kinase C is involved in the evolutionarily conserved par protein complex and plays a critical role in establishing epithelia-specific junctional structures." J.Cell Biol. 152.6 (2001): 1183-96.

Tadros, W., et al. "SMAUG is a major regulator of maternal mRNA destabilization in Drosophila and its translation is activated by the PAN GU kinase." Dev.Cell 12.1 (2007): 143-55.

Tadros, W., et al. "Regulation of maternal transcript destabilization during egg activation in Drosophila." Genetics 164.3 (2003): 989-1001.

Tadros, W. and H. D. Lipshitz. "Setting the stage for development: mRNA translation and stability during oocyte maturation and egg activation in Drosophila." Dev.Dyn. 232.3 (2005): 593-608.

Tadros, W., J. T. Westwood, and H. D. Lipshitz. "The mother-to-child transition." Dev.Cell 12.6 (2007): 847-49.

Tanentzapf, G., et al. "Apical, lateral, and basal polarization cues contribute to the development of the follicular epithelium during Drosophila oogenesis." J.Cell Biol. 151.4 (2000): 891-904.

Tang, F., et al. "Maternal microRNAs are essential for mouse zygotic development." Genes Dev. 21.6 (2007): 644-48.

Tepass, U. and V. Hartenstein. "The development of cellular junctions in the Drosophila embryo." Dev.Biol. 161.2 (1994): 563-96.

---. "The development of cellular junctions in the Drosophila embryo." Dev.Biol. 161.2 (1994): 563-96.

Tepass, U., et al. "Epithelial cell polarity and cell junctions in Drosophila." Annu.Rev.Genet. 35 (2001): 747-84.

Tomari, Y., T. Du, and P. D. Zamore. "Sorting of Drosophila small silencing RNAs." Cell 130.2 (2007): 299-308.

Tomari, Y., et al. "A protein sensor for siRNA asymmetry." Science 306.5700 (2004): 1377-80.

Tran, S. L. and M. A. Welte. "In-vivo centrifugation of Drosophila embryos." J.Vis.Exp.40 (2010).

Turner, F. R. and A. P. Mahowald. "Scanning electron microscopy of Drosophila embryogenesis. 1. The structure of the egg envelopes and the formation of the cellular blastoderm." Dev.Biol. 50.1 (1976): 95-108.

Ullrich, O., et al. "Rab11 regulates recycling through the pericentriolar recycling endosome." J.Cell Biol. 135.4 (1996): 913-24.

Vale, R. D., J. A. Spudich, and E. R. Griffis. "Dynamics of myosin, microtubules, and Kinesin-6 at the cortex during cytokinesis in Drosophila S2 cells." J.Cell Biol. 186.5 (2009): 727-38.

Valiente, M., et al. "Binding of PTEN to specific PDZ domains contributes to PTEN protein stability and phosphorylation by microtubule-associated serine/threonine kinases." J.Biol.Chem. 280.32 (2005): 28936-43.

van der Bliek, A. M. and E. M. Meyerowitz. "Dynamin-like protein encoded by the Drosophila shibire gene associated with vesicular traffic." Nature 351.6325 (1991): 411-14.

Vaughan, P. S., J. D. Leszyk, and K. T. Vaughan. "Cytoplasmic dynein intermediate chain phosphorylation regulates binding to dynactin." J.Biol.Chem. 276.28 (2001): 26171-79.

Vazquez, F., et al. "Phosphorylation of the PTEN tail regulates protein stability and function." Mol.Cell Biol. 20.14 (2000): 5010-18.

Walden, P. D. and N. J. Cowan. "A novel 205-kilodalton testis-specific serine/threonine protein kinase associated with microtubules of the spermatid manchette." Mol.Cell Biol. 13.12 (1993): 7625-35.

Wang, D., et al. "Coexpression of MAST205 inhibits the activity of Na+/H+ exchanger NHE3." Am.J.Physiol Renal Physiol 290.2 (2006): F428-F437.

Watanabe, N., et al. "Cooperation between mDia1 and ROCK in Rho-induced actin reorganization." Nat.Cell Biol. 1.3 (1999): 136-43.

Webb, R. L., et al. "Using total internal reflection fluorescence (TIRF) microscopy to visualize cortical actin and microtubules in the Drosophila syncytial embryo." Dev.Dyn. 238.10 (2009): 2622-32.

Welte, M. A. "Bidirectional transport: matchmaking for motors." Curr.Biol. 20.9 (2010): R410-R413.

Welte, M. A., et al. "Regulation of lipid-droplet transport by the perilipin homolog LSD2." Curr.Biol. 15.14 (2005): 1266-75.

Welte, M. A., et al. "Developmental regulation of vesicle transport in Drosophila embryos: forces and kinetics." <u>Cell</u> 92.4 (1998): 547-57.

Wen, Y., et al. "EB1 and APC bind to mDia to stabilize microtubules downstream of Rho and promote cell migration." <u>Nat.Cell Biol.</u> 6.9 (2004): 820-30.

Wenzl, C., et al. "Localization of RhoGEF2 during Drosophila cellularization is developmentally controlled by slam." <u>Mech.Dev.</u> 127.7-8 (2010): 371-84.

Wieschaus, E. "Embryonic transcription and the control of developmental pathways." <u>Genetics</u> 142.1 (1996): 5-10.

Wieschaus, E. and D. Sweeton. "Requirements for X-linked zygotic gene activity during cellularization of early Drosophila embryos." <u>Development</u> 104.3 (1988): 483-93.

Williams, R. W. and G. M. Rubin. "ARGONAUTE1 is required for efficient RNA interference in Drosophila embryos." <u>Proc.Natl.Acad.Sci.U.S.A</u> 99.10 (2002): 6889-94.

Woods, D. F., et al. "Dlg protein is required for junction structure, cell polarity, and proliferation control in Drosophila epithelia." <u>J.Cell Biol.</u> 134.6 (1996): 1469-82.

Xiong, H., et al. "Interaction of TRAF6 with MAST205 regulates NF-kappaB activation and MAST205 stability." <u>J.Biol.Chem.</u> 279.42 (2004): 43675-83.

Xu, K., et al. "The fragile X-related gene affects the crawling behavior of Drosophila larvae by regulating the mRNA level of the DEG/ENaC protein pickpocket1." <u>Curr.Biol.</u> 14.12 (2004): 1025-34.

Yan, K. S., et al. "Structure and conserved RNA binding of the PAZ domain." <u>Nature</u> 426.6965 (2003): 468-74.
Zhang, C. X., et al. "Isolation and characterization of a Drosophila gene essential for early embryonic development and formation of cortical cleavage furrows." <u>J.Cell Biol.</u> 134.4 (1996): 923-34.

9.   Supplementary material:

S1: Olinucleotides:

Purpose	Name	Sequence 5` to 3`
ago2 sequencing	see Meyer, 2007	
ago2 RTqPCR	Q-PCR long fwd	AACAACAACCGCATCAGC
	Q-PCR short fwd	TTCGAAGAGTTTGCTTGCAG
	Q-PCR both rev	CGTCTTGGGATTTTTGCTGT
	RPL32 fwd	CCGCTTCAAGGGACAGTATC
	RPL32 rev	GACAATCTCCTTGCGCTTCT
Deficiency mapping	ago2(321)_1fwd	GCCCGCCTAGTCCGTATGTTC
	ago2(321)_1rev	TGGCTGAGGCGGTAATGGTAAT
(ago2 only-	ago2(321)_2fwd	TTTGCCGGATACATGCTTTTCA
Df(3L)XG9 mapping	ago2(321)_2rev	CCTTGGCTCTGGGTTTGGTTT
Primers available upon	ago2(454)_1fwd	TGCCGGATACATGCTTTTCAAC
request)	ago2(454)_1rev	GCTCACGCCATCTCGGTAGTAG
	ago2(454)_2fwd	TTTGGGGGCTTTCCGTAATCTC
	ago2(454)_2rev	CGCGCAAGTGCTCCAAAGTAAT
Candidate sequencing	CG6498_1fwd	GTGACCGTTCGGCTGATTGAT
	CG6498_1 rev	GTTGCGATTACGGGGTTTTTG
	CG6498_2 fwd	AGCGCCTTGCCAGCCGTATG
	CG6498_2 rev	CTGCCCGACCGCGAAATGTT
	CG6498_3 fwd	CAGCGGTACTTGATTTTCGGTTGG
	CG6498_3 rev	TTTTGCGGCGTTGAGGTGGATA
	CG6498_4 fwd	CGGGGTTCAGCTGGAGGAGGTG
	CG6498_4 rev	TGGCGTTTGAGGAGGCTGTTGAGG
	CG6498_5 fwd	CGAGGCGGCAGCTGAACTAAATG
	CG6498_5 rev	AGGCGCTACCCGAACCACTACCAC
	CG6498_6 fwd	TTTGCCGCGTTTCTCCATCTCG
	CG6498_6 rev	ATTGCCCCCGCCTGCTATTACG
	CG6498_7 fwd	CACGTCGCCCTCATCCTCTTC
	CG6498_7 rev	CCGCGCCCATTCTCATCAC
	CG6498_8 fwd	CCATCGCGTGCCCAGGAGACT
	CG6498_8 rev	GAGATGGAGAAACGCGGCAAAATG
	CG6498_9 fwd	CGTCCAACTTGCTGCGTATGC
	CG6498_9 rev	CCGGGCGGAATGTTGTGC
	CG6498_10 fwd	CTTTTCGCGCAGCACACCAGA
	CG6498_10 rev	GCCGCAGTCCCGCCTCAA
	CG7427_1 fwd	TCCCGAGATATTTAAGTCACACG
	CG7427_1 rev	GGATGCCGGCGAGGAGTC
	CG7427_2 fwd	GGCCAGCGACAATTACTTCCAGA
	CG7427_2 rev	ATTTACCGGCCGTGCTTAGATTC
	CG16979 1 fwd	ACCGCGTATTGCCGAGGAGAA

Continuation of S1: Oligos used in this work

	CG16979 1 rev	GCAGCCGGGTGAAGCAGAAGTC
	CG16979 2 fwd	TGCGGGCCTCGTTTTTCGTC
	CG16979 2 rev	CCTTCCAGCCGCACCAACCTT
	CG16979 3 fwd	GCGCAGTCGTGATCCCGTGTC
	CG16979 3 rev	CGTGCTAACCCGCGATTCAGTG
	CG12304 1 fwd	GACCCGTCCGGCAGTAATCAC
	CG123041 rev	TGTCGGCCTAAAGAGTCCAAATCA
	CG123042 fwd	CGCCGCGAAAATGTACGAACTGAA
	CG123042 rev	CGACATCCGCCACCGACATCTG
	CG123043 fwd	GTCGGTGGCGGATGTCGGTGTCTA
	CG123043 rev	CAGGCCAGGGTCGCGTCATCTCTT
	Tfb2 1 fwd	CCAGCGTCCCATTTTGTATTAGGT
	Tfb2 1 rev	GCTGGCGTTGCGTGTTGC
	Tfb2 2 fwd	GTTAGCACGCCCACGACGAGATT
	Tfb2 2 rev	CACCCGCCAAACGCCAGAGT
	Tfb2 3 fwd	TCCCTGGGCTTCGAGTCCTTATCC
	Tfb2 3 rev	TGCGGCCCATCACAATTTCTACCT
	CG12301 fwd 1	AAGGGCGTTACGAAGGGGGTTTT
	CG12301 rev 1	GGGCTTGCCTTGGCTTCTTTCTGA
	CG12301 fwd 2	ACGGGCCAAGTACGACAAGGATG
	CG12301 rev 2	CGGCCAACTGGAGCACGGATAC
	CG12301 fwd 3	AGCTCGCCCTGCCTGGATGG
	CG12301 rev 3	CTCACTGGCCCGGCAAATAAACTT
cloning of dop cDNA	Dopfull NotI fwd	CA**GCGGCCGC**ATGAGTCGCCAGGAGGGAGC
	Dopfull KpnI XbaI rev	CT**TCTAGA**GGTACC CTTCCTCTGCTTGGCAGCAGA
cloning of dopΔDUF	dDUF1rev	AC**GCGGCCGC**CCGAGTATGGGGAATGGGTTCG
	dDUF2fwd	AC**GCGGCCGC**CAGCAGGAATTAAGGGAAACACAGC
cloning of dopΔKinase	Delta Kinase 1 fwd	TA**GGTACC**ATGAGTCGCCAGGAGGGAGCT
	Delta Kinase 1 rev	TA**GCGGCCGC**GTTGTTGGGCTCCACTGCCAG
	Delta Kinase 2 fwd	CT**GCGGCCGC**CATGCCACTCCCACGTCTACCG
	Delta kinase 2 rev	GA**TCTAGA**CTTCCTCTGCTTGGCAGCAGAAG
cloning of dopΔPDZ	dPDZ1fwd	**GGTACC**ATGAGTCGCCAGGAGGGAGCTG
	dPDZ1rev	**GCGGCCGC**CACGACGTATGATGATCGGAGGC
	dPDZ2fwd	**GCGGCCGC**CACACCAGCATCCAGAGCGGTGG
	dPDZ2rev	**TCTAGA**CTTCCTCTGCTTGGCAGCAGAAGTG
cloning of DUF-HA	DUF-NotI fwd	TG**GCGGCCGC**ATGTCCCGAACCCATTCCCCATAC
	DUF-KpnI rev	TC**GGTACC**GGTGACTTGCTCCGAGCACATC
cloning of PDZ-HA	Dop-PDZ fwd	TA**GCGGCCGC**ATG GGCTCCAGTACGGCCAGC
	Dop-PDZ rev	TA**GGTACCGC**CACCGCTCTGGATGCTGG
cloning of GFP	GFP-fwd	TC**TCTAGA**ATGGTGAGCAAGGGCGAGGA
	GFP-rev	GC**TCTAGA**TCTTACTTGTACAGCTCGTCCATG

Continuation of S1: Oligos used in this work

Plasmid rescue	Pry4	CAATCATATCGCTGTCTCACTCA
	Plw3-1	TGTCGGCGTCATCAACTCC
	Plac4	ACTGTGCGTTAGGTCCTGTTCATTGTT
	Plac1	CACCCAAGGCTCTGCTCCCACAAT
cloning of HA tag	HA_insert_fwd	CTAGATACCCATACGATGTTCCTGACTATGCGG GCTATCCCTATGACGTCCCGGACTATGCAGGA TCCTATCCATATGACGTTCCAGATTACGCTTGAT
	HA_insert_rev	CTAGATCAAGCGTAATCTGGAACGTCATATGGA TAGGATCCTGCATAGTCCGGGACGTCATAGGG ATAGCCCGCATAGTCAGGAACATCGTATGGGTAT

S2: Ago2 western blot
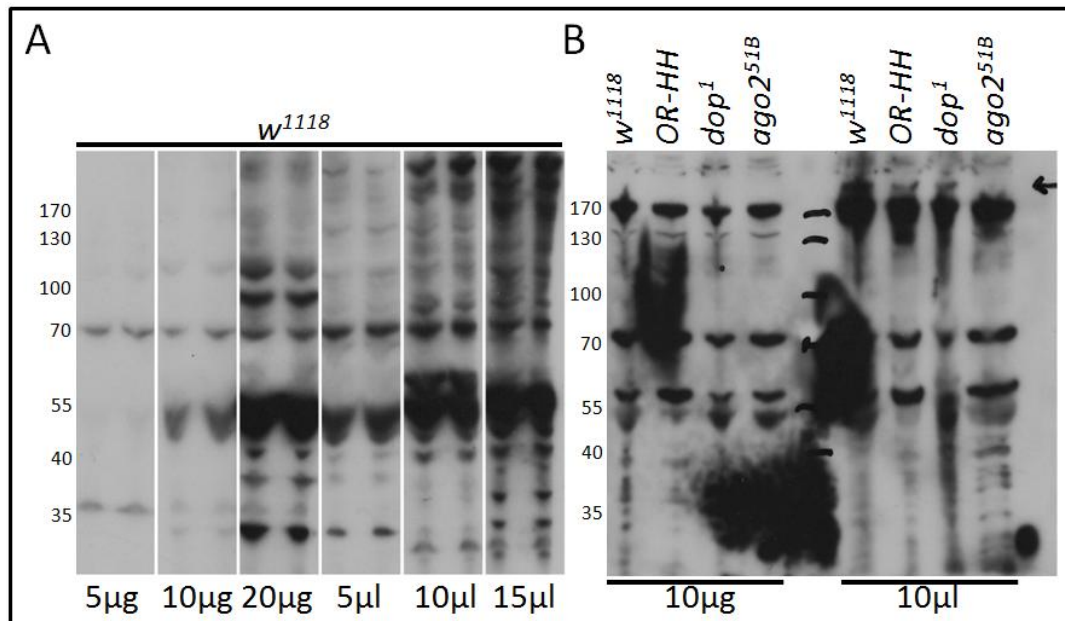
S3: Alignment of Dop with MAST1-4. Jalview alignment of Dop and the human MAST1-4 kinases. The colours indicate identical residue classes. Coloured bars indicate DUF (red), Kinase (green) and PDZ (blue) domains.

S4: anti Dop WB for LH alleles using different peptide antibodies. (A) αDop1303 (left) and affinity purified αDop1303 (right). (B) using affinity purified αDop2074.
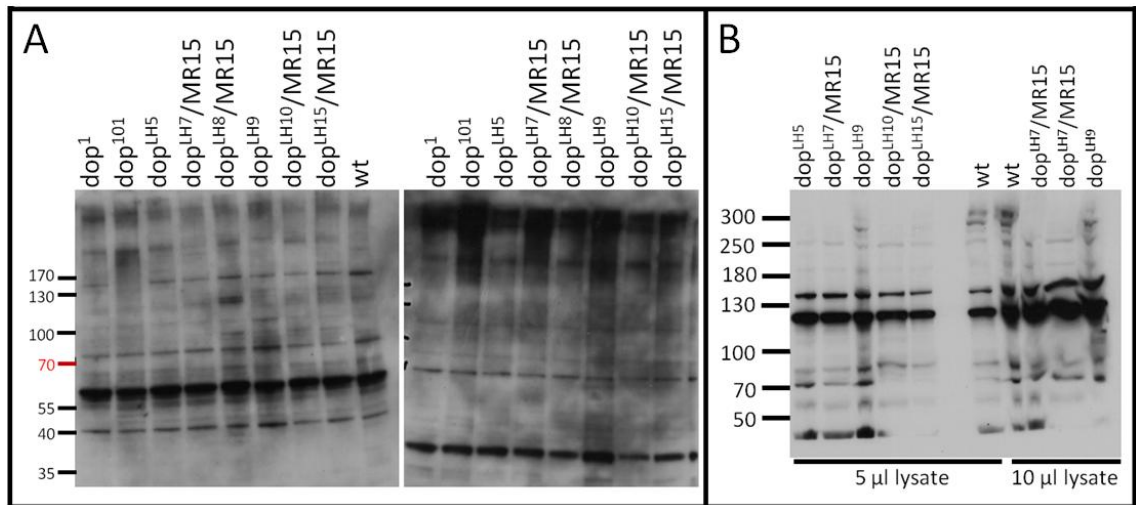
S5: DIC 2DGE - Variations in DIC phosphorylation and phosphatase treatment. (A) Four independent DIC 2DGE experiments show that the pattern of DIC is highly variable. In parallel phosphatase treatment reveals the phosphorylated protein fraction of DIC. (B) DIC separates most likely into 3 different fractions. Fraction 1 (pH 5.7-5.9)(green) and fraction 2 (pH 5.1-5.2)(red) are smear bands, while fraction 3 (pH 4.8-5.0) appears as single dots. Only fraction 1 is sensitive to phosphatase treatment.
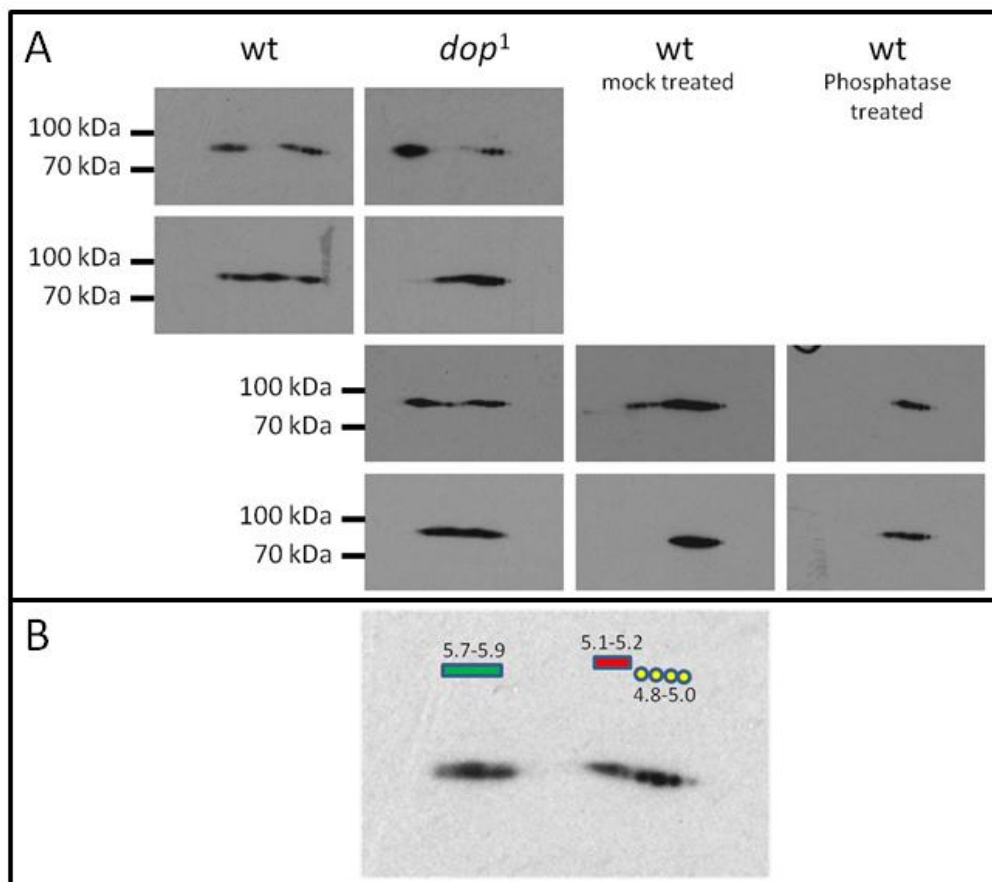
S6: Defects in adult *dop* mutants. Wing defects are previously described; Leg defects include shortening and thickening of femur (f), tibia (ti) and tarsus (ta) but not in the coxa (c). Occasionally legs appear to have ectopic joints in the femur (*).
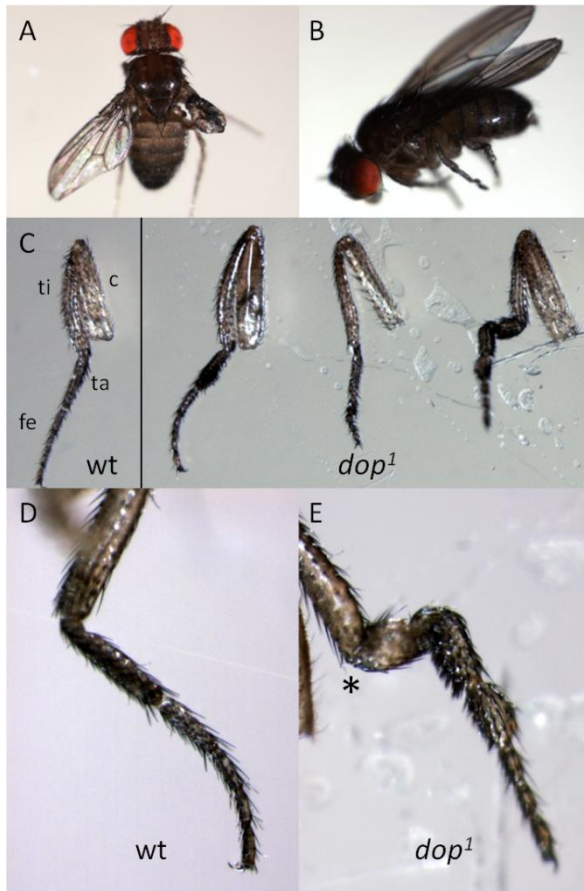

**S7: Yolk streaming in *dop^{LH10}* mutants (on attached DVD)**

**S8: Interaction between Baz-GFP overexpression and *dop^1* phenotype**
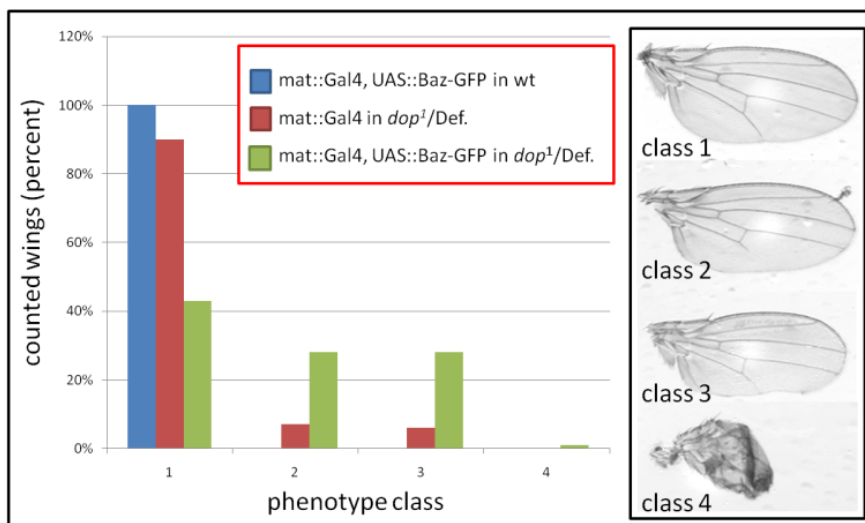
S9: Cellularisation in *dop^LH5^* mutants. Homozygous dopLH5 flies were used for embryo collection and embryos were fixed usin 4% FA. Fixed embryos were stained with antibodies against Dlg (red) and DPatJ (green). Most found embryos resembled to the embryo shown in A (optical section) and B (en face view). Some embryos displayed low level of membrane growth (C, D). E shows a detail view of lateral membranes connected to expanded furrow canals (marked by upwards facing arrow).
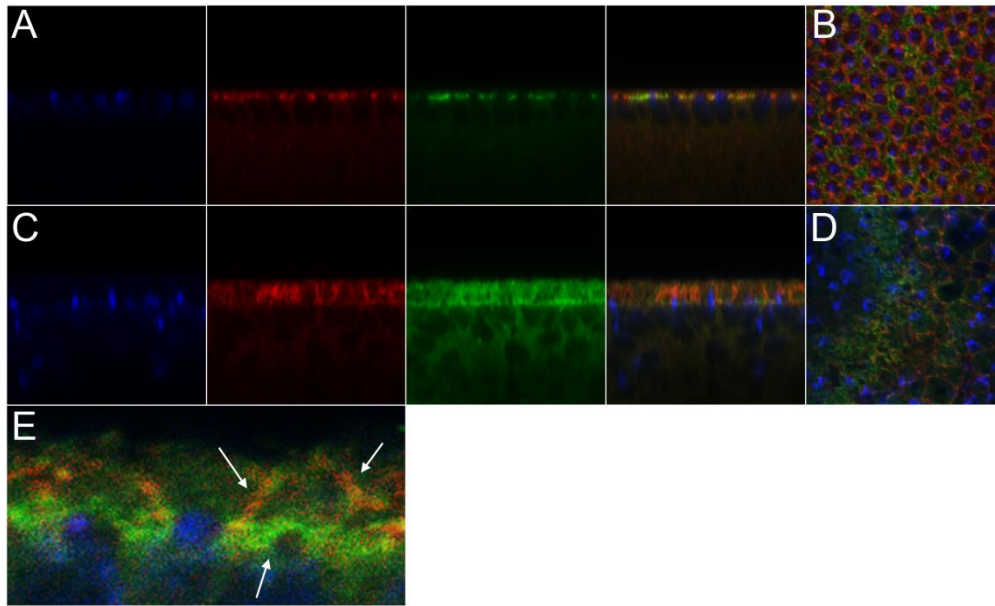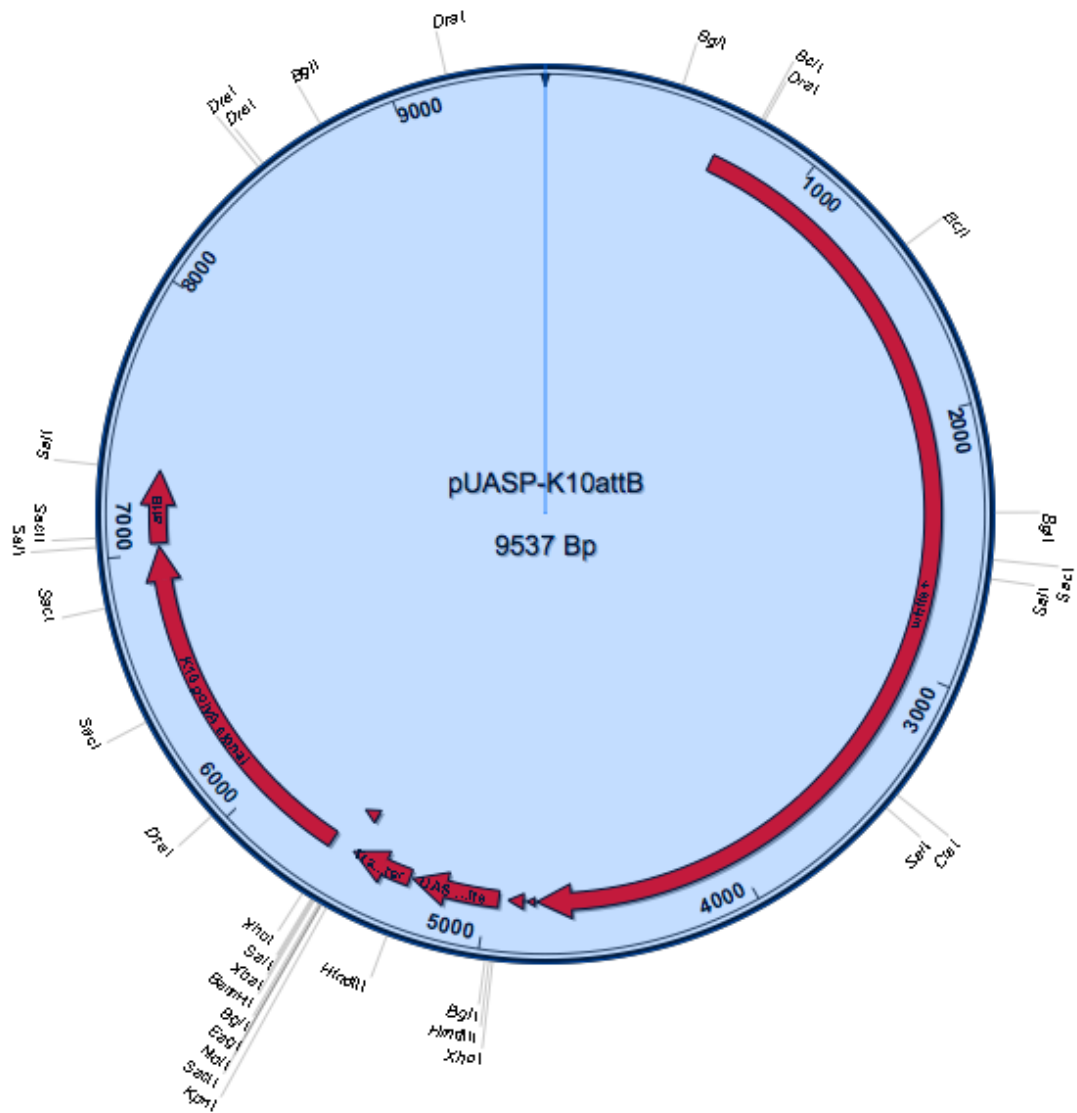

S10: Dop antibody staining
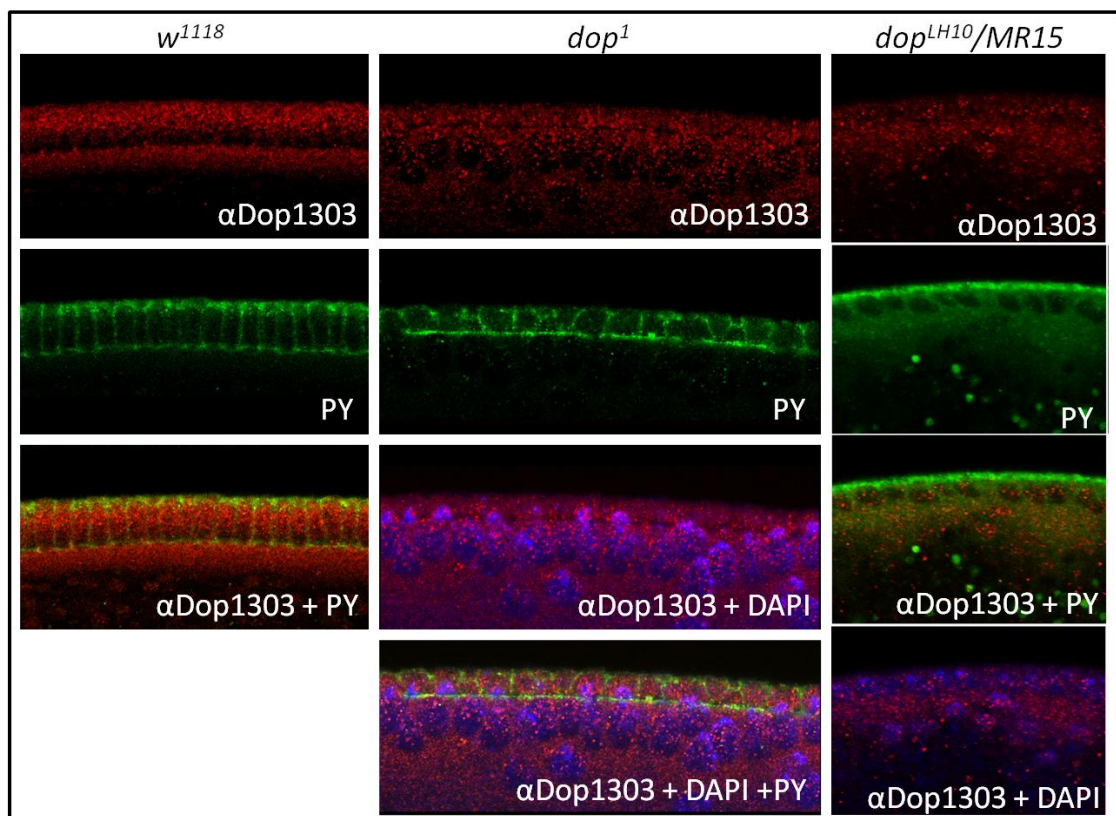
S11: GFP-LSD2 localisation. Life imaging of the lipid droplet marker LSD2 fused to eGFP. Time is shown in min:sec.
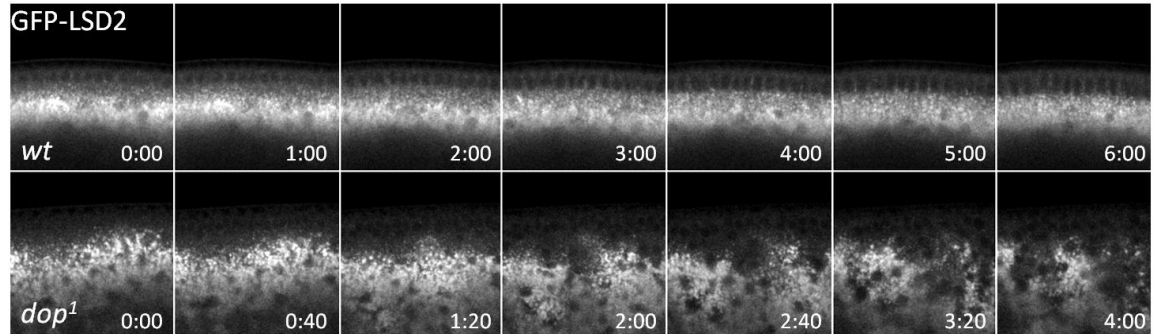
S12: Detailed construct information

Molecular map of the expression vector pUAS-K10

Description of some of the cloned inserts:

dop$^{\Delta DUF}$-HA: Expressing a Dop protein lacking AA 341-703 (ectopic G,R,R at the break point). The used restriction sites were KpnI—NotI--XbaI

dop$^{\Delta Kinase}$-HA: Expressing a Dop protein lacking AA 828-1181 (ectopic G,R at the break point). The used restriction sites were KpnI—NotI--XbaI

dop$^{\Delta PDZ}$-HA: Expressing a Dop protein lacking AA 1512-1593 (ectopic G,R,R at the break point). The used restriction sites were KpnI—NotI—XbaI

DUF-HA and PDZ-HA constructs express AA341-703 and 1512-1593 respectively.